UNIVERSITÄTSKLINIKUM HAMBURG-EPPENDORF

Zentrum für Geburtshilfe, Kinder- und Jugendmedizin
Klinik für Kinder- und Jugendmedizin

Direktorin Prof. Dr. med. Ania C. Muntau

Strukturelle und funktionelle Charakterisierung des humanen Peroxins PEX26

Dissertation

zur Erlangung des Grades eines Doktors der Medizin
an der Medizinischen Fakultät der Universität Hamburg.

vorgelegt von:

Philipp Guder
aus Bad Segeberg

Hamburg 2020

Angenommen von der Medizinischen Fakultät am: **18.03.2021**

Veröffentlicht mit Genehmigung der Medizinischen Fakultät der Universität Hamburg.

Prüfungsausschuss, der/die Vorsitzende: **Prof. Dr. Ania C. Muntau**

Prüfungsausschuss, 2. Gutachter/in: **PD Dr. Maja Hempel**

Prüfungsausschuss, 3. Gutachter/in: **Prof. Dr. Wolfgang Schliebs**

Inhaltsverzeichnis

1. Originalarbeit

Isoform-specific domain organization determines conformation and function of the peroxisomal biogenesis factor PEX26

Philipp Guder[1,2]♦Amelie S. Lotz-Havla[3]♦, Mathias Woidy[1,2], Dunja D. Reiß[3], Marta K. Danecka[1], Ulrich A. Schatz[4], Marc Becker[3,5], Regina Ensenauer[3,6], Philipp Pagel[7,8], Lars Büttner[3], Ania C. Muntau[2] and Søren W. Gersting[1,2]*

[1]University Children's Research@Kinder-UKE and [2]Children's Hospital, University Medical Center Hamburg-Eppendorf, 20246 Hamburg, Germany, [3]Dr. von Hauner Children's Hospital, Ludwig-Maximilians-University, 80337 Munich, Germany, [4]Department for Medical Genetics, Molecular and Clinical Pharmacology, Medical University Innsbruck, 6020 Innsbruck, Austria, [5]Labor Becker Olgemöller und Kollegen, 81671 Munich, Germany, [6]Experimental Pediatrics, Department of General Pediatrics, Neonatology and Pediatric Cardiology, University Children's Hospital, Heinrich Heine University Düsseldorf, 40225 Düsseldorf, Germany, [7]Lehrstuhl für Genomorientierte Bioinformatik, Technische Universität, 85350 Freising, Germany, [8]numares GmbH, Josef-Engert-Str. 9, 93053 Regensburg, Germany

♦ These authors contributed equally to this work.

BBA - Molecular Cell Research 1866 (2019) 518–531

Contents lists available at ScienceDirect

BBA - Molecular Cell Research

journal homepage: www.elsevier.com/locate/bbamcr

Isoform-specific domain organization determines conformation and function of the peroxisomal biogenesis factor PEX26

Philipp Guder[a,b,1], Amelie S. Lotz-Havla[c,1], Mathias Woidy[a,b], Dunja D. Reiß[c], Marta K. Danecka[a], Ulrich A. Schatz[d], Marc Becker[c,e], Regina Ensenauer[c,f], Philipp Pagel[g,h], Lars Büttner[c], Ania C. Muntau[b], Søren W. Gersting[a,b,*]

[a] University Children's Research@Kinder-UKE, University Medical Center Hamburg-Eppendorf, 20246 Hamburg, Germany
[b] Children's Hospital, University Medical Center Hamburg-Eppendorf, 20246 Hamburg, Germany
[c] Dr. von Hauner Children's Hospital, Ludwig-Maximilians-University, 80337 Munich, Germany
[d] Department for Medical Genetics, Molecular and Clinical Pharmacology, Medical University Innsbruck, 6020 Innsbruck, Austria
[e] Labor Becker Olgemöller und Kollegen, 81671 Munich, Germany
[f] Experimental Pediatrics, Department of General Pediatrics, Neonatology and Pediatric Cardiology, University Children's Hospital, Heinrich Heine University Düsseldorf, 40225 Düsseldorf, Germany
[g] Lehrstuhl für Genomorientierte Bioinformatik, Technische Universität, 85350 Freising, Germany
[h] numares GmbH, Josef-Engert-Str. 9, 93053 Regensburg, Germany

ARTICLE INFO

Keywords:
PEX26
Oligomerization
Heptad repeat
Bioluminescence resonance energy transfer (BRET)
Peroxisomal biogenesis
Peroxisomal function
Peroxisomal biogenesis disorders (PBD)
Zellweger syndrome

ABSTRACT

Peroxisomal biogenesis factor PEX26 is a membrane anchor for the multi-subunit PEX1-PEX6 protein complex that controls ubiquitination and dislocation of PEX5 cargo receptors for peroxisomal matrix protein import. PEX26 associates with the peroxisomal translocation pore *via* PEX14 and a splice variant (PEX26Δex5) of unknown function has been reported. Here, we demonstrate PEX26 homooligomerization mediated by two heptad repeat domains adjacent to the transmembrane domain. We show that isoform-specific domain organization determines PEX26 oligomerization and impacts peroxisomal β-oxidation and proliferation. PEX26 and PEX26Δex5 displayed different patterns of interaction with PEX2-PEX10 or PEX13-PEX14 complexes, which relate to distinct pre-peroxisomes in the *de novo* synthesis pathway. Our data support an alternative PEX14-dependent mechanism of peroxisomal membrane association for the splice variant, which lacks a transmembrane domain. Structure-function relationships of PEX26 isoforms explain an extended function in peroxisomal homeostasis and these findings may improve our understanding of the broad phenotype of PEX26-associated human disorders.

1. Introduction

Disorders of peroxisomal biogenesis (PBD) are mostly fatal autosomal recessive disorders. They are characterized by impaired peroxisomal assembly resulting in a deficiency of essential peroxisomal functions or a complete loss of functional peroxisomes [1–3]. Peroxisomes are required for normal health and development [4] and the membrane-bound organelles, found within almost all eukaryotic cells [5], are formed through replication by fission [6,7] or *de novo* by pre-peroxisome vesicles budding from the endoplasmic reticulum (ER) [8] or from mitochondria [9]. PBD are caused by mutations leading to impaired function of peroxins, which are proteins responsible for peroxisome assembly and biogenesis [3]. Although major progress in the understanding of peroxisomal biology has been achieved, there is still a lack of knowledge on structure and function of specific peroxins [3,10]. For PBD, genotype-phenotype correlations are often weak [11] and treatment is mostly symptomatic or supportive [1]. This emphasizes the need for a more detailed understanding of biological function and biochemical pathways associated with proteins involved in peroxisomal biogenesis and disease.

Approximately 80% of PBD patients present with a phenotype of the Zellweger spectrum continuum (Zellweger syndrome, neonatal adrenoleukodystrophy, infantile Refsum disease, Heimler syndrome [12]), which has an overall incidence of 1:50,000 births in the US [13,14].

* Corresponding author at: University Children's Research@Kinder-UKE and University Children's Hospital, University Medical Center Hamburg-Eppendorf, Hamburg, Germany.
E-mail address: gersting@uke.de (S.W. Gersting).
[1] These authors contributed equally to this work.

https://doi.org/10.1016/j.bbamcr.2018.10.013
Received 29 January 2018; Received in revised form 11 October 2018; Accepted 18 October 2018
Available online 23 October 2018

The Zellweger spectrum continuum was classified into 12 complementation groups based on the underlying genetic defects [15]. Mutations in the *PEX26* gene (MIM 608666) [15] are assigned to complementation group 8 [16] and lead to an import defect of peroxisomal matrix proteins type 1 [17] and type 2 [16]. *PEX26* encodes a 34-kDa type 2 peroxisomal membrane protein of 305 amino acids with one transmembrane domain (TMD, aa252–269) near to the C-terminus and a cytosol-faced N-terminal part. The PEX26 protein binds to the peroxin PEX6 with its N-terminal part (aa29–174) and thus recruits the PEX1-PEX6 complex to the peroxisomal membrane [17–19]. Tamura et al. suggested PEX26 residues aa13–48 to be sufficient for PEX6 binding [20]. PEX1 and PEX6 form hetero-hexamers with each other and ternary complexes with PEX26 [21–24]. It is assumed that the PEX26 yeast homologue Pex15 acts as a monomer within this complex [22,25]. Import of the > 50 peroxisomal matrix proteins *via* the peroxisomal translocon [26] requires recycling of the cargo receptor PEX5 [27]. PEX1 and PEX6 are members of the AAA protein family that is involved in ubiquitination [28] and dislocation of PEX5 from the peroxisomal membrane to the cytosol and thus play a key role in matrix protein import [5]. PBD patient-derived PEX26 mutants show insufficient binding to the PEX1-PEX6 complex leading to impaired matrix protein import [16,17,21]. This implies that binding of PEX26 to PEX6 is essential for its function.

The alternative splice variant *PEX26Δex5* encodes a PEX26 isoform that is truncated for aa223–271 comprising the TMD [17]. The splice variant is expressed in a 1:2 ratio to the full-length protein [17]. PEX26Δex5 overexpression in PEX26-deficient cells (GM17398) complemented PEX26-deficiency as efficiently as full-length PEX26. However, PEX26Δex5 showed a subcellular distribution to the cytosol as well as to the ER [17]. A potential physiological function of the splice variant has not been investigated to date. Recently, Tamura et al. [20] showed that PEX26 binds PEX14, therefore, PEX26 may additionally act as a scaffold protein to recruit the PEX13-PEX14 docking complex to the peroxisomal translocon. Increased pexophagy was associated with dysfunction of the peroxisomal AAA^+ ATPase complex [29].

It is well established that the multi-subunit PEX1-PEX6 protein complex is anchored to peroxisomes by binding to PEX26. In order to better understand the role of this peroxin in peroxisome assembly, homeostasis, and metabolic function, we aimed to investigate PEX26 domain organization and binding to other peroxisomal proteins involved in peroxisomal matrix protein import and peroxisomal biogenesis.

2. Materials and methods

2.1. Plasmids

PEX26 (NM_001127649.1), *PEX26*Δex5, and truncated PEX26 fragments were introduced by Invitrogen Gateway recombination cloning (Invitrogen, Carlsbad, CA) into expression clones with C-terminal V5 and HA tag (pEF-DEST51-V5, pEF-DEST51-HA) as well as BRET expression clones coding for N- and C-terminal fusion proteins with Renilla luciferase (Rluc) or yellow fluorescent protein (YFP). BRET expression clones were designed based on pcDNA 6.2. DEST general Gateway vector (Invitrogen, Carlsbad, CA). BiFC expression clones were designed based on pCR3.1 DEST general Gateway vector (Invitrogen, Carlsbad, CA) harboring N-terminally YFP1 or YFP2 fragments. To design the artificial $PEX26_{dimer}$, a sequence coding for a flexible amino acid linker [30] and a synthetic *PEX26* with reverse order of amino acids (Sloning BioTechnology, Puchheim, Germany) were added to the 3′-end of the *PEX26* sequence by In-Fusion cloning (Clontech, Saint-Germain-en-Laye, France) (Supplementary Fig. 1A, B). Mutations for PEX26-C173S, PEX26-HR1, PEX26-HR1HR2, and PEX26Δex5-HR2 were introduced by site-directed mutagenesis. For details see Supplementary Information.

2.2. Cell lines

HEK293 cells, COS-7 cells, and the PBD skin fibroblast cell line GM17398 were used. GM17398 harbors a homozygous mutation *PEX26intG231T*, which is a splice site mutation between exon 1 and 2. Only aa1–77 are identical with PEX26. The mutation leads to a temperature sensitive Zellweger syndrome phenotype with a failure of PTS1 protein import [19].

2.3. Transfection

For transfection of HEK293 cells, COS-7 cells, and the PBD skin fibroblast cell line GM17398, electroporation was performed using the Nucleofector 96-well Shuttle System (Lonza, Basel, Switzerland) according to the supplier's protocols for HEK293 cells, COS-7 cells or primary fibroblasts.

2.4. BRET experiments

The interaction of proteins in living cells was analyzed by bioluminescence resonance energy transfer (BRET) as described before [31,32]. Binary interactions were tested in all eight possible combinations of two proteins of interest either N- or C-terminally fused to Rluc (energy donor) or YFP (energy acceptor) or in four combinations for homomeric interactions, at an acceptor to donor ratio of 3:1. The BRET tag orientation (N-terminal *vs.* C-terminal) had an impact on luciferase signals (Supplementary Fig. 2). All combinations were tested in duplicates and at least two independent experiments if not stated differently. For BRET saturation experiments [32,33] HEK293 cells were transfected with increasing acceptor to donor ratios. After 48 h coelenterazine (30 µM; PJK, Kleinblittersdorf, Germany) was added to living cells and light emission was collected in a 96-well microplate luminometer LUMIstar OPTIMA (BMG Labtech, Ortenberg, Germany) for 10 s at 475 nm (Rluc signal) and 535 nm (YFP signal) as relative light units (RLU). The BRET ratio was calculated based on $R = I_A/I_D - cf$, where R is the BRET ratio, I_A is the intensity of light emission at 535 nm, I_D is the intensity of light emission at 475 nm, and cf is a correction factor = $(I_{A\_control}/I_{D\_control})$ with the control being the co-transfection of a donor fusion-protein and YFP not fused to a protein of interest. An interaction of an investigated protein pair was assumed, if at least 1 tested combination resulted in a BRET ratio above the method-specific threshold of 0.094. The threshold was determined by a reference data set of known interacting and non-interacting protein pairs. A positive control interaction (bJun-bFos) and the expression of a YFP-Rluc fusion protein to monitor BRET efficiency were included in every individual experiment. Parameters for saturation experiments were calculated by $Y = BRET_{max} * (X/BRET_{50} + X)$, where $BRET_{max}$ is the maximal BRET ratio and $BRET_{50}$, a measure of relative binding affinities, is the acceptor to donor ratio required to reach the half-maximal BRET ratio.

2.5. Bimolecular fluorescence complementation (BiFC)

Bimolecular fluorescence complementation (BiFC) was used to analyze binary protein-protein interactions according to Nyfeler et al. [34]. Proteins were N-terminally tagged with YFP fragments, either YFP1 (amino acids 1–158) or YFP2 (amino acids 159–239). 200,000 COS-7 cells were transfected with 400 ng of each cDNA harboring YFP1 and YFP2, respectively, seeded to black 96-well microtiter plates (Corning/Merck, Darmstadt, Germany) and incubated at 30 °C with 5% CO_2 over 48 h. For measurement, growth media (RPMI, 1% antibiotics, 10% FCS; Gibco/Thermo Fisher Scientific, Waltham, MA, USA) was replaced by 40 µl PBS and fluorescence was determined with a plate reader (Pherastar, BMG Labtech, Ortenberg, Germany) at excitation and emission wavelengths of 510 and 545 nm, respectively. The interaction bJun-bFos served as positive control. Interaction of YFP1-PEX26 and YFP2-PEX2 served as a negative control. A detection limit was set as

mean of negative control plus 3 times standard deviation of $n = 6$ experiments (threshold, 344 relative fluorescence units).

2.6. Co-immunoprecipitation

Lysates of COS-7 cells co-transfected with *PEX26*-V5 and Flag-*PEX26* were incubated with mouse anti-Flag antibody (dilution 1:1000; Agilent Technologies, Oberhaching, Germany) and μMac beads (dilution 1:20; Miltenyi biotec, Bergisch Gladbach, Germany). Lysates incubated with beads only were used as a mock-immunoprecipitation control. Pre-equilibrated μMac columns were loaded with the lysate followed by washing and preincubated with LDS sample buffer (95 °C) for 5 min. Bound material was resuspended in 45 μl of LDS buffer and proteins were separated by SDS-PAGE (4–12% Novex NuPAGE Bis-Tris gel system, Invitrogen, Carlsbad, CA) at a constant voltage of 200 V for 90 min.

2.7. Non-reducing SDS-PAGE

COS-7 cells transfected with *PEX26-V5*, *PEX26Δex5-V5* or respective plasmids carrying a C173S mutation were lysed (0.03 M Tris, 0.2 M KCl, protease inhibitors, pH 7.2) and subjected to one step of centrifugation (1000*g* for 10 min). Supernatants were mixed with lysis buffer and LDS with or without the addition of reducing agent. Proteins were separated by SDS-PAGE (see above).

2.8. BN-PAGE

COS-7 cells transfected with *PEX26*-V5 or *PEX26*Δex5-V5 were resuspended in binding buffer (50 mM NaCl, 2 mM aminocaproic acid, 20 mM sodium phosphate, 10% glycerol, 20 mM imidazole, and 1.5% Brij58 for PEX26 (all Sigma-Aldrich)) and lysed for 30 min on ice followed by 30 min centrifugation (20,000*g*). Detergent-solubilized PEX26 and PEX26Δex5 were separated by native PAGE (4–16% Novex NativePAGE Bis-Tris gel system, Invitrogen, Carlsbad, CA) at 150 V for 60 min and continued at 250 V for 90 min.

2.9. Immunoblotting

Proteins were blotted onto nitrocellulose membranes (BA-S 85; Schleicher & Schuell, Dassel, Germany) subsequent to SDS-PAGE or PVDF membrane after BN-PAGE. Blocked membranes were incubated overnight with primary antibodies: mouse anti-V5 (dilution 1:5000; Invitrogen, Carlsbad, CA) or rabbit anti-PMP70 (dilution 1:1000; Thermo Fisher Scientific, Waltham, MA) followed by 3 hour incubation with secondary antibodies: goat anti-mouse IgG-HRP or donkey anti-rabbit IgG-HRP (both in 1:10,000 dilution; Santa Cruz Biotechnology, Dallas, TX). Blots were visualized with SuperSignal West Femto Substrate (Thermo Scientific, Waltham, MA) or Clarity Max Western ECL Substrate (Bio-Rad Laboratories GmbH, Munich, Germany) and chemiluminescence was monitored with a Diana III-1-300 imaging system (Raytest, Straubenhardt, Germany) or ChemiDoc MP Imaging System (Bio-Rad Laboratories GmbH, Munich, Germany).

2.10. Acylcarnitine assay

GM17398 cells transfected with *PEX26*-V5, *PEX26*Δex5-V5, $PEX26_{dimer}$-V5, or *PEX26*aa29–174-V5 were permeabilized with digitonin (20 μg/ml) followed by incubation with lignoceric acid (C24:0; 100 μM), carnitine (0.4 mM), and CoA (0.11 mM) for 3 h [35] (all from Sigma-Aldrich, St. Louis, MO) as described before [36]. Subsequently, cellular extracts and media were subjected to solid-phase extraction and tandem mass spectrometry [37,38] to quantify C24:0- and C20:0-carnitines. Results were normalized to protein concentrations determined by BCA assay (Thermo Scientific, Waltham, MA). All samples were tested in triplicates and in two independent experiments. Normalized values for acylcarnitines of cells transfected with *PEX26* were compared to those transfected with *PEX26*Δex5, $PEX26_{dimer}$ or *PEX26*aa29–174, and a non-transfected control.

2.11. Immunostaining and confocal microscopy

Confocal microscopy was used to determine the subcellular distribution of the peroxisomal targeting sequence SKL fused to eGFP on its N-terminus [13]. GM17398 cells were co-transfected with eGPF-SKL and PEX26 constructs (*PEX26*-V5, *PEX26*Δex5-V5, $PEX26_{dimer}$-V5, *PEX26-HR1HR2*-V5, *PEX26Δex5-HR2*-V5, *PEX26-C173S*-V5, *PEX26Δex5-C173S*-V5, and *i-PEX26*-V5) or with eGFP-SKL alone. Following an expression period of 48 h at 30 or 37 °C, cells were fixed by formaldehyde 3.7% or paraformaldehyde 4%, permeabilized with 0.1% Triton X-100 (both Sigma-Aldrich, St. Louis, MO), blocked with 1% BSA, and subsequently immunolabeled by a monoclonal mouse anti-V5 antibody (dilution 1:500; Invitrogen, Carlsbad, CA) and an Alexa Fluor 555 goat anti-mouse antibody (dilution 1:200; Invitrogen, Carlsbad, CA). Thereafter, cells were analyzed by the FluoView FV1000 Confocal Microscope (Olympus, Tokio, Japan) using a multi-line argon laser (488 nm), a SDM 560 nm beam splitter, and a BA 505–525 nm barrier filter for the detection of eGFP, or a HeNe-Green laser (543 nm) and a BA 560–660 nm barrier filter for the detection of Alexa Fluor 555, and a 60 × 1.35 objective lens. Images were acquired by a UC30 CCD camera (Olympus, Tokio, Japan) and analyzed by use of the ImageJ Software (ImageJ, National Institute of Health, Bethesda, MD). The number, size and intensity of eGFP-positive peroxisomes were determined with a threshold for signal intensity (brightness) of 101–255 in 8-bit images to set the region of interest (ROI).

Localization of the PEX26 constructs (*PEX26*-V5, *PEX26Δex5*-V5, *PEX26-HR1HR2*-V5, *PEX26Δex5-HR2*-V5, *PEX26-C173S*-V5, *PEX26Δex5-C173S*-V5, and *i-PEX26*-V5) was investigated in transfected COS-7 cells after their cultivation at 37 °C for 24 h. For organelle labeling the following primary antibodies were used: mouse anti-V5 (dilution 1:500), rabbit anti-PMP70 (dilution 1:500) and rabbit anti-calnexin (dilution 1:100) in combination with the following secondary antibodies: donkey anti-mouse Alexa Fluor 488 and goat anti-rabbit Alexa Fluor 546 (both in dilution 1:1000). For mitochondria labeling the MitoTracker in 200 nmol working concentration was used. All antibodies and the MitoTracker were from Molecular Probes (Thermo Fisher Scientific, Waltham, MA) except for anti-calnexin (Enzo Life Sciences, Inc., Farmingdale, NY). Nuclei were visualized with DAPI-Fluoromount-G (SouthernBiotech, Birmingham, AL). Analysis was performed using Zeiss Axiovert 200 M equipped with ApoTome for basic structured illumination. Objective: 63× Plan-Apochromat Oil DIC. UV-Lamp: HBO 100 W with Hg lamp. Filtersystems for DAPI: Beamsplitter FT395, excitation lens G365; for GFP/AF488: Beamsplitter FT500, excitation lens BP475/40; for AF546: Beamsplitter FT570, excitation lens BP545/25. The images were acquired with CCD AxioCam HRm 1.4 MP monochrome.

2.12. Computational analyses

ENDscript 2.0 [39] was applied for secondary structure analysis. Alignment was created using ESPript 3.0 [39]. Tertiary structure of PEX26 was predicted by the I-TASSER platform [40] and subsequent structural analysis was performed using the PyMol visualization software [41].

2.13. Statistical analyses

Statistical significance was assessed by unpaired *t*-test or one-way ANOVA with Dunnett's or Bonferroni's post-tests for multiple comparisons. Standard error of mean (s. e. m.) and degrees of freedom (*df*) are given. Analyses were performed using the GraphPad Prism 5 Software, GraphPad Software Inc., La Jolla, CA.

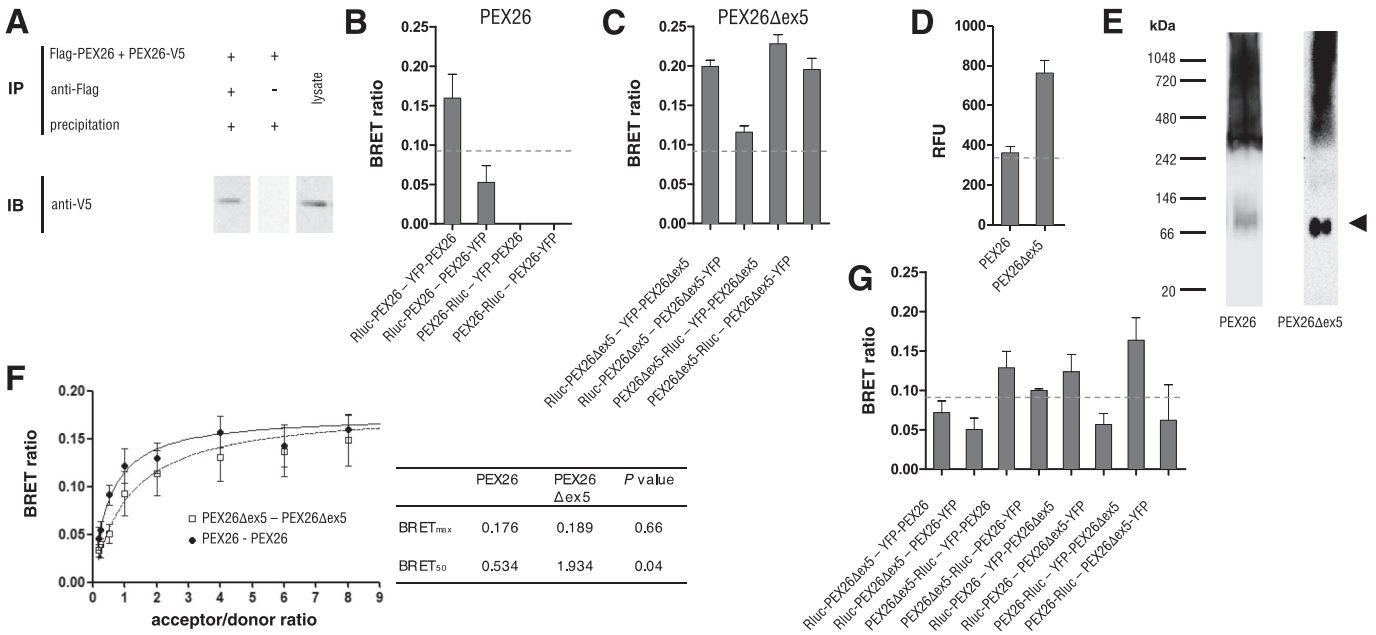

	PEX26	PEX26 Δex5	*P* value
$BRET_{max}$	0.176	0.189	0.66
$BRET_{50}$	0.534	1.934	0.04

Fig. 1. Homooligomerization of PEX26 and its splice variant PEX26Δex5. (A) Homomeric interaction of full-length PEX26 analyzed by co-immunoprecipitation. Lane 1 shows the co-immunoprecipitation experiment (IP) using an anti-Flag antibody. Immunoblotting (IB) demonstrated that PEX26-V5 co-precipitates with Flag-PEX26. Lane 2 shows the mock-immunoprecipitation control that was incubated with μMac beads but not with anti-Flag antibody. In lane 3, the cell lysate as input was analyzed. The complete blot is depicted in Supplementary Fig. 3. (B) Homomeric interaction of full-length PEX26 and (C) PEX26Δex5 analyzed by BRET. Experiments were performed in 4 possible combinations of PEX26 or PEX26Δex5 (Δex5) with N-terminal and C-terminal tags of Rluc or YFP. BRET ratios are given as means ± s. e. m. of $n = 6$ independent experiments. The dashed line depicts the method specific threshold for a protein-protein-interaction of 0.094. (D) Homomeric interaction of full-length PEX26 and PEX26Δex5 analyzed by BiFC. Relative fluorescence units (RFU) are given as means of $n = 6$ independent experiments. The dashed line depicts the mean RFU plus 3 standard deviations (344) of a negative control as threshold. (E) BN-PAGE analyzing the oligomeric state of PEX26 and PEX26Δex5. Protein constructs were expressed in COS-7 cells, after detergent-solubilization distinct bands (arrow) at the size of dimeric PEX26 and dimeric PEX26Δex5 (~66 kDa) were detected. (F) BRET saturation experiments for PEX26 or PEX26Δex5 determined the acceptor to donor ratio at half-maximal BRET ratio ($BRET_{50}$) as a measure for the relative binding affinity and the maximal BRET ratio ($BRET_{max}$) as a measure of the distance of BRET tags. Experiments were performed with N-N terminal tags and BRET ratios as a function of the acceptor to donor ratio are shown. Data are given as means ± s. e. m. of $n = 6$ experiments for PEX26 and $n = 7$ for PEX26Δex5. Differences of means were analyzed by unpaired *t*-test with $df = 11$, for $BRET_{max}$ $t = 0.4522$, for $BRET_{50}$ $t = 2.293$. (G) Heteromeric interaction of PEX26Δex5 and PEX26 analyzed by BRET. Experiments were performed in 8 possible tag combinations of PEX26 or PEX26Δex5 with N-terminal and C-terminal tags of Rluc or YFP. BRET ratios are given as means ± s. e. m. of $n = 9$ independent experiments.

3. Results

3.1. PEX26 and PEX26Δex5 oligomerize with different affinity of subunit association

Higher oligomeric structures and multi-subunit protein complexes were described for the PEX1-PEX6 complex [22,23] as well as for PEX14 [42]. The larger scaffolds of oligomers played an important role in evolution to increase protein functionality [43] and homooligomers have been shown to establish more protein interactions than non-self-interacting proteins [44]. In line with recent data on an extended function of PEX26, we hypothesized that also PEX26 forms homo-oligomers and investigated the quaternary structure of PEX26 by use of co-immunoprecipitation, binary protein interaction analysis in living cells (BRET, BiFC), and native electrophoresis (BN-PAGE). Cells were co-transfected with plasmids coding for PEX26-V5 and Flag-PEX26. We detected PEX26-V5 upon immunoprecipitation with anti-Flag, whereas no PEX26-V5 was detected in the control without anti-Flag antibody (Fig. 1A, Supplementary Fig. 3). To confirm formation of homo-oligomers, we performed BRET experiments in living cells. PEX26 constructs were co-expressed in four possible combinations, either N- or C-terminally tagged with Rluc or YFP (Fig. 1B). In this study, 4 combinations of BRET constructs for homomeric and 8 combinations of BRET constructs for heteromeric binary protein interactions were tested to take potential steric hindrances and conformational alterations into account. hRluc- and YFP-tags were fused to both N-terminus and C-terminus of each protein of interest, which resulted in 4 different BRET expression vectors per individual protein. Peroxisomal localization of PEX26 constructs carrying BRET-tags at the N- terminus was verified by fluorescence microscopy (Supplementary Fig. 4C). The highest BRET ratio (0.160) was observed for N-N-terminally tagged PEX26 indicating binary interaction of these PEX26 fusion proteins in living cells. Co-expression of Rluc-PEX26 and PEX26-YFP resulted in a BRET ratio of 0.052, which was below the threshold of 0.094 for interactions. PEX26 C-terminally fused to Rluc displayed luciferase signals below a method-specific cutoff of 13,000 relative light units (RLU), not allowing for the calculation of BRET ratios. Next, we analyzed oligomerization of the splice variant PEX26Δex5. As for the full-length protein, a protein interaction was observed for PEX26Δex5 N-terminally tagged with Rluc and YFP with a BRET ratio of 0.199 (Fig. 1C). However, the highest BRET ratio (0.228) was detected in cells co-expressing PEX26Δex5-Rluc and YFP-PEX26Δex5. Moreover, C-terminal fusion proteins displayed high luciferase signals. To confirm homooligomerization of PEX26 and PEX26Δex5 in living cells, BiFC experiments were performed (Fig. 1D). Both, the full-length protein (362 relative fluorescence units, RFU) and the splice variant (763 RFU) showed signals above the threshold for a positive protein interaction in this experiment of 344 RFU.

In order to determine the number of subunits in PEX26 oligomers, PEX26-V5 or PEX26Δex5-V5 were expressed in eukaryotic cells and cell lysates were subjected to detergent solubilization. Specific bands were detected by blue native PAGE gel electrophoresis (BN-PAGE) and subsequent immunoblotting with anti-V5 (Fig. 1E). The bands migrated with apparent masses of ≥66 kDa, which is close to the expected values for dimeric PEX26-V5 (~68 kDa) or PEX26Δex5-V5 (~60 kDa).

To analyze the affinity of subunit association in homooligomers of PEX26 or the truncated splice variant PEX26Δex5, we performed BRET saturation experiments (Fig. 1F). For binary protein-protein interactions, a sequential increase in the ratio of proteins carrying the YFP tag (acceptor) over proteins carrying the Rluc tag (donor) results in hyperbolic behavior of the BRET ratios [33]. For proteins with similar structure, the maximum BRET ratio ($BRET_{max}$) can be taken as a measure of the relative orientation of the tags to each other and hence gives information about differences in the protein conformation [45,46]. Co-expression of homomeric protein pairs with N-terminal tags resulted in $BRET_{max}$ of 0.176 for PEX26 and 0.189 for PEX26Δex5. $BRET_{max}$ values did not differ significantly ($P = 0.66$) indicating a comparable protein conformation at the N-terminal part of both protein species. A relative binding affinity index can be determined by use of the YFP to Rluc ratio (acceptor/donor ratio) at half-maximal BRET ($BRET_{50}$) to determine binding affinities of protein pairs. Hyperbolic BRET saturation indicated a specific protein-protein-interaction with a $BRET_{50}$ value of 0.534 for PEX26 and of 1.934 for PEX26Δex5. Thus, a higher relative affinity for homooligomerization of PEX26 compared to PEX26Δex5 was observed (factor 3.6, $P = 0.04$).

Last, we analyzed heteromeric subunit association of full-length PEX26 and the splice variant (Fig. 1G). BRET ratios above the threshold were detected in 4 out of 8 tag combinations, with the strongest signal observed for PEX26-Rluc and YFP-PEX26Δex5 (0.164), demonstrating potential heterooligomerization of PEX26 and PEX26Δex5 *in vivo*.

In conclusion, we showed that PEX26 and its splice variant PEX26Δex5 can form dimeric or higher-order homo- and hetero-oligomers in the environment of living cells. Both proteins oligomerized with similar structural conformation, but PEX26Δex5 engaged into the homomeric interaction with significant lower affinity than the full-length protein.

3.2. Oligomerization is mediated by heptad repeats and disulfide bonding

To identify the domains that promote subunit association, truncated fragments of PEX26 (aa1–251, aa1–269, aa29–174, aa175–251, aa175–305, aa270–305) were constructed based on known functional and structural domains [17,18,20]. We performed BRET experiments with fragments and full-length PEX26 in all 8 possible tag combinations for each protein pair. Interaction experiments of truncated fragments with full-length PEX26 resulted in BRET ratios above the threshold (0.094) for at least one tag-combination except for PEX26aa29–174 corresponding to the PEX6 binding domain (Fig. 2A). The PEX6 binding domain fragment did not interact with full-length PEX26 or any other fragment. All interacting BRET-pairs contained the sequences aa175–251 or aa270–305. These data pointed to two motifs involved in the homooligomerization of PEX26 within the limits of aa175–251 and aa270–305, both located outside the PEX6 binding domain (aa29–174). Interestingly, these truncation constructs also interacted with each other showing high BRET ratios. To analyze the pathophysiological relevance of PEX26 oligomerization, we analyzed known patient mutations in *PEX26* that result in truncated proteins. W99X (aa1–99), R192X (aa1–192) and M1T (aa96–305), either N- or C-terminally fused to Rluc or YFP, were co-expressed in four possible combinations and BRET ratios were determined. The N-terminally truncated protein M1T, which contained motifs 1 and 2, showed homooligomerization with a BRET ratio (0.167) comparable to the full-length protein (0.168) (Fig. 2B). Both nonsense mutations with C-terminal truncation did not oligomerize (W99X, 0.028; R192X, 0.024), however, both interacted with PEX6 (Supplementary Fig. 5). Therefore, the presence of one of the two motifs, as it is the case for the PEX26Δex5 splice variant, is sufficient for association of PEX26 subunits in homo- or heterooligomers of different protein species, whereas the presence of the TMD is not a prerequisite for oligomerization.

With regard to the membrane topology of PEX26 [18], motif 1 (aa175–251) N-terminally precedes the TMD and is supposed to be exposed to the cytosol, whereas motif 2 (aa270–305) composes the C-terminus of PEX26 that faces the matrix side of the peroxisome (Fig. 2A). Based on the similar interaction pattern of both motifs with full-length PEX26 and all other truncation constructs, we hypothesized a sequence similarity in these two regions. Alignment of motif 1 and motif 2 (ESPript, [47]) revealed two regions (aa227–251 and aa278–301) with seven identical amino acids and twelve amino acids with similar biochemical properties (Fig. 3A). Prediction of the secondary structure (ENDscript 2.0, [39]) yielded α-helices for both regions. We further analyzed these helices for motifs that are known to be involved in protein-protein-interactions and can give rise to oligomeric structures. In both α-helices, LxxLxxxL/I sequences (aa232–239, aa283–290) were identified constituting heptad repeats of seven amino acids [48,49] with leucine residues at first (a) and fourth (d) position followed by either a leucine or an isoleucine. Structural alignment by molecular visualization [41] of the predicted tertiary structure of PEX26 (Fig. 6A) based on I-TASSER [40] demonstrated similar position and orientation of the leucine or isoleucine residues in the cytosolic heptad repeat region (HR1, aa227–251) and the C-terminal heptad repeat region (HR2, aa278–301) (Fig. 3B). The information derived from primary and secondary structures revealed leucine zip motifs that are common structural elements driving helical oligomerization [48,50,51]. To further investigate the impact of HR1 and HR2 on PEX26 oligomerization, we created four PEX26 constructs with replacements of HR1 and HR2 leucine and isoleucine residues by alanine. The construct PEX26-HR1 consisted of a mutated heptad repeat 1 and an intact heptad repeat 2, PEX26-HR1HR2 was mutated in heptad repeats 1 and 2. For PEX26Δex5, which lacks HR1, only HR2 was mutated (PEX26Δex5-HR2). BRET saturation experiments (Fig. 3C and D) demonstrated that a loss of both heptad repeats for PEX26 and loss of HR2 for PEX26Δex5 leads to a complete loss of homooligomerization. Loss of HR1 only impaired homooligomerization with a decrease in affinity by 5-fold. The PEX26 LxxLxxxL/I heptad repeats in HR1 and HR2 are highly conserved among mammals with leucine residues at positions (a) and (d) and a conserved leucine or isoleucine, respectively, at the first position after the heptad repeat (Fig. 3E). A loss of oligomerization due to mutations of heptad repeats also impacted cellular localization for PEX26 and PEX26Δex5 (Supplementary Fig. 6). The PEX26-HR1HR2 construct displayed a mitochondrial distribution pattern instead of peroxisomal localization. For PEX26Δex5-HR2, co-localization with the ER was found without any peroxisomal punctuate fluorescence pattern. Instead, a partially cytosolic distribution was observed.

To investigate a potential contribution of disulfide bonds to PEX26 dimerization, sequences of full-length PEX26 and the splice variant were compared (Fig. 3F). In the full-length sequence, one cysteine (C263) maps to the TMD, whereas the splice variant PEX26Δex5 lacks the transmembrane domain. We did not assume disulfide bonding in this position as a critical factor for subunit association because PEX26Δex5 lacking the TMD showed oligomerization. Four cysteine residues are located in the core of the PEX6 binding domain, however, the construct aa29–174 harboring the PEX6 binding domain did not show homooligomerization. No cysteine residues were found in oligomerization domains HR1 and HR2. Cysteine residue C173, at the margin of the putative PEX6-binding domain, is close to HR1, which may contribute to PEX26 homooligomerization. The position of cysteine 173 in the predicted 3D structural model of PEX26 is depicted in Supplementary Fig. 7. To investigate the impact of C173 disulfide bonding on PEX26 dimerization, cysteine 173 was replaced by serine, which is a common approach for disulfide bond assignment in proteins [52,53]. BRET experiments were performed for PEX26, PEX26Δex5, PEX26-C173S, and PEX26Δex5-C173S. Functionality of PEX26-C173S was shown by interaction with PEX26 binding partners PEX6, PEX19, PEX13, and PEX14 in a BRET assay (Supplementary Fig. 8). We observed a peroxisomal distribution similar to the wild type for PEX26-C173S. PEX26Δex5 and PEX26Δex5-C173S both showed a pronounced overlay with the ER-marker and, to a much lesser extent, a peroxisomal

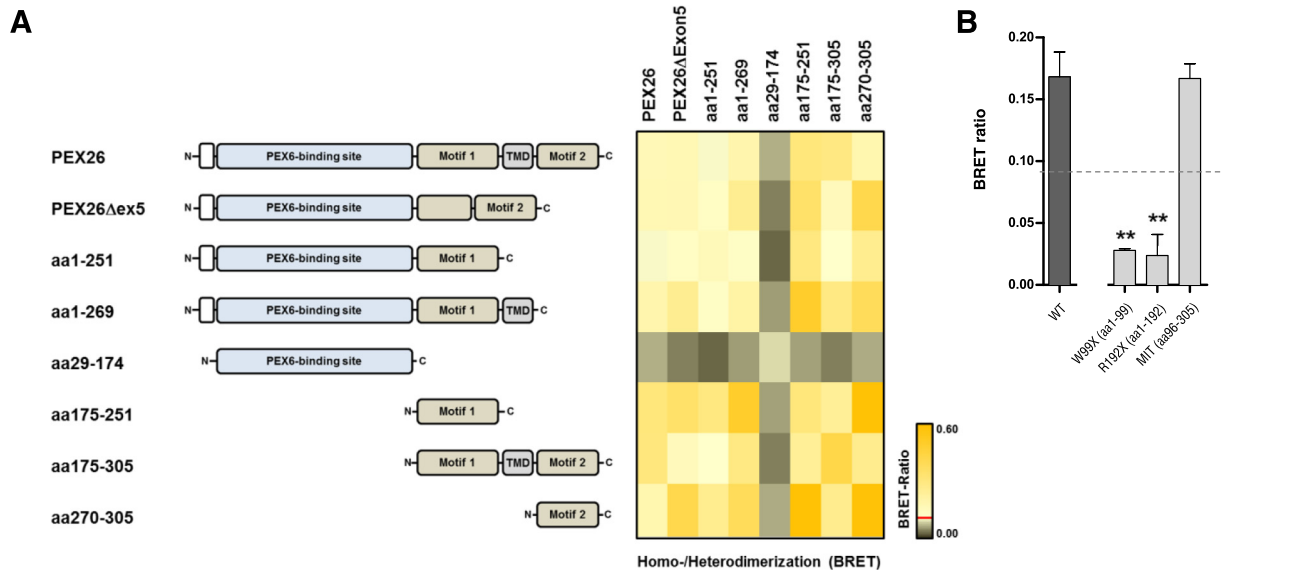

Fig. 2. Identification of PEX26 oligomerization domains. (A) Full-length PEX26 and truncations were constructed based on the PEX6 interaction domain (PEX6-binding site), the transmembrane domain (TMD) and protein sequences adjacent to the TMD (motif 1, motif 2). BRET experiments were performed in 8 possible tag combinations for binary interactions of constructs with N-terminal and C-terminal tags of Rluc or YFP and the highest BRET ratio of binary experiments is shown in the color-coded interaction matrix with high BRET ratios (orange; positive interaction) to low BRET ratios (grey; no interaction). The method specific threshold for a protein-protein-interaction of 0.094 is indicated by a red line. (B) Oligomerization of full-length PEX26 or truncated PEX26 variants resulting from known patient mutations. BRET experiments were performed in 4 possible tag combinations of constructs with N-terminal and C-terminal tags of Rluc or YFP. Highest BRET ratios were determined for N-terminal fusion proteins (Rluc-W99X, Rluc-R192X, and Rluc-M1T with YFP-PEX26) and are shown in the graph. BRET ratios are given as means ± s. e. m. of $n = 9$ for WT, $n = 2$ for W99X and R192X, and $n = 4$ for M1T as independent experiments. The dashed line depicts the method specific threshold for a protein-protein-interaction of 0.094. Differences of means were analyzed by one-way ANOVA with Dunnett's post-test (** $P = 0.0021$ as compared to the full-length protein, $F = 8.636$, $df = 16$).

punctuate fluorescence pattern (Supplementary Fig. 6A). In addition, PEX26-C173S and PEX26Δex5-C173S showed functional complementation of PEX26-deficient cells, however, the efficacy of functional complementation was impaired (Supplementary Fig. 6B, C). A serine in position aa173 resulted in a significant reduction of the BRET ratio for the full-length protein ($P < 0.05$) and the splice variant ($P < 0.01$), with values ranging below the threshold for protein-protein interaction (0.094) (Fig. 3G). Using a BiFC assay, we determined a lower fluorescence signal for homooligomerization of PEX26-C173S (234 RFU) compared to PEX26 (362 RFU). These signals were above the level of the negative control in this experiment (155 RFU) (Fig. 3H). Next, we performed PAGE analysis under reducing and non-reducing conditions (Fig. 3I, Supplementary Fig. 9). Bands with a size corresponding to dimeric PEX26 or PEX26Δex5 were observed for non-reducing conditions but not for reducing conditions. For the mutant constructs PEX26-C173S and PEX26Δex5-C173S, the signal intensity of bands with the size of dimers (60–68 kDa) was lower compared to PEX26 and PEX26Δex5, respectively. In both conditions, intensities of bands for PEX26Δex5 and PEX26Δex5-C173S were higher compared to PEX26 and PEX26-C173S. A similar load of peroxisomal fractions for all lanes was demonstrated using the peroxisomal membrane protein PMP70 as control. These data pointed to a contribution of disulfide bonding to dimerization of PEX26 and PEX26Δex5. In addition, we performed a blast analysis to investigate conservation of PEX26 cysteine residues among mammals (Fig. 3J). All 4 cysteine residues mapping to the PEX6 binding site are highly conserved among mammals. In addition, residue C263 mapping to the transmembrane domain is highly conserved. At aa position 173, an aromatic residue (Tyr or Trp), which is present in dog, mouse, and rat, is replaced by cysteine in humans. Therefore, a potential contribution of C173 to PEX26 oligomerization in humans is not conserved among mammals.

In summary, experimental data gave rise to two PEX26 homooligomerization domains (HR1, aa232–239; HR2, aa283–290) that contained heptad repeats constituting leucine zip coiled-coil motifs. These domains are positioned close to the peroxisomal membrane facing the cytosol and the peroxisomal matrix. In addition, disulfide bonding may contribute to dimerization of PEX26 and PEX26Δex5. Both, a cysteine to serine mutation of aa173 and reducing conditions induced loss of binary interactions of dimeric PEX26. In the absence of HR1 and HR2, *e. g.* in truncated PEX26 due to the natural mutation R192X or in PEX26-HR1HR2, cysteine 173 was not sufficient to promote oligomerization.

3.3. *Different interaction patterns of PEX26 and PEX26Δex5 with the translocon*

PEX26 interacts directly with PEX14, which forms the docking complex with PEX13 [20]. Recently, pre-peroxisomes, which contain distinct subsets of the import machinery protein complex, have been described in yeast [54] and human cells [9]. In order to map PEX26 interactions with the import machinery protein complex (translocon) and to investigate potential association with pre-peroxisome vesicles containing either PEX2-PEX10 or PEX13-PEX14, we analyzed binding of PEX26 and PEX26Δex5 with these peroxins by means of BRET (Fig. 4A). The interaction with PEX6 and PEX19 served as controls. We confirmed the interaction of PEX26 with PEX14 (BRET ratio 0.101). In addition, PEX26Δex5 interacted with PEX14 (BRET ratio 0.122). Furthermore, we found interaction of PEX26 with PEX13 (0.173), but not with PEX2 (0.005) and PEX10 (0.003). Interestingly, PEX26Δex5 did not interact with PEX13 (BRET ratio −0.027). By means of BiFC experiments, interactions of PEX26 and PEX26Δex5 with PEX14 and PEX19 were confirmed (Fig. 4B). However, the functional interaction of PEX26 and PEX26Δex5 with PEX6 could not be detected using this method. In addition, relative fluorescence units (RFU) for interactions with PEX2, PEX10, and PEX13 remained below an experiment-specific threshold for protein-protein-interactions.

To identify structural domains promoting the newly identified interactions of PEX26 and PEX26Δex5, we expanded these analyses using

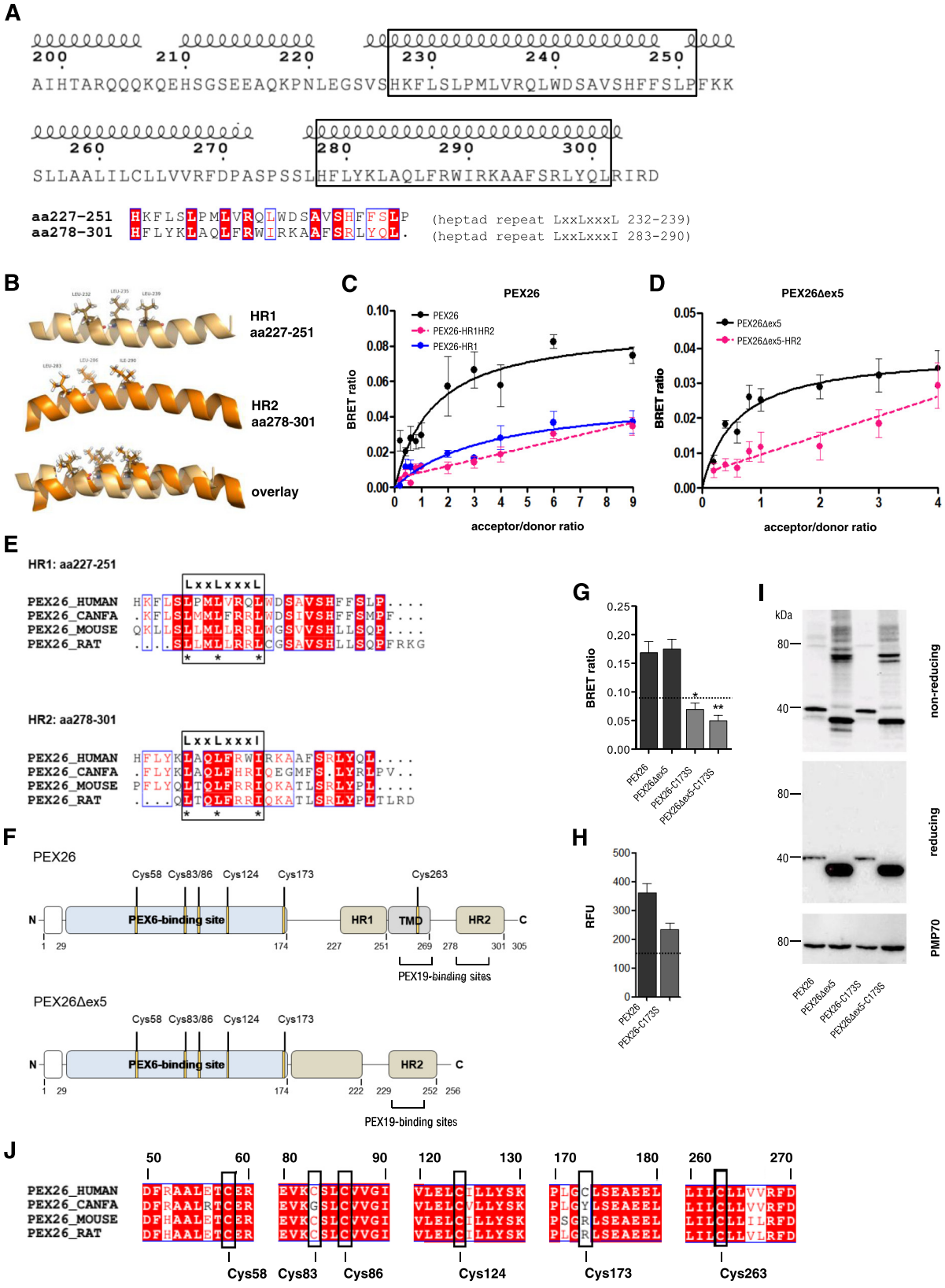

(caption on next page)

the artificial truncated fragments of PEX26 (aa1–251; aa1–269; aa29–174; aa175–251; aa175–305; aa270–305) (Fig. 4C). The N-terminal PEX6 binding domain (Fig. 3D) [54,55] was confirmed in our experimental setup as all constructs containing aa29–174 interacted with PEX6. In addition, the C-terminal PEX19 binding domain (aa276–290) was confirmed by interactions with PEX19 for constructs containing motif 2 (aa270–305), whereas the presence of the TMD (aa252–269), which was reported to be involved in binding of PEX19 *in*

Fig. 3. Characterization of PEX26 oligomerization domains. (A) Predicted secondary structures of two regions bearing potential oligomerization domains are indicated and sequences spanning 25 amino acids (black frames) were aligned to identify identical (red frame) and similar (white frame) amino acids. Heptad repeats with leucine zip motifs (LxxLxxxL/I) are shown. (B) Tertiary structure of helical heptad repeat motifs (HR1 aa227–251, HR2 aa278–301) as predicted by I-TASSER. Leucine and isoleucine residues of the heptad repeat motifs are represented as sticks and an overlay of both structural regions is shown. (C, D) Homooligomerization of PEX26 constructs with mutated HR motifs tested by BRET saturation experiments. Experiments were performed with N-N terminal tags and BRET ratios as a function of the acceptor to donor ratio are shown. Data are given as means ± s. e. m. of $n = 4$ experiments. (C) PEX26 (black; $BRET_{50}$, 1.46), mutation of HR1 (PEX26-HR1, blue; $BRET_{50}$, 7.77). Mutation of both HR motifs (PEX26-HR1HR2, pink) resulted in non-hyperbolic binding-behavior, which indicated non-interacting protein pairs. (D) PEX26Δex5 (black) only contains HR2. Mutation of HR2 (PEX26Δex5-HR2, pink) resulted in non-hyperbolic binding-behavior, which indicated non-interacting protein pairs. (E) Blast analysis of the predicted heptad repeat motifs to identify highly conserved amino acids (red frame, identical; white frame, similar; $_{*}$, heptad repeat) among mammals. (F) Domain organization of PEX26 and PEX26Δex5. The positions of cysteine residues, PEX6-binding site, transmembrane domain (TMD), heptad repeat domains adjacent to the TMD (HR1, HR2), and PEX19-binding sites are indicated. (G) BRET experiments using N-N terminal tags were performed with PEX26 and PEX26Δex5 compared to constructs harboring cysteine to serine mutations of aa173 (PEX26-C173S, PEX26Δex5-C173S). BRET ratios are given as means ± s. e. m. of $n \geq 6$ experiments and the dashed line depicts the method specific threshold for a protein-protein-interaction of 0.094. Differences of means were analyzed by unpaired *t*-test for PEX26 with $t = 4.283$, $df = 13$ (** $P < 0.05$) and for PEX26Δex5 $t = 6.604$, $df = 12$ (** $P < 0.001$). (H) BiFC experiments of PEX26 compared to a construct harboring a cysteine to serine mutation of aa173 (PEX26-C173S). Results are given as means ± s. e. m. of $n = 6$ as relative fluorescent units (RFU) of $n = 6$ experiments and the dashed line depicts the threshold for a negative control experiment of 155 RFU. (I) Denaturing PAGE under reducing/non-reducing conditions with subsequent immunoblot probing the impact of disulfide bonding on PEX26 dimerization. PEX26, PEX26Δex5, PEX26-C173S, and PEX26Δex5-C173S were expressed in COS-7 cells. Bands at the size of monomeric (35–40 kDa) and dimeric (70–80 kDa) V5-tagged proteins were detected (anti-V5). The peroxisomal membrane protein PMP70 served as control. (J) Blast analysis of cysteine residues (red frame, identical; white frame, similar; black frame, cysteine residue) in mammals. Amino acid positions are given as numbers. (For interpretation of the references to color in this figure legend, the reader is referred to the online version of this chapter.)

vitro [56], was not a prerequisite. Binding of both PEX14 and PEX13 required motif 2. However, binding of PEX13 was only observed for constructs additionally harboring the transmembrane domain. The splice variant that lacks aa223–271 including the TMD did not interact with PEX13, which is in line with our data using artificial fragments for domain mapping.

Taken together, PEX26Δex5 showed a distinct interaction pattern compared to PEX26 as it did not bind to PEX13. Hence, the PEX13 binding domain either involves the TMD or binding of PEX13 requires C-terminal anchoring of PEX26 in the peroxisomal membrane. Interaction of PEX26Δex5 with PEX14 and domain mapping showed that the TMD is not required for binding. PEX26 and PEX26Δex5 interacted completely or partially with PEX13 and PEX14, which are part of the docking complex, but not with PEX2 and PEX10, which are part of the ubiquitination machinery [3].

3.4. PEX26 dimerization impacts PEX14 interaction and peroxisomal metabolism

PEX26 may play a role in early steps of peroxisomal biogenesis and

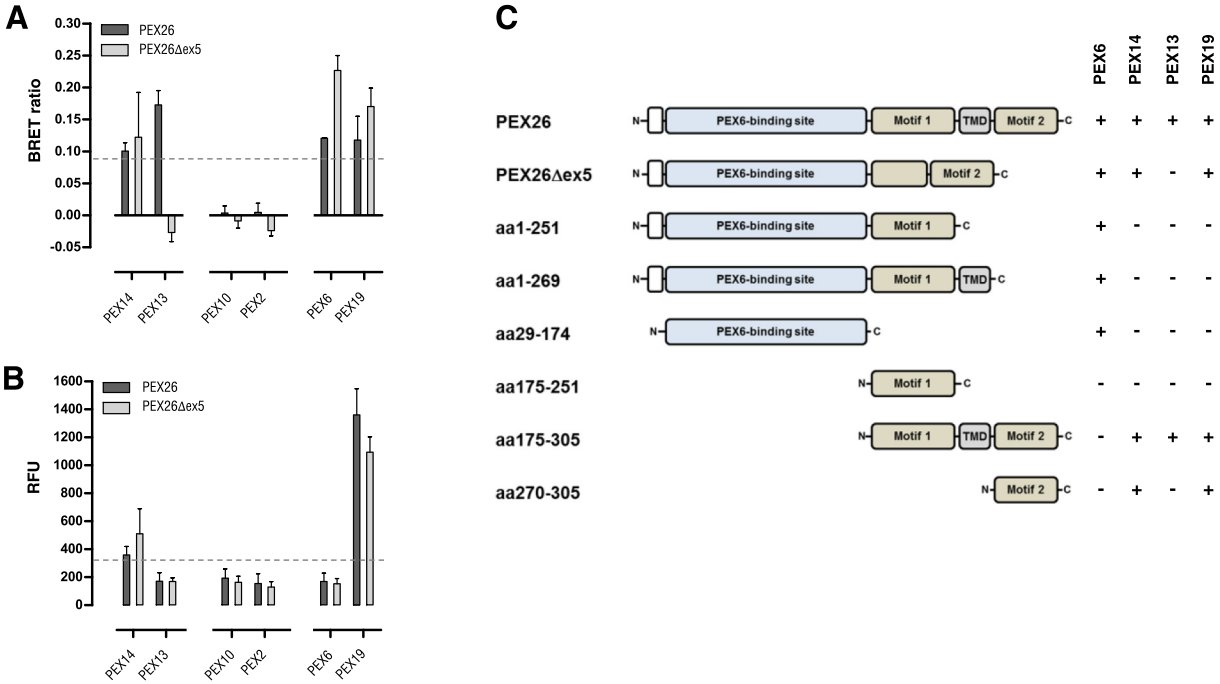

Fig. 4. Interaction patterns and domains for interaction of PEX26 isoforms with peroxins. (A) BRET experiments were performed in 8 possible tag combinations of N-terminal and C-terminal tags of Rluc or YFP to investigate interactions between PEX26 or PEX26Δex5 with PEX13-PEX14, PEX2-PEX10 as well as PEX6 and PEX19. Interaction of PEX26 with PEX6 and PEX19 served as positive controls. The respective tag-combination resulting in the highest BRET ratio is depicted (Rluc-PEX26, Rluc-PEX26Δex5 with YFP-PEX14; YFP-PEX26, YFP-PEX26Δex5 with Rluc-PEX13, Rluc-PEX6, and with Rluc-PEX19). BRET ratios are given as means ± s. e. m. of $n = 6$ for all PEX26 combinations except for PEX26 with PEX6 ($n = 2$), $n = 6$ for PEX26Δex5 with PEX6 and PEX19, and $n = 2$ for PEX26Δex5 with PEX2, PEX10, PEX13, PEX14. (B) Results of BiFC experiments are given as means ± s. e. m. of $n = 6$ as relative fluorescent units (RFU). PEX26 (dark grey) and PEX26Δex5 (light grey) were N-terminally tagged with YFP1 and tested against proteins tagged with N-terminal YFP2 (see labeling of x-axis). A positive result exceeded 344 RFU (dashed line). (C) PEX26 truncation constructs analyzed by BRET to determine interaction domains with PEX6, PEX13, PEX14, and PEX19 (+, interaction; −, no interaction).

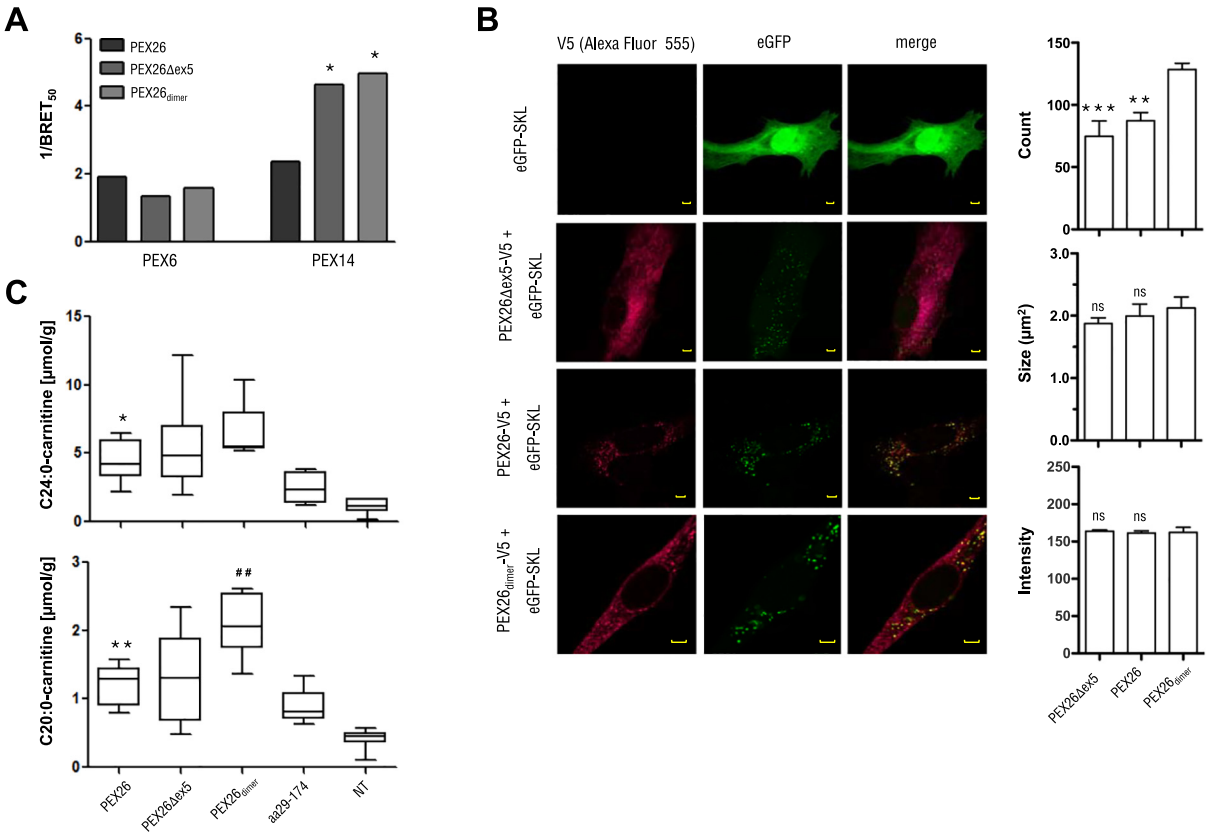

Fig. 5. Impact of dimerization and domain organization on PEX26 biological function. (A) Relative affinity of PEX26, PEX26Δex5 and $PEX26_{dimer}$ for binding to PEX6 and PEX14 was analyzed by BRET saturation experiments of N-terminally tagged constructs. Data are given as means of $1/BRET_{50}$ for $n \geq 5$ experiments. Analysis by one-way ANOVA with Bonferroni's post-test for PEX6 with $F = 3.264$ and $df = 17$, and for PEX14 with $F = 12.18$ and $df = 14$ (* $P < 0.01$). (B) Functional complementation of PEX26-deficient fibroblasts with PEX26Δex5 (PEX26Δex5-V5), full-length PEX26 (PEX26-V5), and dimeric PEX26 ($PEX26_{dimer}$-V5) with a fluorescent protein carrying a peroxisomal targeting signal (eGFP-SKL). Scale bars indicate 5 µm. Complementation was analyzed with respect to the number (count), size (size), and signal intensity (intensity) of peroxisomes showing fluorescence at 505–525 nm (eGFP). Data are given as means ± s. e. m. of $n = 11$ different transfections. Differences were analyzed by one-way ANOVA with Bonferroni's post-test with $df = 32$, and with $F = 10.86$, 0.62, and 0.06 for count, size, and intensity, respectively (** $P < 0.01$, *** $P < 0.001$). (C) Impact of PEX26 oligomeric states on peroxisomal fatty acid metabolism. PEX26-deficient fibroblasts were complemented with full-length PEX26, PEX26Δex5, dimeric PEX26 ($PEX26_{dimer}$), or monomeric construct comprising the PEX6-binding domain (aa29–174). Non-transfected cells served as a control (NT). After loading of complemented cells with C24:0 fatty acid concentrations of C24:0- and C20:0-carnitines were quantified by tandem mass spectrometry. Data are given as boxplots of $n = 2$ independent experiments with three replicates per experiment and differences were analyzed by one-way ANOVA with $df = 29$, for C24:0-carnitines $F = 7.047$ and for C20:0-carnitines $F = 13.41$, (Dunnett's post-test: * $P < 0.05$/** $P < 0.01$ as compared to NT, ## $P < 0.01$ as compared to PEX26).

the protein contributes to the peroxisomal importomer, which coordinates the import of peroxisomal matrix proteins. Thus, we intended to investigate the impact of PEX26 dimerization on PEX6 and PEX14 binding on the import of peroxisomal matrix proteins and on downstream parameters of peroxisomal metabolic function. We designed an artificial covalent PEX26 dimer ($PEX26_{dimer}$), which is composed of two C-terminally fused PEX26 peptide chains with inversed order of amino acids for the C-terminal copy of the PEX26 sequence (Supplementary Fig. 1A). We aimed to investigate the impact of an obligatory dimeric state as both oligomerization domains (motifs 1 and 2) are supposed to come to close proximity mediated by a C-terminal linker. Functionality of PEX26 with inverse order of amino acids (i-PEX26) was confirmed by western blot (Supplementary Fig. 10), homooligomerization, interaction with PEX6 and PEX19 (Supplementary Fig. 1D–F), localization to peroxisomes, and functional complementation of PEX26-deficient cells (Supplementary Fig. 6). BRET saturation experiments were performed to determine the relative binding affinities of PEX26, PEX26Δex5, or $PEX26_{dimer}$ to PEX6 and PEX14, respectively (Fig. 5A). We defined a relative binding affinity index as reciprocal values of acceptor/donor ratios at half-maximum BRET ratios ($1/BRET_{50}$) and observed comparable relative binding affinities for all three PEX26 protein species with PEX6 (PEX6-PEX26, 1.90; PEX6-PEX26Δex5, 1.35; PEX6-$PEX26_{dimer}$, 1.59; $P = 0.0665$). In contrast, relative binding affinities of PEX26Δex5 and $PEX26_{dimer}$ to PEX14 were significantly higher (4.64 and 4.98) compared to full-length PEX26 (2.37, $P = 0.0013$). Considering that (i) PEX26Δex5 is a physiological isoform, and (ii) $PEX26_{dimer}$ constitutes an artificial covalent PEX26 dimer, these results may indicate that isoform abundance and oligomeric state of PEX26 have an impact on its binding affinity to PEX14, but not to PEX6.

Next, we determined functional complementation of PEX26-deficient cells (GM17398) by PEX26, PEX26Δex5, and the $PEX26_{dimer}$. The consensus targeting sequence for peroxisomal matrix proteins type 1 (SKL) fused to eGFP at the N-terminus (eGFP-SKL) showed a homogeneous distribution pattern for eGFP-SKL in PEX26-deficient cells indicating cytosolic localization (Fig. 5B). This substantiated the known impairment in import of peroxisomal matrix proteins in patient cells. When PEX26 or PEX26Δex5 were overexpressed in PEX26-deficient cells, eGFP-SKL displayed peroxisomal localization confirming complementation of PEX26-deficient cells by both isoforms [17]. Cells overexpressing the artificial $PEX26_{dimer}$ also showed complementation with a peroxisomal localization of eGFP-SKL. PEX26Δex5 and $PEX26_{dimer}$ displayed bimodal distribution patterns indicating both cytosolic and peroxisomal localization (see also Supplementary Fig. 1C). This substantiated that the artificial PEX26 dimer is functional

and has the capacity to restore the import of peroxisomal matrix proteins of type 1. However, the efficiency of complementation with respect to the number of eGFP-positive peroxisomes per cell differed significantly. More eGFP-positive peroxisomes were found in cells transfected with the artificial dimer (129) compared to *PEX26*Δex5 (75, $P < 0.001$) and full-length *PEX26* (88, $P < 0.01$). The sizes of eGFP-positive peroxisomes and the amount of imported eGFP (fluorescence intensity of each peroxisome) were in the same range. When PEX26-deficient cells were transfected with mutant constructs showing impaired (mutation C173S) or deficient (mutations in HR1 and HR2) oligomerization, functional complementation with respect to the number of complemented cells or the cellular distribution of eGFP-SKL was impaired accordingly (Supplementary Fig. 6B, C).

A main function of peroxisomal metabolism is the β-oxidation of very-long-chain fatty acids (VLCFA) [57]. Upstream of this process, VLCFA are activated by CoA and imported into peroxisomes [58]. After chain shortening inside the peroxisomal matrix, long-chain fatty acids are converted into the corresponding carnitine esters for subsequent β-oxidation in mitochondria [59,60]. Reduced activation of VLCFA has been demonstrated in fibroblasts of patients with Zellweger syndrome [61] not allowing for the transesterification to carnitine esters [62]. To analyze the potential impact of PEX26 dimerization on parameters of peroxisomal metabolic function, we quantitated C24:0- and C20:0-carnitines in fibroblasts in order to determine VLCFA activation and subsequent conversion into carnitine esters as well as the breakdown of VLCFA. PEX26-deficient skin fibroblasts (GM17398) were functionally complemented with PEX26, PEX26Δex5, $PEX26_{dimer}$ or the truncated construct PEX26aa29–174 comprising the PEX6 binding domain only. The cells were subsequently loaded with 100 μM of the VLCFA lignoceric acid (C24:0). The median C24:0-carnitine concentration was 1.12 μmol/g for the non-transfected cells and 4.43 μmol/g for cells transfected with full-length PEX26 ($P < 0.05$) (Fig. 5C). This finding indicated functional reconstitution of VLCFA activation with subsequent transesterification to carnitine esters by overexpression of PEX26. Cells complemented with PEX26Δex5 or $PEX26_{dimer}$ did not show a statistically significant difference in C24:0-carnitine concentrations compared to PEX26 (5.45 and 6.49; $P > 0.05$). Hence, further evidence was gained for full functionality of the covalent PEX26 dimer. For cells expressing the monomeric construct PEX26aa29–174, C24:0-carnitines of 2.45 μmol/g were detected, showing higher concentrations than non-transfected cells but lower levels than cells complemented by full-length PEX26. This is consistent with a previously described rescue activity of 36% for the PEX6 binding domain (aa29–174) [17].

As chain shortening of VLCFA is predominantly performed by peroxisomal β-oxidation [58,63], the detection of acylcarnitines with a chain length of C20 is considered to be indicative of effective peroxisomal fatty acid metabolism. Concentrations of C20:0-carnitines were in general lower as compared to C24:0-carnitines, with a mean value of 0.42 μmol/g for non-transfected cells. Cells transfected with PEX26 showed a significant increase in C20:0-carnitines to 1.22 μmol/g ($P < 0.01$), indicating the restoration of VLCFA metabolism. There was no significant difference in C20:0-carnitine concentrations of cells transfected with PEX26 when compared to cells expressing PEX26Δex5 (1.32 μmol/g) or monomeric PEX26aa29–174 (0.89 μmol/g). However, C20:0-carnitine concentrations were significantly higher in cells expressing the $PEX26_{dimer}$ (2.08 μmol/g) than those expressing PEX26 ($P < 0.01$).

In summary, our data demonstrated that $PEX26_{dimer}$ is functionally active. It has the capacity to bind the peroxisomal biogenesis factor PEX6 and PEX14 as well as to rescue the import of peroxisomal matrix proteins. The oligomeric state did neither influence the binding affinity of PEX26 to PEX6 nor the efficiency of matrix protein import. However, stabilization of the dimeric state enhanced the binding affinity to PEX14, increased the number of peroxisomes in complemented PEX26-deficient cells and improved peroxisomal metabolic function, where the latter might be a consequence of the former. Furthermore, enhanced binding affinity to PEX14 was found for the physiological splice variant PEX26Δex5. These data gave evidence that domain organization and dimerization influence the biological function of PEX26.

4. Discussion

Human PEX26 is known to be the anchor for the PEX1-PEX6 complex in the peroxisomal membrane [17–19] and the peroxin is thus involved in recycling of the PEX5 cargo receptor [20]. In addition, PEX26 binds to PEX14 as part of the docking complex and mediates conformational changes of PEX14 [20]. An expanded view of PEX26 function was recently suggested in different organisms [64,65]. Deficiency of PEX26 causes PBD with considerable phenotypic variability [15]. The physiological splice variant PEX26Δex5 without transmembrane domain is functionally active and can rescue PEX26-deficient cells [17,18]. The existence of this splice variant with unknown function, the recent finding of interaction with PEX14, an involvement in PEX5 degradation in *Arabidopsis* [64], and the formation of peroxisomal subpopulations in *Neurospora* [65] led to the view of a complex role of PEX26 in matrix protein import and peroxisomal homeostasis. To gain more insight into the molecular function of this peroxin, which causes severe human disorder in the presence of mutations, we characterized conformational dynamics of PEX26 isoforms and investigated their structure-function relationships.

Homomeric interactions of proteins facilitate the constitution of larger structures with higher stability as well as expanded conformational complexity enabling proteins to engage in specific cellular functions [43,66]. Moreover, this complexity allows for the formation of additional specific bindings sites [44]. We demonstrated homo-oligomerization and characterized subunit association of PEX26 and its splice variant PEX26Δex5. Interestingly, PEX26Δex5 oligomerized with a threefold lower relative binding affinity than the full-length protein. Full-length PEX26 and PEX26Δex5 also displayed interaction with each other suggesting that PEX26 may exist *in vivo* in homo- and heteromeric states with distinct structural properties and/or functional behavior. Binary interaction of PEX26 was only detected for constructs that carried a BRET-tag or BiFC tag at the N-terminus. PEX26 is a C-tail anchored membrane protein, therefore, our observation may reflect steric hindrance induced by C-terminal fusion of tags to PEX26. This is supported by the fact that all 4 possible combinations of N- and C-terminal BRET-constructs showed binary interaction of PEX26Δex5, which lacks a transmembrane domain.

Further analysis of the quaternary structure of PEX26 and PEX26Δex5 provided evidence for the existence of dimeric states for both homooligomers. BRET interaction studies of truncated PEX26 fragments gave rise to two independent homooligomerization domains located within the boundaries of aa175–251 (motif 1) and aa270–305 (motif 2). Subsequent *in silico* predictions suggested α-helical secondary structures assigned to aa227–250 and aa278–301 and sequence alignment revealed similarity for 24 amino acids in these regions. We identified the heptad repeat regions HR1 and HR2 in the helical domains, which are both highly conserved among mammals. An overlay of the predicted tertiary structures demonstrated similar three-dimensional orientation of the leucine/isoleucine residues inside the putative oligomerization domains. These findings indicated the presence of leucine zip motifs that enable coiled-coil interactions as the basis of oligomerization [48,50,51]. Mutations of both heptad repeats led to a loss of homomeric interaction and mutation of only one heptad repeat in PEX26 significantly impaired the propensity of homomeric interaction. Based on experimental data, sequence alignments, and structural predictions, we therefore hypothesize that two independent domains (HR1 and HR2) mediate oligomerization, where leucine zip motifs may allow for coiled-coil interactions between two subunits. Motif 2 includes a basic charge motif described by Yagita and colleagues [67] that is responsible for peroxisomal targeting. A loss of basic residues leads to

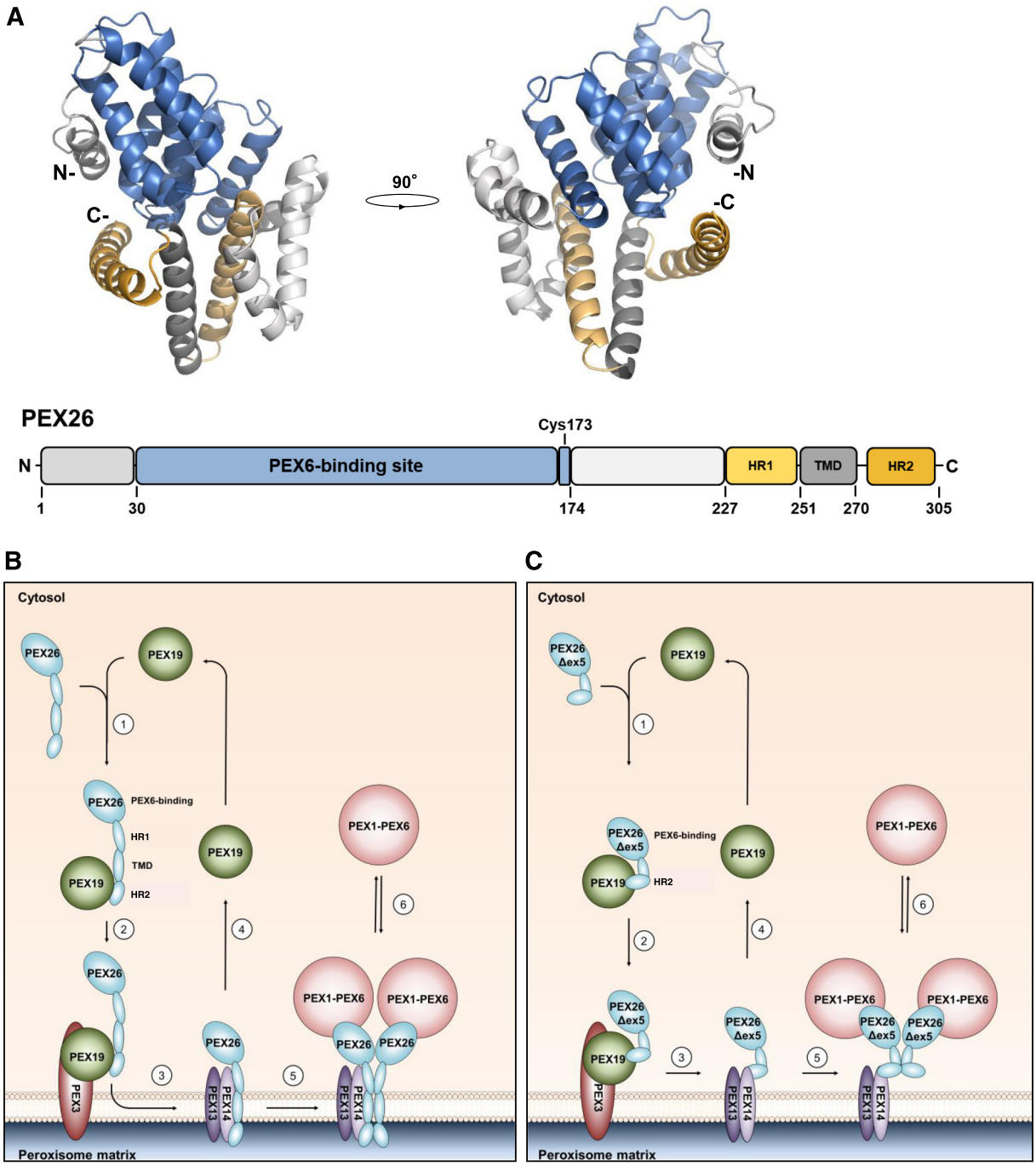

Fig. 6. Models of PEX26 tertiary structure and PEX26 association with peroxins. (A) *In silico* prediction of the tertiary structure of a PEX26 monomer by I-TASSER demonstrated in two views rotated by 90°. The N-terminus (grey), the PEX6 binding domain (blue, aa29–174), and two homooligomerization domains identified in this study (HR1, light orange, aa227–250; HR2, dark orange, aa278–301) are highlighted. The oligomerization domains are positioned close to the transmembrane domain (TMD, dark grey) and separated from the PEX6 binding domain by a linker region (light grey). (B) Model for insertion of PEX26 into the peroxisomal membrane and complex formation with peroxins. C-terminal interaction of PEX26 (HR2 and TMD) with PEX19 in the cytosol (1), PEX26 forms a ternary complex with PEX19 and PEX3 at the peroxisomal membrane (2) and is inserted into the peroxisomal membrane (3). PEX19 is released from the complex for recycling (4). (5) PEX26 dimers form multi-subunit complexes with PEX13, PEX14, and the PEX1-PEX6 AAA+ motor complex, which subsequently dislocates from the peroxisomal membrane (6). (C) Model for recruitment of PEX26Δex5 to the peroxisomal membrane and complex formation with peroxins. PEX26Δex5 interacts with its C-terminal domain (HR2) with PEX19 in the cytosol (1) and forms a ternary complex with PEX19 and PEX3 at the peroxisomal membrane (2). PEX26Δex5, which lacks the TMD, is not inserted into the peroxisome membrane. Interaction of PEX26Δex5 with PEX14 is mediated by the C-terminal domain (HR2), in contrast to PEX26 not in the peroxisomal matrix but in the cytosol (3). PEX19 is released for recycling (4). (5) PEX26Δex5 dimers interact with PEX14 and the PEX1-PEX6 AAA+ motor complex, which subsequently dislocates from the peroxisomal membrane (6). (For interpretation of the references to color in this figure legend, the reader is referred to the online version of this chapter.)

mistargeting to mitochondria. Halbach and colleagues [56] reported PEX26 mislocalization to mitochondria when the C-terminal PEX19 binding site, which overlaps with HR2, was missing. Weller et al. [17] described functional complementation of PEX26-deficient cells for an artificial fusion protein consisting of N-terminal PEX26 and a mitochondrial targeting sequence, which localized to mitochondria,

directed PEX1 and PEX6 to mitochondria and showed full complementation ability when compared to wild-type PEX26, indicating that peroxisomal localization is not an essential prerequisite for PEX26 function. We therefore conclude that motif 2, which contains HR2, is essential for dimerization as well as for peroxisomal targeting. PEX26Δex5 lacks motif 1 and the TMD but contains the C-terminus including the basic charge motif and HR2. However, the basic charge motif alone is likely to be insufficient for peroxisomal targeting because PEX26Δex5, when overexpressed in PEX26-deficient cells, mainly localizes to the ER [17], which was substantiated by overexpression of PEX26Δex5 constructs in COS-7 cells. Patient mutations W99X and R192X [14,68] are associated with Zellweger spectrum phenotypes. The resulting C-terminally truncated PEX26 proteins lack HR1, HR2, and the transmembrane domain. We showed that these proteins bind PEX6 *in vitro* but do not homooligomerize. Loss of function of these mutations may be related to loss of oligomerization, however, impaired interaction with other peroxisomal proteins and mistargeting may also contribute to pathogenicity.

With regard to a potential contribution of disulfide bonding on PEX26 homooligomerization our data pointed towards an involvement of the cysteine residue at position aa173, as all other cysteine residues map to the PEX6 binding domain, which does not homooligomerize, or to the transmembrane domain, which is not present in the oligomerization-competent splice variant PEX26Δex5. Mutagenesis of cysteine to serine at position aa173 (C173S) resulted in significant impairment of subunit association for PEX26-C173S and PEX26Δex5-C173S. The constructs showed similar cellular localization compared to wild type PEX26 and PEX26Δex5, however, functional complementation of PEX26-deficient cells was impaired. A natural mutation PEX26-R192X, which harbors C173 but no heptad repeat binding motif, showed loss of homooligomerization. Hence, residue C173 alone is not sufficient to mediate homooligomerization without heptad repeats. Non-reducing PAGE analysis further increased the evidence that disulfide bonding contributes to formation of PEX26 and PEX26 dimers and that C173 is involved in this process. We conclude that C173 contributes to oligomerization mediated by heptad repeats HR1 and HR2, putatively by formation of a disulfide bond. Surprisingly, cysteine 173 is not conserved among mammals. An aromatic amino acid at position 173, which is present in other mammals, is replaced by cysteine in humans. Acquisition of disulfide bonds in eukaryotic protein evolution can increase protein stability and induce gain of function [69]. Our data does not preclude that an additional disulfide bond in the transmembrane domain (C263) may exist and contribute to PEX26 dimerization. Hence, the observed differences in the relative binding affinity for homomeric interaction of full-length PEX26 and PEX26Δex5 may be explained by the absence of motif 1 with HR1 in the primary sequence of the splice variant. The heptad repeat is a prerequisite for homooligomerization, whereas a putative disulfide bond at C173 may play a stabilizing role.

The physiological relevance of PEX26 homooligomerization domains is emphasized by the analysis of truncated PEX26 variants resulting from known disease causing nonsense mutations (W99X, R192X, M1T) [14,16]. W99X and R192X, both lacking the homooligomerization domains motif 1 and motif 2, were not able to homooligomerize when analyzed by BRET experiments. By contrast, M1T (aa96–305), which lacks the N-terminus, homooligoomerized with similar BRET ratios as PEX26. Interestingly, the mutation M1T has been shown to be functionally active in restoring peroxisomal matrix protein import even though it showed reduced binding to PEX6 [16,19]. For M1T a dominant-positive effect has been suggested because patients carrying the M1T mutation in compound heterozygosity with L45P, a mutation without rescue activity, displayed a milder phenotype than patients homozygous for L45P [16,17].

In light of the expanded function of PEX26 in peroxisomal biogenesis and in the importomer complex, we revealed a so far unknown interaction of PEX26 with PEX13 and we confirmed the recently described interaction of PEX26 with PEX14. PEX13 and PEX14 both contribute to the docking complex. Binding domain mapping revealed a C-terminal binding domain within motif 2 for both, PEX13 and PEX14, and binding of PEX13 required the transmembrane domain. In addition, we confirmed the known PEX6 binding domain (aa29–174). In contrast to our BRET results, Tamura et al. [20] identified in co-immunoprecipitation experiments amino acid residues aa78–85 as sufficient for binding to PEX14. This difference might be due to the different nature of assays and cell lines.

PEX26 was not amenable to protein purification precluding the analysis of the protein crystal structure. Therefore, we performed *in silico* prediction of the 3D-structure (Fig. 6A). Although structural prediction still must be regarded as an auxiliary means for the understanding of protein conformation, recent advances in this technique resulted in high confidence results as shown for iterative assembly structure simulations (I-TASSER) [70]. Based on the model generated by I-TASSER, the PEX6 binding domain consists of a 7-helix bundle that is spatially separated from the C-terminal part of the protein. The predicted structure revealed that the oligomerization domains are positioned on the opposite side of the PEX6 binding domain and thus substantiated the experimental finding that oligomerization and PEX6 binding are functionally independent. The structural arrangement of the two helices carrying the putative oligomerization domains HR1 and HR2 would allow for the formation of a dimerization interface. The crystal structure of PEX15 [71], the yeast homologue of mammalian PEX26, was recently solved in complex with Pex1-Pex6. Yeast Pex15 has only 15% similarity with PEX26 in the primary sequence but shows significant functional overlap with PEX26. Pex15 binds the Pex1-Pex6 complex and serves as an anchor in the peroxisomal membrane [56,72]. The Pex15 crystal structure shows a fully helical 3D structure, where the N-terminal part is arranged in an orthogonal position to the C-terminus. This structural arrangement is in accordance with the prediction presented in our study. Here we propose a model of PEX26 domain organization that shares similarity with mitofusin, which is involved in fusion of mitochondria. Mitofusin is composed of a N-terminal cytosolic functional domain (GTP-binding domain) and 2 heptad repeat domains flanking a transmembrane region. However, organization of the mitofusin transmembrane region as 2 subsequent domains results in cytosolic position for both HR domains [73].

Next, we aimed to investigate the impact of conformation and domain organization on the function of PEX26 and the isoform PEX26Δex5. We compared binding affinities to PEX6 and PEX14 as well as peroxisomal β-oxidation and peroxisomal proliferation after complementation of PEX26-deficient cells. An obligate dimeric state of PEX26 was used as a control. PEX26, PEX26Δex5, and $PEX26_{dimer}$ interacted with PEX6 with similar binding affinity, although these proteins displayed different propensities to form dimers. Hence, we speculate that dimeric PEX26 would adopt a back-to-back position between two clusters of PEX1 and PEX6 (Fig. 6B). This is also consistent with a computational dimerization model of PEX26 created by the GalaxyWEB Server (Supplementary Fig. 11) and with the current debate questioning that Pex15 acts as a monomer [74]. In contrast, experimental data showed a higher affinity of $PEX26_{dimer}$ binding to PEX14. Thus, we suggest that one PEX26 dimer binds one PEX14-PEX13 complex. PEX13 and PEX14 constitute a docking complex where they promote binding of the PTS1 cargo receptor PEX5 and are part of precursor peroxisomal vesicles. PEX2, PEX10, and PEX12 form a RING complex responsible for PEX5 ubiquitination [8,29]. In addition, PEX2-PEX10 are part of pre-peroxisomes distinct from pre-peroxisomes containing PEX13-PEX14 [8]. With regard to a potential association of PEX26 with pre-peroxisomes, we found that PEX26 exclusively interacts with PEX13 and PEX14 but not with PEX2 and PEX10. The splice variant showed a different pattern, interacting with PEX14 but not with PEX13. Furthermore, we found that oligomeric state and domain-organization impact the binding affinity of PEX26 isoforms to PEX14. PEX26Δex5 showed a higher affinity towards PEX14. This may be due to the lack of binding motif 1 in the splice variant, which is not essential for PEX14

binding. We confirmed that the splice variant located mainly to the ER when a PEX26Δex5 construct was overexpressed without additional overexpression of PEX14 and/or PEX19 (Fig. 5B, Supplementary Fig. 4A, B). Recent findings demonstrated that peroxisomes can originate from the ER [8] or mitochondria [9] and peroxisomal membrane proteins can be inserted into the ER membrane prior to their transit to peroxisomes [75]. Considering (i) its ER origin, (ii) a distinct subcellular distribution pattern together with (iii) a different interaction pattern and (iv) different interaction properties, it is tempting to assume that PEX26Δex5 is more involved in early peroxisomal biogenesis, whereas PEX26 functions in the peroxisomal protein import machinery of mature peroxisomes. PEX26 is integrated into the peroxisomal membrane by PEX19 and its membrane receptor PEX3 [67]. We here propose different models for recruitment to and insertion into (PEX26) or association with (PEX26Δex5) the peroxisomal membrane. A C-terminal tail-anchored position of PEX26 in the peroxisomal membrane allows for PEX13 binding, which requires the transmembrane domain, and binding to PEX14 by HR2 (Fig. 6B). In the peroxisomal membrane, PEX26 dimers form multi-subunit complexes with PEX13, PEX14, and the PEX1-PEX6 AAA+ motor complex. PEX26Δex5 lacks the transmembrane domain, which includes one of two putative PEX19 binding domains. Binding to PEX19 *in vivo* does not require the presence of the TMD, but aa276–290 located in HR2 are an essential part of the PEX19 binding domain. Our data demonstrate that the splice variant is still capable of binding to PEX19 and to PEX14, which is mediated by HR2. Based on these findings, we suggest a mechanism how dimeric PEX26Δex5 associates with peroxisomes *via* PEX14, without integration of a tail-anchor into the membrane, to form multi-subunit complexes with the PEX1-PEX6 AAA+ motor complex (Fig. 6C). This alternative peroxisomal targeting or peroxisomal association mediated by PEX14 may explain how the splice variant can join early peroxisomal vesicles (ER or cytosolic localized) enabling the suggested function in early peroxisomal biogenesis, an issue for further investigations.

To investigate the impact of oligomerization on peroxisomal matrix protein import we analyzed the efficiency of PEX26, PEX26Δex5 and $PEX26_{dimer}$ to translocate eGFP-SKL into peroxisomes of PEX26-deficient cells. Size and fluorescence intensity of single peroxisomes was similar in cells complemented by all three constructs. Interestingly, overexpression of $PEX26_{dimer}$ was associated with an increase in the number of peroxisomes in complemented cells. These results indicate that the oligomeric state of PEX26 does not influence the PEX1-PEX6 dependent process of matrix protein import but PEX26 oligomerization may be an additional factor for cellular control of peroxisome homeostasis. To further differentiate the impact of the PEX26 oligomeric state on peroxisomal metabolism, we measured very long-chain (C24:0) and long-chain (C20:0) acylcarnitines in PEX26-deficient fibroblasts loaded with lignoceric acid (C24:0). The detection of the corresponding C24:0-carnitines indicates their activation and subsequent transesterification to carnitine esters. C20:0-carnitines additionally require the breakdown of VLCFA by peroxisomal β-oxidation. Overexpression of all three constructs resulted in equally increased C24:0-carnitine concentrations, when compared to non-transfected cells, however, the artificial covalent $PEX26_{dimer}$ induced significantly higher C20:0-carnitine concentrations compared to the putatively partially dimeric state of full-length PEX26. In light of an increase in the number of peroxisomes per cell in the presence of $PEX26_{dimer}$, improved β-oxidation capacity may be a consequence of the former rather than a result of a so far unknown function of PEX26 in peroxisome metabolism.

In conclusion, characterization of the tertiary and quaternary structure of PEX26 revealed dimerization based on two domains harboring leucine-zip coiled-coil motifs and a potential contribution of cysteine residue C173 to subunit association. Two oligomerization motifs with heptad repeat regions (HR1 and HR2) were identified that are structurally distinct from the PEX6 binding domain and positioned close to the transmembrane domain facing both the cytosol and the peroxisomal matrix. HR1 is not present in the PEX26Δex5 splice variant, which also lacks the transmembrane domain, and HR2 overlaps with a basic charge motif responsible for peroxisomal targeting. We provide a model how membrane-bound PEX26 may link multi-subunit PEX1-PEX6 complexes and the docking complex (PEX13-PEX14) and suggest an alternative mechanism of peroxisomal membrane association for a PEX26 isoform. At a functional level, isoform-specific domain organization drives oligomerization and interaction patterns. Our findings may give rise to an extended function of PEX26 isoforms in different steps of peroxisomal function and homeostasis.

Funding

This work was supported by the Bavarian Genome Research Network [to A.C.M]; the LMUexcellent grant [42595-6 to A.C.M]; the German Federal Ministry of Education and Research [01EA1307 to R.E.]; and a Fritz Thyssen Stiftung scholarship [to A.S.L.].

Transparency document

The Transparency document associated with this article can be found, in online version.

Acknowledgements

We wish to thank Jutta Gärtner and Hendrik Rosewich for providing the GM17398 cell line and the eGFP-SKL plasmid. We also thank Sven Thoms, Ralf Erdmann, Wolfgang Schliebs, Hans Waterham, Ronald Wanders, and Ineke Braakman for valuable discussion and Anja Schultze, Anna Heckel-Pompey, Ilona Dahmen, Sonja Schriever and Barbara Fink for excellent technical assistance. Fluorescence imaging was supported by the UKE Microscopy Imaging Facility. This article is part of a thesis by P.G. at the University of Hamburg.

Author contribution

A.C.M. and S.W.G. designed the study, analyzed the data and wrote the manuscript. A.S.L-H. and P.G. performed protein interaction assays and contributed to data analysis and manuscript preparation. M.W. performed structural predictions and statistical evaluation. D.D.R., M.K.D. and L.B. performed complementation assays and western blots. U.A.S. contributed BRET vectors and truncation constructs. M.B., R.E. and P.P. performed metabolic assays and statistical evaluation. All authors reviewed and approved the manuscript.

Conflicts of interest

The authors declare they have no conflicting interests and no competing financial interests.

Appendix A. Supplementary data

Supplementary data to this article can be found online at https://doi.org/10.1016/j.bbamcr.2018.10.013.

References

[1] N.E. Braverman, et al., Peroxisome biogenesis disorders in the Zellweger spectrum: an overview of current diagnosis, clinical manifestations, and treatment guidelines, Mol. Genet. Metab. 117 (3) (2016) 313–321.
[2] S. Ferdinandusse, et al., The important role of biochemical and functional studies in the diagnostics of peroxisomal disorders, J. Inherit. Metab. Dis. 39 (4) (2016) 531–543.
[3] H.R. Waterham, S. Ferdinandusse, R.J. Wanders, Human disorders of peroxisome metabolism and biogenesis, Biochim. Biophys. Acta 1863 (5) (2016) 922–933.
[4] R.J. Wanders, Metabolic functions of peroxisomes in health and disease, Biochimie 98 (2014) 36–44.
[5] J.J. Smith, J.D. Aitchison, Peroxisomes take shape, Nat. Rev. Mol. Cell Biol. 14 (12) (2013) 803–817.
[6] P.B. Lazarow, Y. Fujiki, Biogenesis of peroxisomes, Annu. Rev. Cell Biol. 1 (1985)

489–530.
[7] R. Hua, P.K. Kim, Multiple paths to peroxisomes: mechanism of peroxisome maintenance in mammals, Biochim. Biophys. Acta 1863 (5) (2016) 881–891.
[8] A. van der Zand, et al., Biochemically distinct vesicles from the endoplasmic reticulum fuse to form peroxisomes, Cell 149 (2) (2012) 397–409.
[9] A. Sugiura, et al., Newly born peroxisomes are a hybrid of mitochondrial and ER-derived pre-peroxisomes, Nature 542 (7640) (2017) 251–254.
[10] R. Erdmann, Assembly, maintenance and dynamics of peroxisomes, Biochim. Biophys. Acta 1863 (5) (2016) 787–789.
[11] R.L. Farr, et al., Peroxisome biogenesis in mammalian cells: the impact of genes and environment, Biochim. Biophys. Acta 1863 (5) (2016) 1049–1060.
[12] C.E. Smith, et al., Spectrum of PEX1 and PEX6 variants in Heimler syndrome, Eur. J. Hum. Genet. 24 (11) (2016) 1565–1571.
[13] C. Krause, et al., Identification of novel mutations in PEX2, PEX6, PEX10, PEX12, and PEX13 in Zellweger spectrum patients, Hum. Mutat. 27 (11) (2006) 1157.
[14] S. Steinberg, et al., The PEX Gene Screen: molecular diagnosis of peroxisome biogenesis disorders in the Zellweger syndrome spectrum, Mol. Genet. Metab. 83 (3) (2004) 252–263.
[15] M.S. Ebberink, et al., Genetic classification and mutational spectrum of more than 600 patients with a Zellweger syndrome spectrum disorder, Hum. Mutat. 32 (1) (2011) 59–69.
[16] N. Matsumoto, et al., Mutations in novel peroxin gene PEX26 that cause peroxisome-biogenesis disorders of complementation group 8 provide a genotype-phenotype correlation, Am. J. Hum. Genet. 73 (2) (2003) 233–246.
[17] S. Weller, et al., Alternative splicing suggests extended function of PEX26 in peroxisome biogenesis, Am. J. Hum. Genet. 76 (6) (2005) 987–1007.
[18] N. Matsumoto, S. Tamura, Y. Fujiki, The pathogenic peroxin Pex26p recruits the Pex1p-Pex6p AAA ATPase complexes to peroxisomes, Nat. Cell Biol. 5 (5) (2003) 454–460.
[19] S. Furuki, et al., Mutations in the peroxin Pex26p responsible for peroxisome biogenesis disorders of complementation group 8 impair its stability, peroxisomal localization, and interaction with the Pex1p × Pex6p complex, J. Biol. Chem. 281 (3) (2006) 1317–1323.
[20] S. Tamura, et al., AAA peroxins and their recruiter Pex26p modulate the interactions of peroxins involved in peroxisomal protein import, J. Biol. Chem. 289 (35) (2014) 24336–24346.
[21] S. Tamura, et al., Dynamic and functional assembly of the AAA peroxins, Pex1p and Pex6p, and their membrane receptor Pex26p, J. Biol. Chem. 281 (38) (2006) 27693–27704.
[22] S. Ciniawsky, et al., Molecular snapshots of the Pex1/6 AAA+ complex in action, Nat. Commun. 6 (2015) 7331.
[23] D. Tan, et al., Structures of the double-ring AAA ATPase Pex1-Pex6 involved in peroxisome biogenesis, FEBS J. 283 (6) (2016) 986–992.
[24] N.B. Blok, et al., Unique double-ring structure of the peroxisomal Pex1/Pex6 ATPase complex revealed by cryo-electron microscopy, Proc. Natl. Acad. Sci. U. S. A. 112 (30) (2015) E4017–E4025.
[25] D. Schwerter, et al., Insight into receptor recognition by the Pex1p/Pex6p AAA complex of the yeast *Saccharomyces cerevisiae*, 5th Open European Peroxisome Meeting Vienna 2016, 2016.
[26] L. Emmanouilidis, et al., Structural biology of the import pathways of peroxisomal matrix proteins, Biochim. Biophys. Acta 1863 (5) (2016) 804–813.
[27] H.W. Platta, et al., The peroxisomal receptor dislocation pathway: to the exportomer and beyond, Biochimie 98 (2014) 16–28.
[28] H.W. Platta, et al., Regulation of peroxisomal matrix protein import by ubiquitination, Biochim. Biophys. Acta 1863 (5) (2016) 838–849.
[29] K.B. Law, et al., The peroxisomal AAA ATPase complex prevents pexophagy and development of peroxisome biogenesis disorders, Autophagy 13 (5) (2017) 868–884.
[30] J.S. Huston, et al., Protein engineering of single-chain Fv analogs and fusion proteins, Methods Enzymol. 203 (1991) 46–88.
[31] S.W. Gersting, A.S. Lotz-Havla, A.C. Muntau, Bioluminescence resonance energy transfer: an emerging tool for the detection of protein-protein interaction in living cells, Methods Mol. Biol. 815 (2012) 253–263.
[32] M. Bakele, et al., An interactive network of elastase, secretases, and PAR-2 protein regulates CXCR1 receptor surface expression on neutrophils, J. Biol. Chem. 289 (30) (2014) 20516–20525.
[33] J.R. James, et al., A rigorous experimental framework for detecting protein oligomerization using bioluminescence resonance energy transfer, Nat. Methods 3 (12) (2006) 1001–1006.
[34] B. Nyfeler, S.W. Michnick, H.P. Hauri, Capturing protein interactions in the secretory pathway of living cells, Proc. Natl. Acad. Sci. U. S. A. 102 (18) (2005) 6350–6355.
[35] M. Morita, et al., Baicalein 5,6,7-trimethyl ether activates peroxisomal but not mitochondrial fatty acid beta-oxidation, J. Inherit. Metab. Dis. 31 (3) (2008) 442–449.
[36] R. Ensenauer, et al., In situ assay of fatty acid beta-oxidation by metabolite profiling following permeabilization of cell membranes, J. Lipid Res. 53 (5) (2012) 1012–1020.
[37] B. Rolinski, et al., The biochemical metabolite screen in the Munich ENU Mouse Mutagenesis Project: determination of amino acids and acylcarnitines by tandem mass spectrometry, Mamm. Genome 11 (7) (2000) 547–551.
[38] P.E. Minkler, C.L. Hoppel, Quantification of free carnitine, individual short- and medium-chain acylcarnitines, and total carnitine in plasma by high-performance liquid chromatography, Anal. Biochem. 212 (2) (1993) 510–518.
[39] X. Robert, P. Gouet, Deciphering key features in protein structures with the new ENDscript server, Nucleic Acids Res. 42 (2014) W320–W324 (Web Server issue).
[40] A. Roy, A. Kucukural, Y. Zhang, I-TASSER: a unified platform for automated protein structure and function prediction, Nat. Protoc. 5 (4) (2010) 725–738.
[41] L.L.C. Schrodinger, The PyMOL Molecular Graphics System, Version 1.8, (2015).
[42] R. Itoh, Y. Fujiki, Functional domains and dynamic assembly of the peroxin Pex14p, the entry site of matrix proteins, J. Biol. Chem. 281 (15) (2006) 10196–10205.
[43] M.H. Ali, B. Imperiali, Protein oligomerization: how and why, Bioorg. Med. Chem. 13 (17) (2005) 5013–5020.
[44] I. Ispolatov, et al., Binding properties and evolution of homodimers in protein-protein interaction networks, Nucleic Acids Res. 33 (11) (2005) 3629–3635.
[45] L. Drinovec, et al., Mathematical models for quantitative assessment of bioluminescence resonance energy transfer: application to seven transmembrane receptors oligomerization, Front. Endocrinol. (Lausanne) 3 (2012) 104.
[46] N. Boute, R. Jockers, T. Issad, The use of resonance energy transfer in high-throughput screening: BRET versus FRET, Trends Pharmacol. Sci. 23 (8) (2002) 351–354.
[47] E. Gasteiger, et al., ExPASy: the proteomics server for in-depth protein knowledge and analysis, Nucleic Acids Res. 31 (13) (2003) 3784–3788.
[48] P. Burkhard, J. Stetefeld, S.V. Strelkov, Coiled coils: a highly versatile protein folding motif, Trends Cell Biol. 11 (2) (2001) 82–88.
[49] Y.L. Cao, et al., MFN1 structures reveal nucleotide-triggered dimerization critical for mitochondrial fusion, Nature 542 (7641) (2017) 372–376.
[50] A.A. McFarlane, G.L. Orriss, J. Stetefeld, The use of coiled-coil proteins in drug delivery systems, Eur. J. Pharmacol. 625 (1–3) (2009) 101–107.
[51] A. Lupas, Coiled coils: new structures and new functions, Trends Biochem. Sci. 21 (10) (1996) 375–382.
[52] L. Cosenza, E. Sweeney, J.R. Murphy, Disulfide bond assignment in human interleukin-7 by matrix-assisted laser desorption/ionization mass spectroscopy and site-directed cysteine to serine mutational analysis, J. Biol. Chem. 272 (52) (1997) 32995–33000.
[53] M.L. Chernaik, P.C. Huang, Differential effect of cysteine-to-serine substitutions in metallothionein on cadmium resistance, Proc. Natl. Acad. Sci. U. S. A. 88 (8) (1991) 3024–3028.
[54] H.F. Tabak, I. Braakman, A. van der Zand, Peroxisome formation and maintenance are dependent on the endoplasmic reticulum, Annu. Rev. Biochem. 82 (2013) 723–744.
[55] C. Nashiro, et al., Recruiting mechanism of the AAA peroxins, Pex1p and Pex6p, to Pex26p on peroxisome membrane, Traffic 12 (2011) 774–788.
[56] A. Halbach, et al., Targeting of the tail-anchored peroxisomal membrane proteins PEX26 and PEX15 occurs through C-terminal PEX19-binding sites, J. Cell Sci. 119 (Pt 12) (2006) 2508–2517.
[57] R.J. Wanders, H.R. Waterham, Biochemistry of mammalian peroxisomes revisited, Annu. Rev. Biochem. 75 (2006) 295–332.
[58] R.J. Wanders, et al., Peroxisomes, lipid metabolism and lipotoxicity, Biochim. Biophys. Acta 1801 (3) (2010) 272–280.
[59] S. Miyazawa, et al., Purification and properties of carnitine octanoyltransferase and carnitine palmitoyltransferase from rat liver, J. Biochem. 94 (2) (1983) 529–542.
[60] S.O. Farrell, et al., Properties of purified carnitine acyltransferases of mouse liver peroxisomes, J. Biol. Chem. 259 (21) (1984) 13089–13095.
[61] R.J. Wanders, et al., Peroxisomal fatty acid beta-oxidation in relation to the accumulation of very long chain fatty acids in cultured skin fibroblasts from patients with Zellweger syndrome and other peroxisomal disorders, J. Clin. Invest. 80 (6) (1987) 1778–1783.
[62] C. Rizzo, et al., Characteristic acylcarnitine profiles in inherited defects of peroxisome biogenesis: a novel tool for screening diagnosis using tandem mass spectrometry, Pediatr. Res. 53 (6) (2003) 1013–1018.
[63] E. Christensen, T.A. Hagve, B.O. Christophersen, The Zellweger syndrome: deficient chain-shortening of erucic acid (22:1 (n-9)) and adrenic acid (22:4 (n-6)) in cultured skin fibroblasts, Biochim. Biophys. Acta 959 (2) (1988) 134–142.
[64] K.L. Gonzalez, et al., Disparate peroxisome-related defects in Arabidopsis pex6 and pex26 mutants link peroxisomal retrotranslocation and oil body utilization, Plant J. 92 (2017) 110–128.
[65] F. Liu, et al., Import oligomers induce positive feedback to promote peroxisome differentiation and control organelle abundance, Dev. Cell 21 (3) (2011) 457–468.
[66] K. Hashimoto, A.R. Panchenko, Mechanisms of protein oligomerization, the critical role of insertions and deletions in maintaining different oligomeric states, Proc. Natl. Acad. Sci. U. S. A. 107 (47) (2010) 20352–20357.
[67] Y. Yagita, T. Hiromasa, Y. Fujiki, Tail-anchored PEX26 targets peroxisomes via a PEX19-dependent and TRC40-independent class I pathway, J. Cell Biol. 200 (5) (2013) 651–666.
[68] M. Al-Sayed, et al., Preimplantation diagnosis in a family affected with Zellweger syndrome, J. Inherit. Metab. Dis. 29 (2006) 138-138.
[69] J.W. Wong, S.Y. Ho, P.J. Hogg, Disulfide bond acquisition through eukaryotic protein evolution, Mol. Biol. Evol. 28 (1) (2011) 327–334.
[70] A. Bazzoli, A.G. Tettamanzi, Y. Zhang, Computational protein design and large-scale assessment by I-TASSER structure assembly simulations, J. Mol. Biol. 407 (5) (2011) 764–776.
[71] B.M. Gardner, et al., The peroxisomal AAA-ATPase Pex1/Pex6 unfolds substrates by processive threading, Nat. Commun. 9 (1) (2018) 135.
[72] J. Buentzel, et al., Conserved targeting information in mammalian and fungal peroxisomal tail-anchored proteins, Sci. Rep. 5 (2015) 17420.
[73] F. Daste, et al., The heptad repeat domain 1 of Mitofusin has membrane destabilization function in mitochondrial fusion, EMBO Rep. 19 (2018) e43637.
[74] EMBL, Peroxisome formation, function and metabolism, 2nd International Conference, 2016 (Hamburg, Germany).
[75] P.U. Mayerhofer, Targeting and insertion of peroxisomal membrane proteins: ER trafficking versus direct delivery to peroxisomes, Biochim. Biophys. Acta 1863 (5) (2016) 870–880.

1.1. Ergänzendes Material zur Originalarbeit

Supplementary data

Isoform-specific domain organization determines conformation and function of the peroxisomal biogenesis factor PEX26

Philipp Guder[1,2]♦Amelie S. Lotz-Havla[3]♦, Mathias Woidy[1,2], Dunja D. Reiß[3], Marta K. Danecka[1], Ulrich A. Schatz[4], Marc Becker[3,5], Regina Ensenauer[3,6], Philipp Pagel[7,8], Lars Büttner[3], Ania C. Muntau[2] and Søren W. Gersting[1,2]*

[1]University Children's Research@Kinder-UKE and [2]Children's Hospital, University Medical Center Hamburg-Eppendorf, 20246 Hamburg, Germany, [3]Dr. von Hauner Children's Hospital, Ludwig-Maximilians-University, 80337 Munich, Germany, [4]Department for Medical Genetics, Molecular and Clinical Pharmacology, Medical University Innsbruck, 6020 Innsbruck, Austria, [5]Labor Becker Olgemöller und Kollegen, 81671 Munich, Germany, [6]Experimental Pediatrics, Department of General Pediatrics, Neonatology and Pediatric Cardiology, University Children's Hospital, Heinrich Heine University Düsseldorf, 40225 Düsseldorf, Germany, [7]Lehrstuhl für Genomorientierte Bioinformatik, Technische Universität, 85350 Freising, Germany, [8]numares GmbH, Josef-Engert-Str. 9, 93053 Regensburg, Germany

Supplementary Figures

Legend to supplementary Figure 1. Characterization of the $PEX26_{dimer}$ construct. (**A**) Cloning of the $PEX26_{dimer}$ construct. PEX26 and a sequence coding for a synthetic PEX26 with reverse order of amino acids (i-PEX26, Sloning BioTechnology) were genetically fused with a sequence coding for a flexible amino acid linker [1] resulting in the $PEX26_{dimer}$ construct. PEX26, i-PEX26 and $PEX26_{dimer}$ are illustrated with the respective N-terminus highlighted in dark grey and the C-terminus highlighted in light grey. **(B)** Inverted PEX26 (i-PEX26) nucleotide and amino acid sequences. (**C**) Subcellular localization of $PEX26_{dimer}$ in complemented PEX26 deficient cells in merge with the peroxisomal marker eGFP-SKL. $PEX26_{dimer}$ showed an overlap with green fluorescent protein carrying a peroxisomal targeting signal (eGFP-SKL) which is located to peroxisomes. (**D)** Protein interactions of full-length PEX26 and i-PEX26 with PEX6. The interaction of PEX26 and i-PEX26 with PEX6 was analyzed by BRET saturation experiments. Hyperbolic curves of BRET ratios as a function of the acceptor to donor concentration indicated that both PEX26 and i-PEX26 showed specific interaction with PEX6. (**E**) Homooligomerization of full-length PEX26 and i-PEX26 protein and interaction with PEX19. Experiments were performed with N-terminal tags of Rluc or YFP at acceptor to donor ratios of 3 to 1. BRET ratios are given as means ± s. e. m. of $n = 3$ independent experiments. (**F**) The matrix highlights that PEX26 and i-PEX26 both homooligomerize and interact with the known PEX26 interaction partners PEX6 and PEX19, demonstrating functionality of the i-PEX26 construct derived from the inversed PEX26 sequence. Yellow square, positive interaction by BRET.

Supplementary Figure 1

A

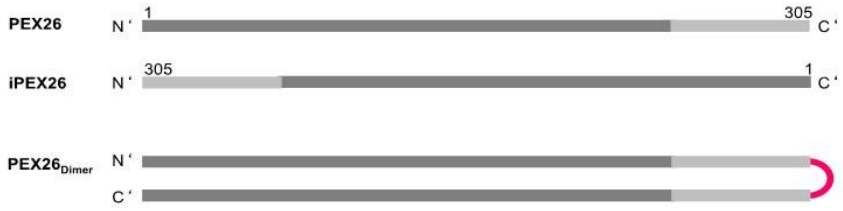

B

i-PEX26 nucleotide sequence

```
ATAGAATTAGACTGCAATATCTGAGATCCTTCGCCGCCAAGAGGATCTGGAGATTTCTGCAGGCCCTGAAGTACCTCTTTCACCTCAGC
TCCCCTTCCGCACCAGACTTCAGAGTGGTGCTGCTGTGTCTGATCCTCGCTGCTCTGCTGAGTAAAAAGTTTCCTCTGAGCTTCTTCCA
TTCCGTGGCATCCGACTGGCTCCAGAGGGTGCTGATGCCCCTCTCCCTGTTCAAGCATAGCGTGAGCGGAGAACTGAACCCTAAGCAGG
CCGAGGAGTCCGGGTCCCATGAGCAGAAACAGCAGCAGCGGGCCACCCATATTGCCCAGCTGGTGGACCTCCGGAGGGAGGAAGGCTTT
GCCGCTTCCGGCGTAGTGCTGGAGGAGGCAGAAAGTCTGTGCGGGCTGCCTCTGCTCGTGAGACAGGTGCATTTCGAGGCTCTGGCCGG
ATACGAACCCCTGAATCAGAACGCCCCAGATCAACTCTGGGCAGGCGTGGTCGACTTGGTTGCCGGACCCGAGCAGATGAAATCTTACC
TGTTAATATGTCTCGAACTGGTGAAACCTCCACTGAAAGAGCCTGTCCAATATTACCAACTCGTATGGTCACTCGTGGAGCAATGGAGA
GACATGGAAGCTCTCGCCCAGATTGGGGTTGTTTGTCTCTCTTGCAAAGTTGAGCTGTCTACCGGAGCTCCCGAAGAAGCTGTGGCCCA
TAACGCCTTGTCTCAATGGGCAAGAGAGTGCACCGAGCTGGCTGCAAGATTTGACCTGCATGTGGTCCTGTTGGACGCAGCAGAGGAAT
TGTTAGATGTTGCTCCCGCTAGAGCCCCTGTGGCTAGAGTGCCAGAGAGTAGCAGATTGCCAGGAGGATTAGGCAGGCTGCCCGCCGCT
AGCACTAGCTCCGACTCCAAGATG
```

i-PEX26 amino acid sequence

```
DRIRLQYLRSFAAKRIWRFLQALKYLFHLSSPSAPDFRVVLLCLILAALLSKKFPLSFFHSVASDWLQRVLMPLSLFKHSVSGELNPKQ
AEESGSHEQKQQQRATHIAQLVDLRREEGFAASGVVLEEAESLCGLPLLVRQVHFEALAGYEPLNQNAPDQLWAGVVDLVAGPEQMKSY
LLICLELVKPPLKEPVQYYQLVWSLVEQWRDMEALAQIGVVCLSCKVELSTGAPEEAVAHNALSQWARECTELAARFDLHVVLLDAAEE
LLDVAPARAPVARVPESSRLPGGLGRLPAASTSSDSKM
```

C

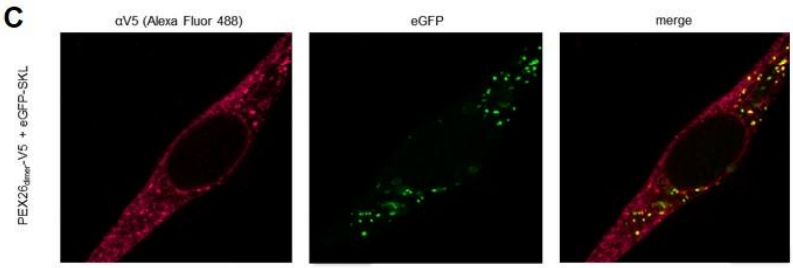

D

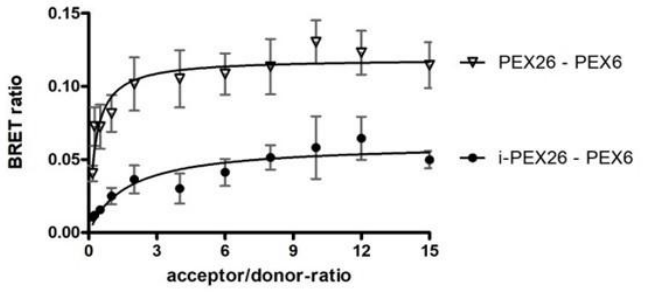

Comparison of fits	PEX26 – PEX6	i-PEX26 – PEX6
Nonlinear regression		
Probability it is correct	98.73%	84.62%
Linear regression		
Probability it is correct	1.27%	15.38%
Ratio of probabilities	77,71	5,50
Preferred model	Nonlinear regression	Nonlinear regression
Difference in AICc	-8,706	-3,410

E

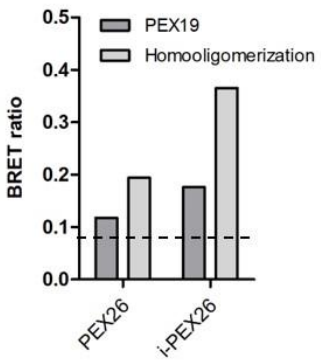

F

	PEX26	i-PEX26
PEX6		
PEX19		
Homo-oligomerization		

Legend to supplementary Figure 2. Impact of BRET tag orientation (N-terminal versus C-terminal) on luciferase signals. A total of 21,112 luciferase signals from N-terminal tagging and 21,112 luciferase signals from C-terminal tagging were analyzed. Data were derived from all BRET experiments performed in our laboratory in the past 6 years. N-terminal tagging (188,395 RLU) resulted in a 5.5 times higher mean compared to C-terminal tagging (34,386 RLU). This is in good agreement with results from BRET experiments in this study. For PEX26, highest luciferase signals resulted from N-terminal tagging.

Supplementary Figure 2

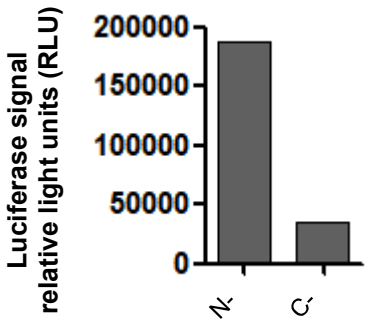

Legend to supplementary Figure 3. Homomeric interaction of full-length PEX26 analyzed by co-immunoprecipitation. (**1**) and (**2**) PEX26-V5 + Flag-PEX26; (**3**) Flag-PAH + PEX26-V5. PEX26-V5 + Flag-PEX26 was either immunoprecipitated (**IP**) with anti-Flag or anti-V5. Mock-immunoprecipitation controls were incubated with µMac beads without anti-Flag or anti-V5 antibody. Precipitated samples were immunoblotted (**IB**) with anti-V5, lysates were immunoblotted with anti-V5 or anti-Flag for control purpose. Controls for Co-immunoprecipitation experiments were performed as recommended [2].

Supplementary Figure 3

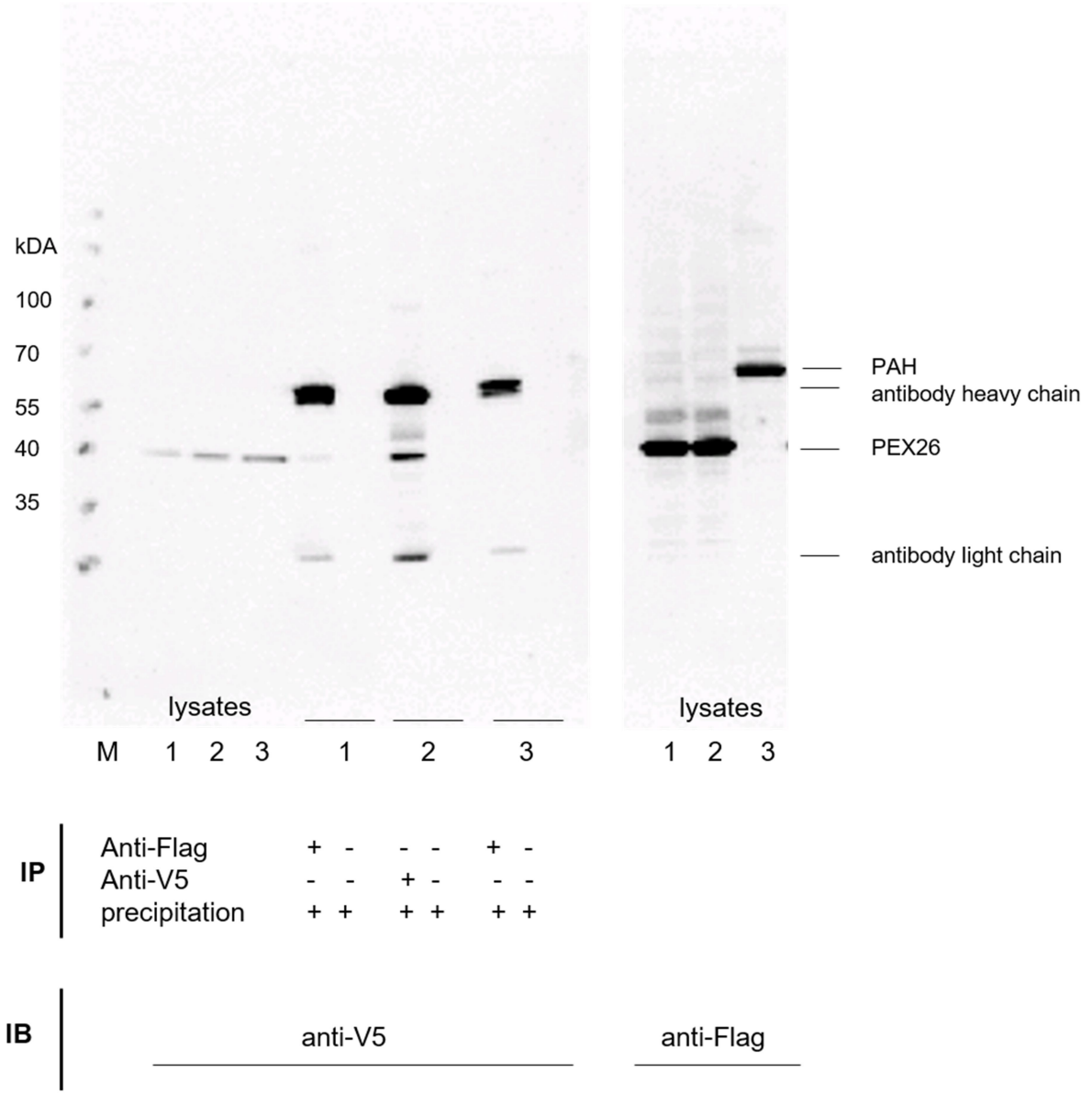

Legend to supplementary Figure 4. Immunofluorescence staining demonstrating the subcellular distribution of PEX26Δex5 carrying a V5 tag and of the BRET construct N-YFP-PEX26. (**A**) Subcellular localization of PEX26Δex5 in merge with the ER marker Calnexin. PEX26Δex5-V5 was expressed in human fibroblasts and detected by indirect immunofluorescence using monoclonal mouse anti-V5 (1:500; Invitrogen, Carlsbad, CA) and Alexa Fluor 488 chicken anti-mouse (1:200; Invitrogen, Carlsbad, CA). PEX26Δex5-V5 showed a subcellular distribution that matched to the ER protein Calnexin that was detected by polyclonal goat anti-Calnexin (1:50; Santa Cruz Biotechnologies, Dallas, TX) and Alexa Fluor 568 donkey anti-goat (1:200; Invitrogen, Carlsbad, CA). The scale bars indicate 5 µm. (**B**) Subcellular localization of PEX26Δex5 in complemented PEX26 deficient cells in merge with the peroxisomal marker eGFP-SKL. PEX26Δex5-V5 did not show a merging subcellular distribution to green fluorescent protein carrying a peroxisomal targeting signal (eGFP-SKL). The scale bars indicate 5 µm. (**C**) COS-7 cells were transfected with N-YFP-PEX26. For immunofluorescence, cells were counterstained with the peroxisomal membrane protein PMP70 and DAPI to visualize the nucleus. The overlay of the green fluorescence signal of N-YFP-PEX26 and red fluorescence of anti-PMP70 yielded a yellow/orange color. This demonstrated peroxisomal localization of the BRET-construct N-YFP-PEX26.

Supplementary Figure 4

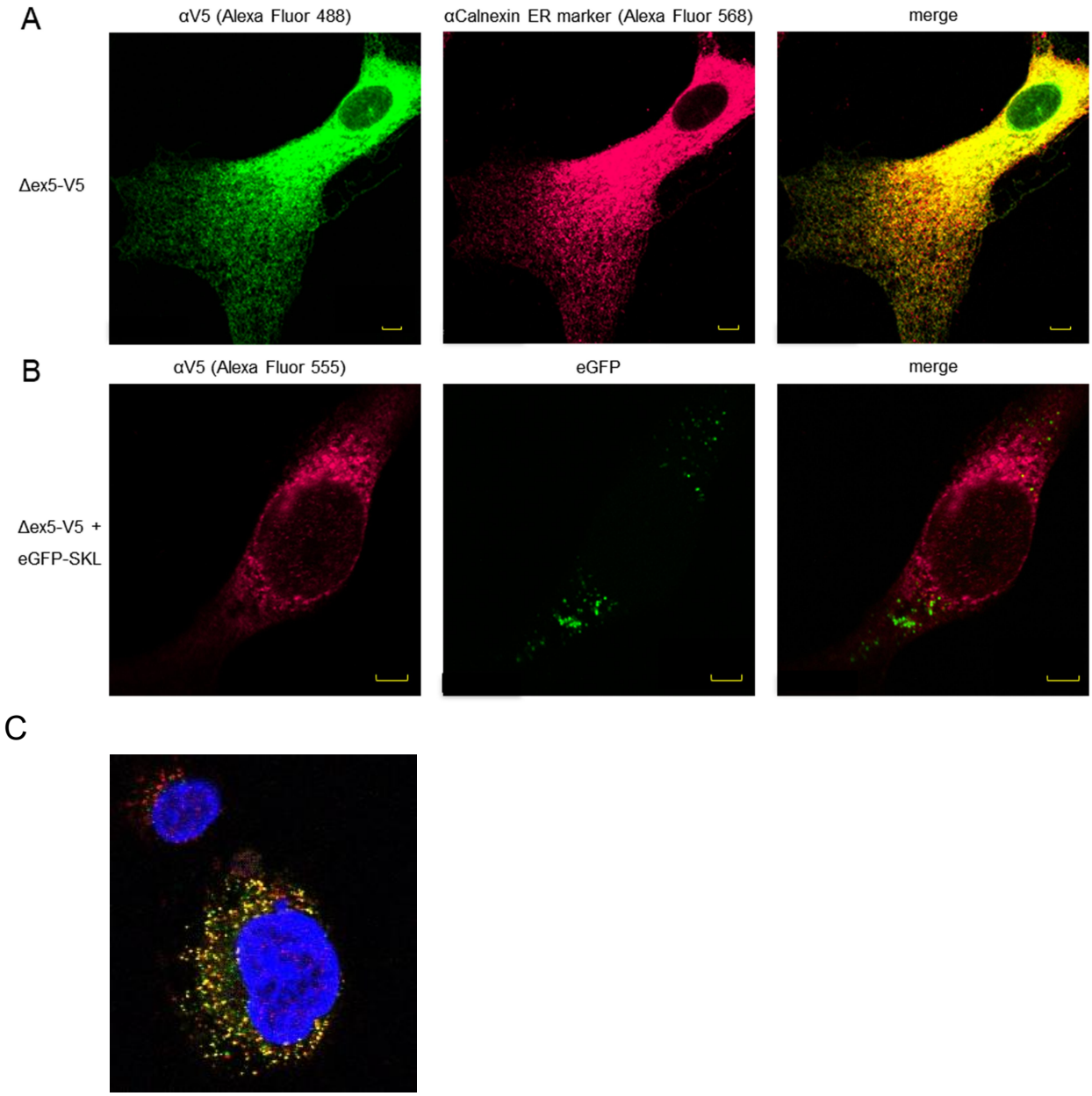

Legend to supplementary Figure 5. Protein interactions of PEX26 mutants with PEX6 to analyze functional activity. Experiments were performed with N-terminal tags of Rluc at PEX6 and with N-terminal tags of YFP at PEX26 mutations at acceptor to donor ratios of 3 to 1. Highest BRET ratios of n = 4 experiments are given for PEX26M1T (0.027), PEX26R192X (0.033), and PEX26W99X (0.053). The dashed line depicts the assay specific threshold for protein-protein-interaction of 0.026.

Supplementary Figure 5

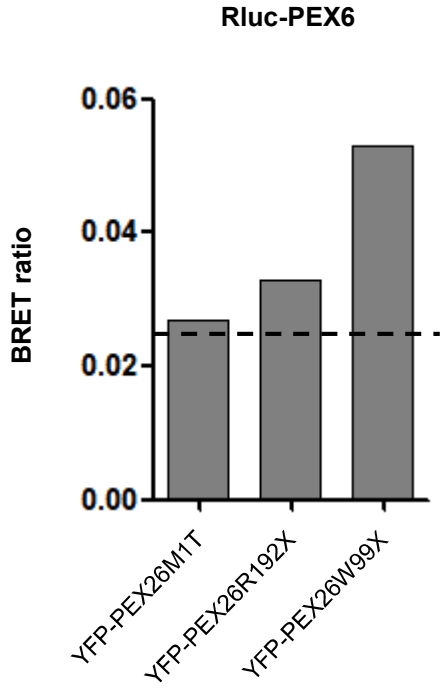

Legend to supplementary Figure 6. Localization and complementation of PEX26 constructs. (A) Localization of PEX26, PEX26-C173S, PEX26-HR1HR2, PEX26Δex5, PEX26Δex5-C173S, PEX26Δex5-HR2 and i-PEX26 in COS-7 fibroblasts. PEX26 constructs are stained against V5 (green), co-staining (red) against PMP70 (peroxisome), calnexin (ER), and with MitoTracker (mitochondria), respectively. Counterstaining with DAPI (nucleus). Co-localization appeared yellow. (B) Complementation of PEX26-deficient cells (GM17398) with co-transfection of the same constructs as used for localization and eGFP-SKL. eGFP-SKL (green) served as the marker for restored peroxisomal function/protein import by showing peroxisomal localization. eGFP-SKL single transfection resulted in a cytosolic distribution pattern as a negative control. PEX26 and PEX26Δex5 served as positive controls. DAPI (blue) as counterstaining. Co-transfection with PEX26 constructs showed peroxisomal localization. (C) 180,000 PEX26-deficient cells (GM17398) were seeded after transfection with constructs for PEX26, PEX26-C173S, and PEX26-HR1HR2. The table shows the number of functionally complemented PEX26-deficient cells after incubation for 48 hours at 30 °C or 37 °C, respectively.

Supplementary Figure 6

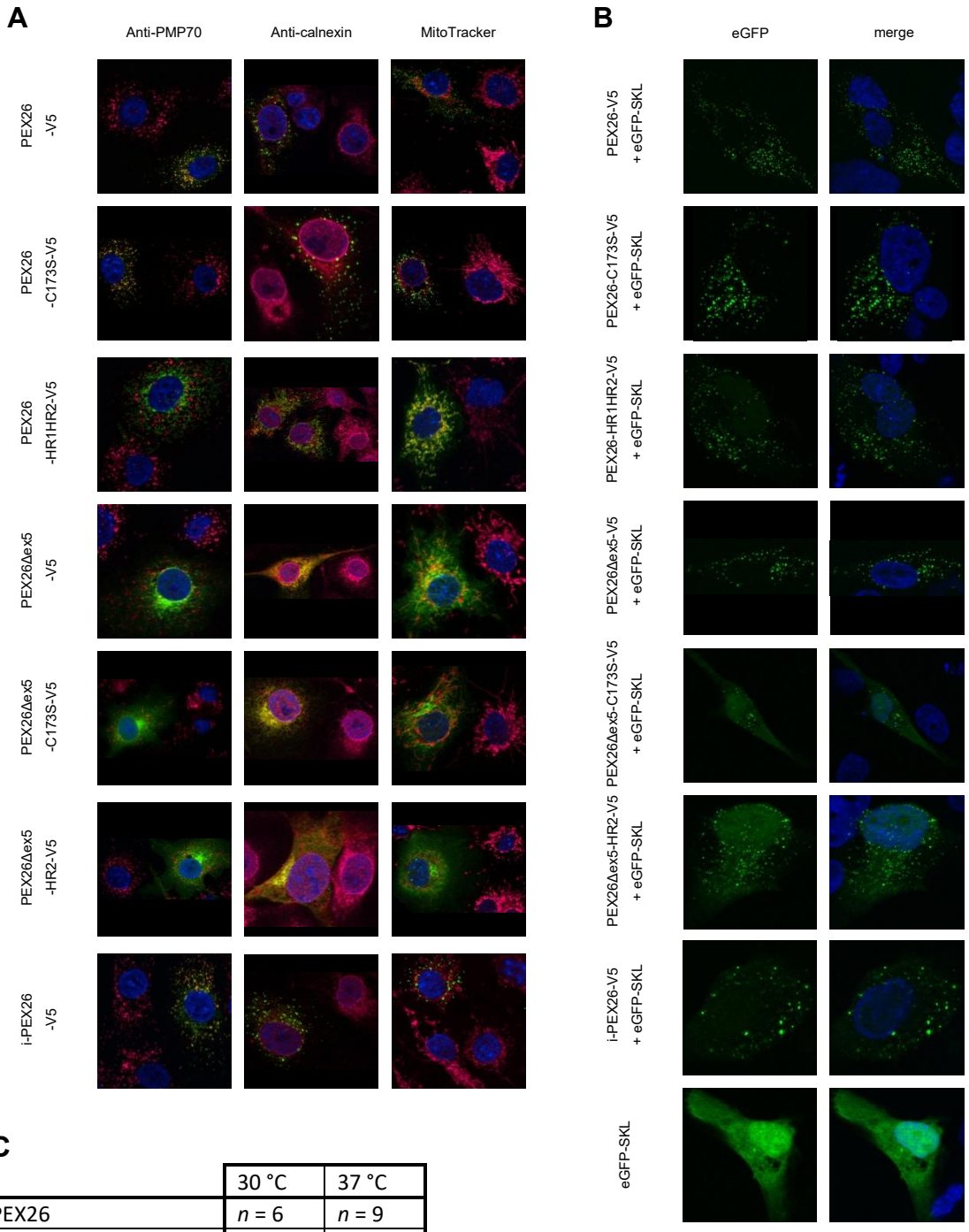

C

	30 °C	37 °C
PEX26	*n* = 6	*n* = 9
PEX26-C173S	*n* = 2	*n* = 4
PEX26-HR1HR2	*n* = 3	*n* = 8

Legend to supplementary Figure 7. Position of cysteine 173 in the predicted 3D model of PEX26, as shown in Figure 6. The cysteine residue at position 173 is depicted as stick model and backbone structure of the PEX6 binding domain (PEX6, blue), the oligomerization domains (HR1, HR2, yellow), and the transmembrane domain (TMD, grey) are color coded.

Supplementary Figure 7

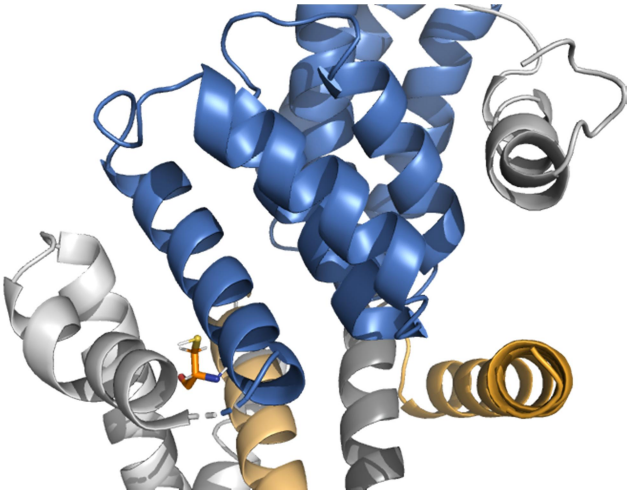

Legend to supplementary Figure 8. Protein interactions of PEX26-C173S to known interaction partners were performed to analyze functionality of mutant constructs in a BRET assay. Experiments were performed with N-terminal tags of Rluc at PEX26-C173S and with N-terminal tags of YFP at binding partners at acceptor to donor ratios of 3 to 1. BRET ratios of $n = 6$ experiments are given for interaction with PEX6, PEX19, PEX13, and PEX14. The dashed line depicts the assay specific threshold for protein-protein-interaction of 0.026.

Supplementary Figure 8

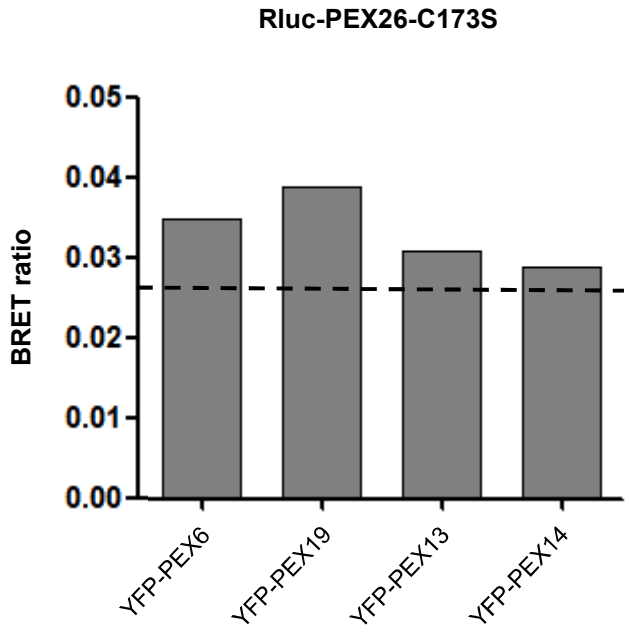

Legend to supplementary Figure 9. PEX26 Homooligomerization under reducing and non-reducing conditions to investigate the influence of disulfide bonding. Denaturing PAGE under reducing and non-reducing conditions was performed for full-length PEX26 (**1**) and PEX26Δex5 (**3**). An artificial covalent PEX26 dimer (**2**, $PEX26_{dimer}$) served as a control. COS-7 cells transfected with respective constructs were lysed by three freeze-thaw cycles in lysis buffer (20 mM HEPES, 200 mM NaCl, pH 7.0 supplemented with 1 % Triton X-100 (all Sigma-Aldrich) and protease inhibitors (Roche)), followed by two steps of centrifugation (1,000 g for 10 min; 20,000 g for 20 min; 4 °C). Supernatants (**S**) and pellets (**P**) were resuspended in lysis buffer and 4 x LDS with or without the addition of reducing agent and denatured for 5 min at 96 °C. Proteins were separated by SDS-PAGE (see material and methods). In reducing PAGE analysis monomeric (35 - 40 kDa) V5-tagged proteins were detected (anti-V5) for PEX26 and PEX26Δex5. For PEX26dimer dimeric (70 – 80 kDa) V5-tagged protein was detected. In non-reducing PAGE analysis, monomeric (35 - 40 kDa) and dimeric (70 – 80 kDa) V5-tagged proteins were detected (anti-V5) for PEX26 and PEX26Δex5. These results support the notion that disulfide bonding may contribute to PEX26 homooligomerization.

Supplementary Figure 9

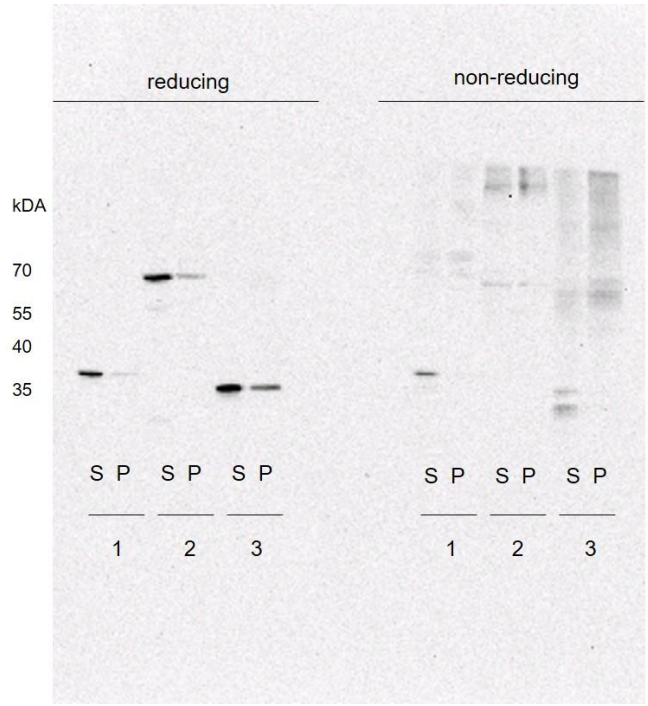

Legend to supplementary Figure 10. PEX26, i-PEX26, and PEX26-HR1 expression shown in a western blot. In PEX26-HR1, all three leucine residues in heptad repeat 1 (HR1) were replaced by alanine. 200,000 COS-7 cells were transfected with 0.2 µg DNA and cultivated over 24 hours at 37 °C. Cell lysis was performed by freeze and thaw cycles using lysis buffer with 1 % Triton X100 in 22.5 mM HEPES and protease inhibitors. A 4-12 % SDS gel was used for PAGE with a run time of 2 hours at 200 V. Blotting was performed using a PVDF membrane with a run time of 1.5 hours at 1.5 mA/cm^2. Membranes were blocked in 10 % milk with 0.05 % TBS-Tween. Primary antibodies (mouse anti V5 antibody, life technologies, Carlsbad, CA or mouse anti-GFP antibody, Clontech Living Colors A.v. Monoclonal Ab, Takara Bio USA, Inc., Mountain View, CA) were diluted 1:5,000 in 5 % milk in 0.05 % TBS-Tween and membranes were incubated with antibody dilutions at 4 °C overnight. The secondary antibody (goat anti-mouse IgG-HRP, Santa Cruz Biotechnology, Dallas, TX) was diluted 1:20,000 in 5 % milk in 0.05 % TBS-Tween and membranes were incubated with antibody dilution at 25 °C for 5 hours. Detection was performed with Clarity Max western ECL Substrate, Bio-Rad Laboratories, Inc., Hercules, CA. Images were acquired for 90 seconds with 1 picture every 10 seconds.
For i-PEX26, 2 different clones were tested, which are indicated by numbers (#2, #3). Clone #3 showed a weaker expression, so it was not used for further experiments. Phenylalaninhydroxylase (PAH) was used as a control. For N-Rluc-PEX26, N-Rluc-i-PEX26 and N-Rluc-PEX26-HR1 the expected size was 70 kDa; for N-YFP-PEX26, N-YFP-i-PEX26 and N-YFP-PEX26-HR1 60 kDa; for N-YFP-PAH 80 kDa.
i-PEX26 and PEX26-HR1 showed the same size as PEX26. CTRL (N-Rluc-PEX26 and N-YFP-PEX26) and N-YFP-PAH harbor a C-terminal stop codon and the V5 tag is not expressed. There was no signal for V5 detection but for GFP detection.

Supplementary Figure 10

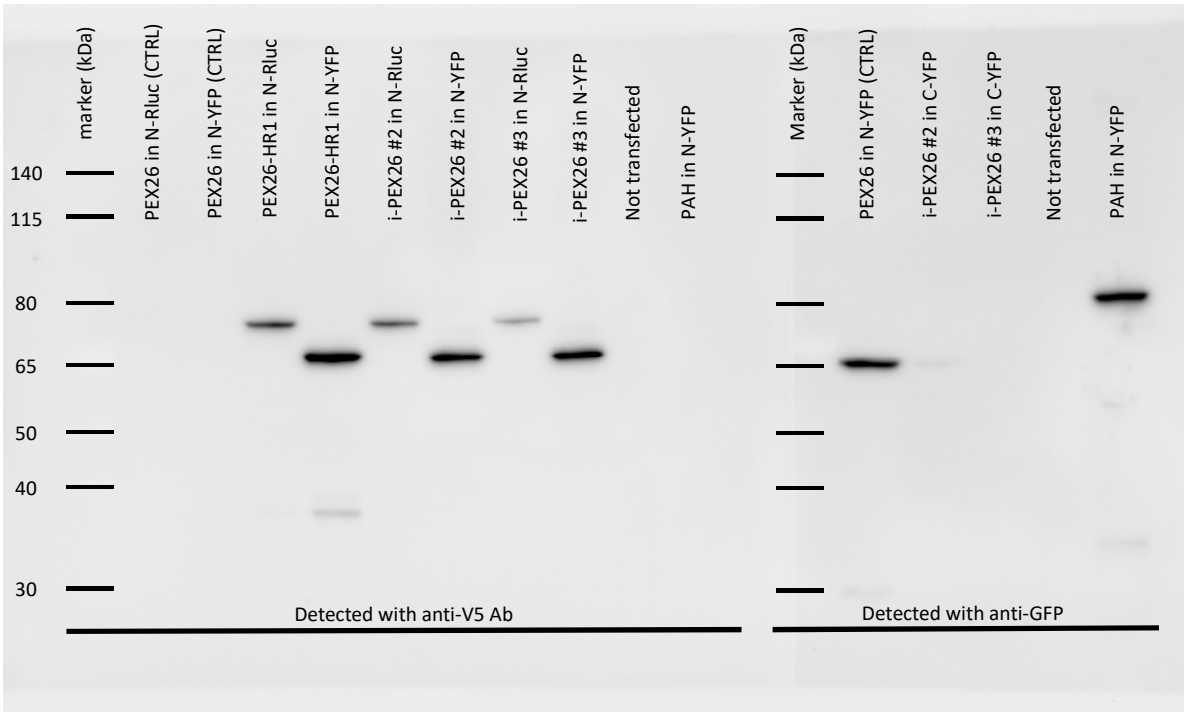

Legend to supplementary Figure 11. Putative PEX26 dimerization model predicted with GalaxyWEB Server (http://galaxy.seoklab.org/index.html) [4, 5]. A computational dimerization model shows good agreement of our hypothesized PEX26 model. The PEX6 binding domain (PEX6, purple), the oligomerization domains (HR1, HR2, yellow), and the transmembrane domain (TMD, grey) are color coded. The prediction is shown in different 90° angels.

Supplementary Figure 11

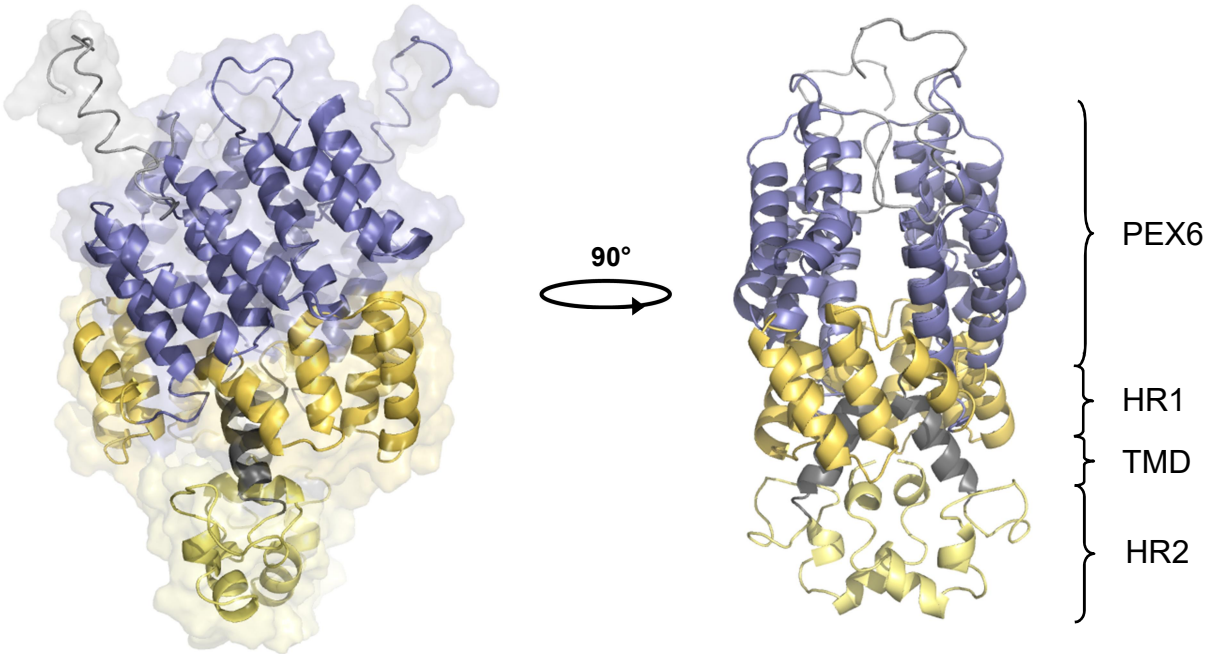

Supplementary Information.
Primer used for site-directed mutagenesis (SDM) with KAPA Hifi Polymerase, Sigma-Aldrich Chemie GmbH, Munich, Germany.

PEX26-C173S and PEX26Δex5-C173S
PEX26_C173S_Pfwd: 5'-ctgcctctgggctccttatcggaggct-3'
PEX26_C173S_Prev: 5'-agcctccgataaggagcccagaggcag-3'

PEX26-HR1
pHR1fwd: 5'-GTTCCTGTCAGCACCGATGGCGGTTCGCCAGGCTTGGGACTCTG-3'
pHR1rev: 5'-CAGAGTCCCAAGCCTGGCGAACCGCCATCGGTGCTGACAGGAAC-3'

PEX26-HR2 and PEX26Δex5-HR2
HR2 mutations were introduced by three consecutive SDM.

pHR2_1_fwd: 5'-CCTCTACAAGGCGGCCCAGCTCTTC-3'
pHR2_1_rev: 5'-GAAGAGCTGGGCCGCCTTGTAGAGG-3'

pHR2_2_fwd: 5'-GGCGGCCCAGGCCTTCCGCTGGATC-3'
pHR2_2_rev: 5'-GATCCAGCGGAAGGCCTGGGCCGCC-3'

pHR2_3_fwd: 5'-GCCTTCCGCTGGGCCCGGAAGGCTG-3'
pHR2_3_rev: 5'-CAGCCTTCCGGGCCCAGCGGAAGGC-3'

PEX26-HR1HR2
PEX26_HR1 served as a template for SDM with pHR2 primers.

PEX26 template:
HR1: LPMLVRQL = CTACCGATGTTGGTTCGCCAGCTT aa694-717 (24 aa)
HR2: LAQLFRWI = CTGGCCCAGCTCTTCCGCTGGATC aa847-870 (24 aa)

Resulting mutations:
HR1: **GCA CCG ATG GCG GTT CGC CAG GCT** = APMAVRQA
HR2: **GCG GCC CAG GCC TTC CGC TGG GCC** = AAQAFRWA

References

[1] J.S. Huston, M. Mudgett-Hunter, M.S. Tai, J. McCartney, F. Warren, E. Haber, H. Oppermann, Protein engineering of single-chain Fv analogs and fusion proteins, Methods Enzymol, 203 (1991) 46-88.
[2] R.A. Hall, Co-immunoprecipitation as a strategy to evaluate receptor-receptor or receptor-protein interactions, in: S.R.G.a.B.F. O'Dowd (Ed.) Receptor Biochemistry and Methodology, John Wiley & Sons, Place Published, 2005.

2. Darstellung der Publikation mit Literaturverzeichnis

2.1 Einleitung

Peroxisomen sind essentielle, mit einer einfachen Membran umgebene Zellorganellen in eukaryoten Organismen (1). Ihre Funktion variiert nach Organismus, Gewebe und Umwelteinfluss (2). Humane Peroxisomen beinhalten ca. 50 verschiedene Enzymaktivitäten, die hauptsächlich von Membran- und Matrixproteinen erfüllt werden (3, 4). An peroxisomalen Prozessen können jedoch auch zytosolische Proteine, beispielsweise PEX19 mit Proteinimport- und Chaperonefunktion (5) und primär mitochondriale Proteine wie der *mitochondrial fission factor*, der für mitochondriale und peroxisomale Teilungsprozesse verantwortlich ist (6), beteiligt sein. Eine wesentliche Aufgabe ist die Verarbeitung reaktiver Sauerstoffspezies (*ROS*, *reactive oxygen species*) bei der Entstehung und dem Abbau von H_2O_2 (1). Weitere wichtige Stoffwechselwege umfassen die α- und β-Oxidation von Fettsäuren (7), die Plasmalogen- (8) und Gallensäuresynthese (9), sowie die Glyoxalat-Entgiftung (10, 11).
Die peroxisomale Biogenese beinhaltet folgende Schritte: die Bildung der Membran des Organells, den Import von peroxisomalen Membran- und Matrixproteinen sowie Wachstum, Teilung und Vermehrung (11, 12). Die dazu benötigten Proteine werden Peroxine (PEX) genannt und durch *PEX* Gene codiert. In Säugetieren wurden 14 Peroxine identifiziert (13). Peroxisomale Membranproteine (PMP) werden mit Hilfe von PEX3, PEX16 und PEX19 in die peroxisomale Membran integriert (Abb. 1) (13, 14). PEX3 und PEX16 wurden auch im endoplasmatischen Retikulum (ER) nachgewiesen, was einen peroxisomalen Ursprung aus dem ER vermuten lässt (15). Somit könnten durch Sprossung aus dem ER *de novo* peroxisomale Vorläuferorganellen (*pre-peroxisomal vesicles*) entstehen, die zu Peroxisomen reifen oder mit präexistenten Peroxisomen fusionieren (16). Zusätzliche sind Sprossungen von Peroxisomen aus Mitochondrien beschrieben (12). Peroxisomale Matrixproteine sind nukleär codiert, werden an freien Ribosomen synthetisiert und anhand ihrer Signalsequenzen (PTS1, PTS2) von Shuttleproteinen (PEX5, PEX7) erkannt, die dann den Transport durch ein Translocon ins peroxisomale Lumen vermitteln (4, 11, 17). PEX5 liegt in zwei Isoformen (PEX5S und PEX5L) vor, die durch alternatives Splicing entstehen (18). PEX5S kann Proteine mit PTS1-Sequenz binden. PEX5L beinhaltet zusätzliche 37 Aminosäuren und kann mit PEX7 interagieren, welches wiederum Proteine mit PTS2-Sequenz binden kann (18).

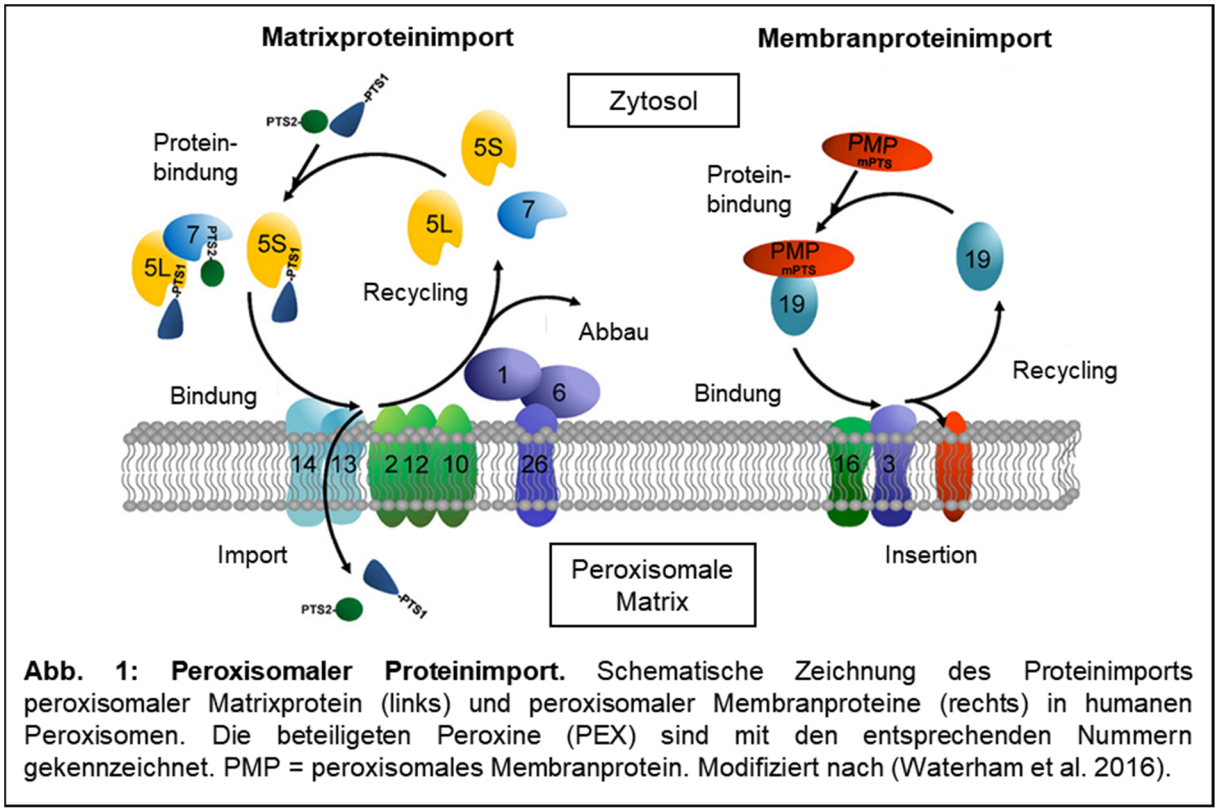

Abb. 1: Peroxisomaler Proteinimport. Schematische Zeichnung des Proteinimports peroxisomaler Matrixprotein (links) und peroxisomaler Membranproteine (rechts) in humanen Peroxisomen. Die beteiligeten Peroxine (PEX) sind mit den entsprechenden Nummern gekennzeichnet. PMP = peroxisomales Membranprotein. Modifiziert nach (Waterham et al. 2016).

Der transmembranöse Transport erfolgt in mehreren Schritten. Zuerst bindet der Matrixprotein-beladene Rezeptor PEX5 an den Bindungskomplex (*docking complex*) bestehend aus PEX13 und PEX14 (19). Das Modell der transienten Pore beschreibt die Entstehung eines Proteinimportkanals in der peroxisomalen Membran, der sich an die Größe des zu importierenden Proteins anpassen kann (20). Dazu bildet das zytosolische PEX5 zusammen mit dem PEX13-PEX14-Komplex der peroxisomalen Membran eine Pore (21). Es erfolgt der Import des Protein-Rezeptor-Komplexes mit anschließender Dissoziation des Matrixproteins vom PEX5 Rezeptor (21). Anschließend wird PEX5 durch die Ligasen des PEX2/PEX10/PEX12-Komplexes ubiquitiniert (22, 23). Die AAA+ ATPasen PEX1 und PEX6 bilden ein Heterohexamer und sind am Export von ubiquitiniertem PEX5 beteiligt (24). Der peroxisomale Membrananker PEX26 bindet an PEX6 und assoziiert so den PEX1-PEX6-Komplex an die peroxisomalen Membran (Abb. 1) (25). In der Hefe wird diese Ankerfunktion von Pex15 übernommen (26). Zur Vermehrung von Peroxisomen stehen wahrscheinlich zwei unterschiedliche Wege zur Verfügung (16). Entweder entstehen sie aus bereits existierenden Peroxisomen über Wachstum, Proteinimport und anschließende Teilung (27) oder durch *de novo*-Synthese (28). Der Teilungsprozess lässt sich wiederum in drei Schritte unterteilen: Verlängerung/Schlauchbildung (*elongation*), Einschnürung (*constriction*) und Abspaltung (*fission*) (Abb. 2) (11). Die daran beteiligten Schlüsselproteine sind auch an Teilungsprozessen des Mitochondriums beteiligt (29).

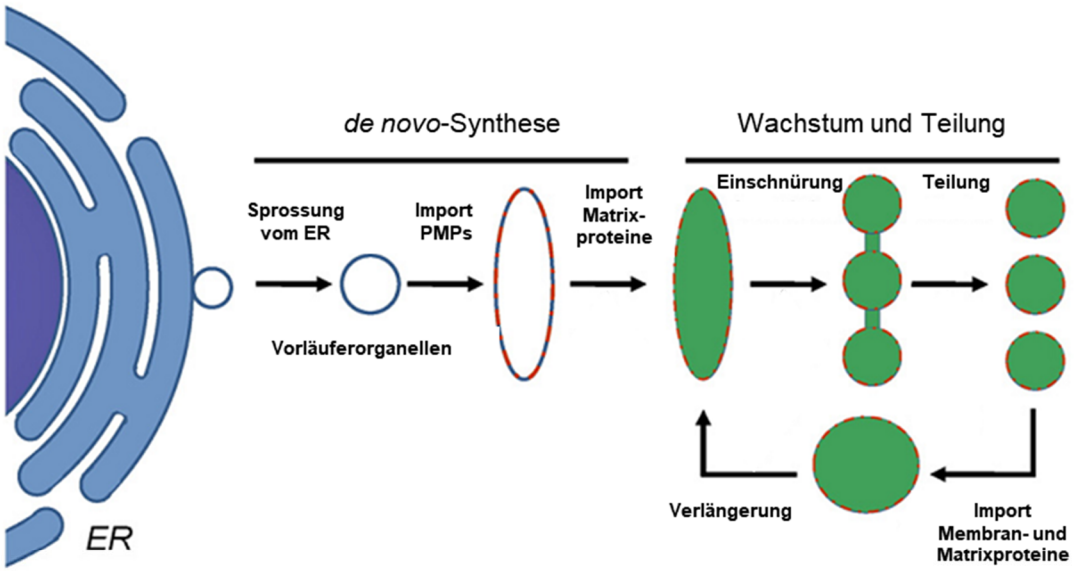

Abb. 2: Modell peroxisomaler Biogenese und Teilung. Eine *de novo*-Synthese kann aus dem endoplasmatischen Retikulum (ER) über Sprossung erfolgen. Die so entstandenen peroxisomalen Vorläuferorganellen reifen über den Import von peroxisomalen Membranproteinen (PMP) und Matrixproteinen zu stoffwechselaktiven Peroxisomen. Die Vermehrung durch Teilung umfasst die konsekutiven Schritte: Verlängerung/Schlauchbildung, Einschnürung und Abspaltung. Modifiziert nach (Waterham et al. 2016).

Mutationen in Genen, die für peroxisomale Proteine codieren, können zu Erkrankungen führen, die sich entweder als Defekte der peroxisomalen Biogenese (*peroxisomal biogenesis disorders, PBD*) oder als Enzymdefekte in peroxisomalen Stoffwechselwegen beschreiben lassen (3). Bisher sind krankheitsrelevante Veränderungen in über 30 Genen beschrieben (30). Bei PBD handelt es sich um autosomal-rezessiv vererbte Erkrankungen, die die peroxisomale Entstehung oder Funktion beeinträchtigen (11). Ca. 80 % der PBD-Fälle können dem Zellweger-Kontinuum-Spektrum zugeordnet werden (31). Das Spektrum umfasst Verläufe, die bereits in den ersten Lebensmonaten letal sind, bis hin zu milden Krankheitsausprägungen mit lebenslang asymptomatischen Betroffenen (32, 33). In abnehmender Schwere des klinischen Phänotyps werden beim Zellweger-Spektrum-Kontinuum

Zellweger-Syndrom, Neonatale Adrenoleukodystrophie, Refsum- und Heimler-Syndrom (34) unterschieden (32). Das Zellweger-Syndrom ist charakterisiert durch eine auf meist unter ein Jahr verkürzte Lebensspanne (35). Klinisch imponiert eine kraniofaciale Dysmorphie (langer Hirnschädel mit großer vorderer Fontanelle), es zeigen sich eine muskuläre Hypotonie, Hepatomegalie und Hepatopathie (Ikterus, Gerinnungsstörung), adrenocorticale Dysfunktion, Nierenzysten, Hör- und Sehstörungen, Entwicklungsstörungen des Gehirns (neuronale Migrationsdefekte mit neocorticaler Dysplasie, Verminderung der weißen Substanz, verzögerter Myelinisierung, Ventrikelerweiterung und germinolytischen Zysten) sowie eine generalisierte Entwicklungsverzögerung (35). Die Schwere des klinischen Phänotyps variiert deutlich (32). Schwere systemische Verläufe manifestieren sich frühzeitig, isolierte Symptome wie Sehprobleme oder Schallempfindungsschwerhörigkeit werden oft erst mit zunehmendem Alter als Ausdruck eines milderen klinischen Verlaufs apparent (Abb. 3) (32, 36). Traditionell erfolgt die Unterteilung der PBD in zwölf Komplementationsgruppen (*complementation groups, CG*) auf Grundlage des betroffenen, für ein PEX-Protein codierenden Gens (37).

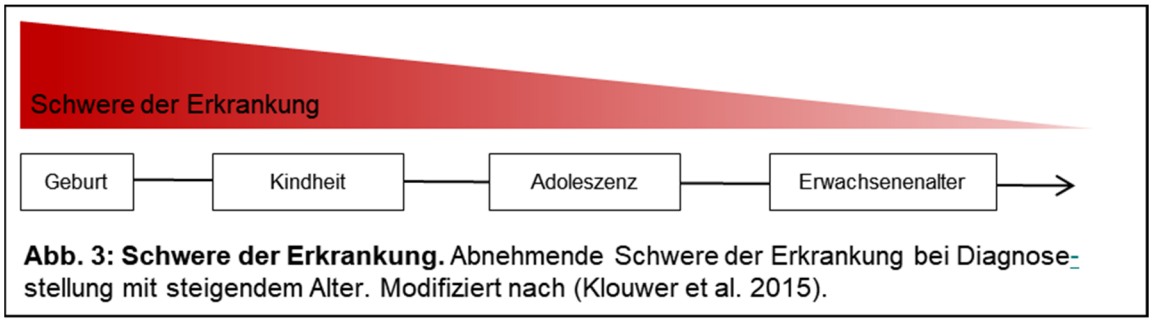

Abb. 3: Schwere der Erkrankung. Abnehmende Schwere der Erkrankung bei Diagnosestellung mit steigendem Alter. Modifiziert nach (Klouwer et al. 2015).

In der vorliegenden Arbeit wurde das humane Peroxin PEX26 strukturell und funktionell charakterisiert. Hierbei handelt es sich um ein Proteinprodukt des krankheitsverursachenden Gens *PEX26* (MIM 608666) (38), das eine wichtige, jedoch nicht vollständig verstandene Rolle im peroxisomalen Matrixproteinmport spielt (39). Strukturell wurden einzelne Domänen beschrieben (40), eine 3D-Kristallstruktur existiert jedoch nicht. Gardner und Kollegen analysierten die 3D-Struktur des PEX26-Hefe-Orthologs Pex15p (41). Mutationen in *PEX26* werden der *CG8* zugeordnet, die durch einen Defekt des peroxisomalen Matrixproteinimports gekennzeichnet ist (38, 40). Der PTS1- und PTS2-vermittelte Import von peroxisomalen Matrixproteinen ist jedoch abhängig von der genetischen Variante unterschiedlich stark beeinträchtigt (40). Für die *CG8* sind alle Formen des Zellweger-Kontinuum-Spektrums beschrieben (42).
PEX26 ist ein 34 kDa großes, peroxisomales Membranprotein. Über eine C-terminale Transmembrandomäne (TMD) erfolgt die Verankerung in der peroxisomalen Membran (*tail-anchored*) mit dem N-Terminus im Zytosol (43). Am eingehendsten ist bisher die Funktion als Membrananker des PEX1-PEX6-Komplexes beschrieben (25). Zusätzlich besteht eine Proteininterkation zu PEX14, einem Bestandteil des Bindungskomplexes und Teil der transienten Pore (19).
Weller und Kollegen haben eine physiologische Splicevariante identifiziert, in der Exon 5 nicht exprimiert wird (PEX26Δex5) und der somit die Transmembrandomäne fehlt (40). Immunfluoreszenz-untersuchungen zeigten eine Lokalisation von PEX26Δex5 sowohl im Zytosol als auch im ER, jedoch nicht im Peroxisom. Trotz intrazellulärer Fehllokalisation verfügt die Splicevariante über die Fähigkeit, PEX26-defiziente Zelllinien funktionell zu komplementieren (*rescue activity*) (40). Der zugrunde liegende Mechanismus ist bisher unbekannt.

Ziel der Arbeit war es, durch strukturelle und funktionelle Untersuchungen von PEX26 und der Splicevariante PEX26Δex5 zu einem besseren Verständnis des Aufbaus und der Funktion von PEX26 bei peroxisomaler Biogenese, Homöostase und metabolischer Funktion beizutragen.

2.2 Methoden

Als cDNA von *PEX26* wurde die Sequenz NM_001127649.1 verwendet. Sämtliche Plasmidklonierungen erfolgten mit dem rekombinanten Gateway©-Klonierungssystem. Als Vektoren zur Proteinexpression fungierten pcDNA 6.2 DEST und pCR3.1 DEST.

Zur Detektion von Protein-Protein-Interaktionen wurden Co-Immunpräzipitation (CoIP), Biolumineszenz-Resonanz-Energie-Transfer (BRET) und bimolekulare Fluoreszenzkomplementation (BiFC) angewendet. Für BRET-Experimente werden die beiden Proteine, deren Interaktion untersucht werden soll, am N- oder C-Terminus mit Luciferase (Donor) oder *Yellow Fluorescent Protein* (YFP, Akzeptor) versehen. Daraus ergeben sich pro Protein vier verschiedene Markierungsmöglichkeiten (Luciferase-N-Protein, Protein-C-Luciferase, YFP-N-Protein, Protein-C-YFP). Zur Untersuchung einer Interaktion von zwei Proteinen mittels BRET ergeben sich aus den verschiedenen Markierungen acht Donor-Akzeptor-Kombinationsmöglichkeiten. Mittels BRET-Sättigungsexperimenten kann die Bindungsaffinität zwischen zwei Proteinen untersucht werden (44). Hierzu wird eine Protein-Markierungskombination (z.B. N-Luciferase-Protein1 und N-YFP-Protein2) in verschiedenen Konzentrationsverhältnissen von Donor zu Akzeptor untersucht. Bei einer positiven Protein-Protein-Interaktion zeigt sich eine hyperbole Kurve mit einem Sättigungsplateau. Durch die Bestimmung des Akzeptor-Donor-Verhältnisses bei halbmaximaler Sättigung kann die relative Bindungsaffinität der Proteinbindungspartner ermittelt werden (44, 45).

Wir nutzten HEK293-, Cos7-Zellen und eine PEX26-defiziente Zelllinie (GM17398) zur Überexpression von Konstrukten, beispielsweise um die Lokalisation und Protein-Protein-Interaktionen zu untersuchen. Patienten mit der PEX26-Variante, die in GM17398 vorliegt, zeigen klinisch einen schweren Phänotyp des Zellwegersyndroms. *PEX26* weist in GM17398 eine homozygote Splicestellenvariante in Intron 2 [c.230+1G>T (IVS2+1G>T)] auf. Diese führt zu einem Frameshift ab Codon 77 und einem verfrühtem Stopp der Translation (T77fs139X) (40). Auf zellulärer Ebene resultiert daraus ein reduzierter Matrixproteinimport von PTS1-Proteinen (42).

Zur Detektion von Proteinen nutzten wir SDS- und BN-PAGE mit anschließendem Immunoblot. Die peroxisomale β-Oxidation wurde in einem Acylcarnitinmessverfahren mittels Tandem-Massenspektroskopie untersucht (46). Zur Bestimmung intrazellulärer Verteilungsmuster und zur Überprüfung des Proteinimports nutzten wir Immunfärbungen und konfokale Mikroskopie. Sekundärstrukturen von PEX26 und PEX26Δex5 wurden mit ENDscript 2.0 analysiert und Tertiärstrukturen mit I-TASSER vorhergesagt. Die visuelle Darstellung der Vorhersage erfolgte mittels PyMol.

2.3 Ergebnisse

2.3.1 PEX26 und PEX26Δex5 bilden Oligomere mit unterschiedlicher Affinität und unter Verwendung verschiedener Proteinuntereinheiten.

Für die PEX26-Interaktionspartner PEX1, PEX6 und PEX14 wurden höhergradige Oligomere beschrieben (47-49). Höhergradige Oligomere können das funktionelle Spektrum eines Proteins erweitern und mehr Proteininteraktionen aufbauen als Monomere (50, 51). Zusätzlich zur Bindung des PEX1-PEX6-Komplexes wurde 2014 die Bindung von PEX26 an PEX14 beschrieben (39). Die Bindungsaffinität wird über die Bindung von PEX5 an PEX14 beeinflusst (39). Der Komplex aus PEX1 und PEX6 scheint die Dissoziation von PEX14 und PEX26 zu regulieren (39). Aufgrund dieser erweiterten Funktion von PEX26, haben wir die Hypothese aufgestellt, dass auch PEX26 homooligomerisiert. Wir konnten eine Homooligomerisierung von PEX26 mittels Co-Immunpräzipitation (CoIP), Biolumineszenz-Resonanz-Energie-Transfer (BRET), bimolekularer Fluoreszenzkomplementation (BiFC) und nativer Gelelektrophorese (BN-PAGE) nachweisen. Für die Splicevariante PEX26Δex5 gelang der Homooligomerisierungsnachweis ebenfalls mittels BRET, BiFC und BN-PAGE. In BRET-Sättigungsexperimenten zeigte PEX26 eine höhere relative Bindungsaffinität für eine Homooloigomerisierung als PEX26Δex5. Darüber hinaus konnten wir eine Heterooligomerisierung von PEX26 mit PEX26Δex5 nachweisen.

2.3.2 Die Olimomerisierung wird durch Heptadenmuster und Disulfidbrücken vermittelt.

Um die an der Oligomerisierung beteiligten Proteinuntereinheiten zu identifizieren, erstellten wir genetische Verkürzungskonstrukte der PEX26-cDNA, die zu einem teilweisen oder kompletten Wegfall einzelner oder mehrerer funktioneller Domänen des Proteins führen. Jedes Verkürzungskonstrukt wurde wie in den Methoden beschrieben für die BRET-Experimente am N- oder C-Terminus mit Luciferase (Donor) oder YFP (Akzeptor) versehen. Bei Anwendung der BRET-Methode interagierten alle Fragmente miteinander, die die Aminosäuren (aa) 175-251 und/oder 270-305 enthielten. Diese beiden Abschnitte flankieren N- bzw. C-terminal die Transmembrandomäne und wurden als „*Motif 1*“ und „*Motif 2*“ bezeichnet, da diesen in der Literatur im Gegensatz zum PEX6-Bindungsfragment und der Transmembrandomäne bisher keine eindeutige Funktion zugeschrieben war. Wir stellten die Hypothese auf, dass diese beiden Motive an der Homooligomerisierung beteiligt sind. Zur Prüfung der physiologischen Relevanz untersuchten wir pathogene Varianten von PEX26, die zu verkürzten Proteinsequenzen führen. Diese bestätigten das vorherige Ergebnis und zeigten keine Homooligomerisierung, wenn die beiden angenommenen Interaktionsdomänen fehlten. Die Funktionalität der Varianten wurde mittels BRET demonstriert, in dem die vorbeschriebene Interaktion zu PEX6 weiterhin nachgewiesen werden konnte.

Die beiden identifizierten Abschnitte aa175-251 und aa270-305 zeigten nicht nur eine Homo-, sondern auch eine Heterooligomerisierung. Ein Identitätsvergleich der Aminosäuresequenzen der Primärstruktur ergab sieben identische und zwölf ähnliche Aminosäuren. Dabei konnten in der Primärstruktur Heptadenmuster identifiziert werden. Hierbei handelt es sich um Proteinsequenzen, die aus 7 Aminosäuren bestehen und an Position 1 und 4 eine hydrophobe Aminosäure aufweisen. Die identifizierten Muster haben wir „*HR1*“ (*heptad repeat 1*; N-terminal der Transmembrandomäne) und „*HR2*“ (*heptad repeat 2*; C-terminal der Transmembrandomäne) genannt. Die hydrophoben Aminosäuren waren Leucine, auf die an Position 7 erneut ein Leucin, respektive ein Isoleucin, folgt. *HR1* und *HR2* sind in Säugetieren hoch konserviert. Die computerbasierte Vorhersage der Sekundärstruktur mittels ENDscrpit 2.0 (52) zeigte α-Helices für beide Motive. Die Vorhersage der Tertiärstruktur mittels I-TASSER (53) ergab in beiden Motiven eine ähnliche räumliche Ausrichtung der Leucinreste. Diese Ausrichtung ist ein typisches Merkmal von Leucin-Zippern, die ein häufiges Proteinmuster für Protein-Protein-Interaktionen (PPI) darstellen (54). Um die Relevanz der beiden Heptadenmuster zu überprüfen, wurden durch Mutagenese BRET-Konstrukte erstellt, in denen die entsprechenden (Iso)Leucine durch Alanine als kleine, apolare Aminosäure ersetzt wurden. In PEX26-HR1HR2 wurden beide Motive mutiert, in PEX26-HR2 nur das distale *HR2*. PEX26Δex5 verfügt lediglich über *HR2*. Dies wurde in PEX26Δex5-HR2 mutiert. An Hand von BRET-Untersuchungen konnten wir zeigen, dass der Verlust beider Motive in PEX26 und des einzigen vorhandenen Motivs in PEX26Δex5 zu einem Verlust der Homooligomerisierungsfähigkeit führt. Der Verlust von nur einem Motiv in PEX26 führt zu einer Schwächung, aber zu keinem Verlust der Homooligomerisierung. Die Mutation der Motive führte zu intrazellulärer Fehllokalisation in die Mitochondrien für PEX26-HR1HR2 und ins ER für PEX26Δex5-HR2.

Disulfidbrücken können ebenfalls eine Oligomerisierung vermitteln. Wir haben die Sequenzen von PEX26 und PEX26Δex5 auf das Vorhandensein von Cysteinen untersucht, die Disulfidbrücken ausbilden könnten. An Aminosäureposition 173 findet sich ein Cystein, das potentiell Disulfidbrücken ausbilden könnte. Dieses ist unter den sechs Cysteinen in PEX26 das einzige, das in Säugetieren nicht konserviert ist. Um den Einfluss von C173 auf die Oligomerisierung von PEX26 zu untersuchen, haben wir durch Mutagenese das Cystein durch ein Serin ersetzt (C173S). Die Funktionalität von C173S-Mutationskonstrukten wurde in Bezug auf die intrazelluläre Lokalisation, die funktionelle Komplementation und Proteininteraktionen mit bekannten Interaktionspartnern verifiziert. BRET-Experimente mit den beiden Mutationskonstrukten PEX26-C173S und PEX26Δex5-C173S zeigten einen Verlust der Homooligomerisierung. In BiFC-Experimenten zeigte PEX26-C173S ein geringeres Fluoreszenzsignal im Vergleich zur PEX26 Homooligomerisierung. Zur weiteren Verifizierung des Einflusses von Disulfidbrücken auf die Oligomerisierung führten wir Gelelektrophoreseuntersuchungen durch. Unter nicht-reduzierenden Bedingungen bleiben Disulfidbrücken im Gegensatz zu reduzierenden Bedingungen erhalten. Die C173S-Mutationskonstrukte zeigten unter nicht-reduzierenden Bedingungen Banden im Bereich der erwarteten Größe eines PEX26-, bzw. PEX26Δex5-Dimers. Diese Banden

waren jedoch von geringerer Intensität als die Banden der entsprechenden Wildtyp-Konstrukte, was einer geringeren Proteinmenge entspricht. Unter reduzierenden Bedingungen, und damit nach Reduktion und Aufhebung der Disulfidbrücken, wurden keine Dimere nachgewiesen. Somit scheinen die Disulfidbrücken einen Einfluss auf die Oligomerisierung zu haben. Die nicht membrangebundenen Konstrukte PEX26Δex5 und PEX26Δex5-C173S zeigten eine höhere Intensität der Banden als das in die peroxisomalen Membran verankerten Konstrukte PEX26 und PEX26-C173S.

2.3.3 Unterschiedliche Interaktionsmuster von PEX26 und PEX26Δex5 mit dem peroxisomalen Translocon

PEX26 interagiert mit PEX14, das zusammen mit PEX13 den Bindungskomplex (*docking complex*) des Translocons bildet (39). Es wurden zwei Gruppen unterschiedlicher peroxisomaler Vorläuferorganellen beschrieben, die verschiedene Peroxine beinhalten, entweder PEX2 und PEX10 oder PEX13 und PEX14 (12). Um eine mögliche Beteiligung von PEX26 am Translocon zu untersuchen, haben wir mittels BRET die Interaktion von PEX26 und PEX26Δex5 mit den entsprechenden Peroxinen untersucht. Die Interaktion mit PEX6 und PEX19 diente als Positivkontrolle. Die bekannte Interaktion mit PEX14 wurde für PEX26 bestätigt. Auch für die Splicevariante PEX26Δex5 konnten wir eine Interaktion mit PEX14 nachweisen. Für PEX26 konnten wir die Interaktion mit PEX13 erstmals zeigen, PEX26Δex5 interagierte hingegen nicht mit PEX13. Die Interaktion der beiden PEX26-Konstrukte mit PEX13 konnten mittels BiFC nicht bestätigt werden. Für PEX2 und PEX10 konnten wir keine Interaktion mittels BRET oder BiFC nachweisen. Um Domänen zu identifizieren, die die Interaktionen mit PEX13 und PEX14 vermitteln, untersuchten wir die zuvor beschriebenen PEX26-Fragmente mittels BRET auf Interaktionen mit PEX6, PEX13, PEX14 und PEX19. Die vorbeschriebene PEX6-Bindedomäne (aa29-174) interagierte mit PEX6. PEX19-Interaktionen wurden für Konstrukte mit *Motif 2* identifiziert. Die TMD (aa252-269) ohne *Motif 2* war nicht ausreichend für eine PEX19-Bindung, obwohl dieser Bereich als zusätzliche PEX19-Bindestelle beschrieben wurde (43). Für die Bindung von PEX13 und PEX14 war *Motif 2* notwendig. Für die PEX13-Bindung war jedoch zusätzlich die TMD notwendig. Dies erklärt die fehlende Bindung von PEX26Δex5 an PEX13.

2.3.4 Die PEX26-Dimerisierung beeinflusst die Interaktion mit PEX14, die Komplementation PEX26-defizienter Zellen und die peroxisomale β-Oxidation überlangkettiger Fettsäuren.

Um den Einfluss der Dimerisierung auf peroxisomale Prozesse zu untersuchen, synthetisierten wir ein künstliches PEX26-Dimer ($PEX26_{dimer}$). Hierbei handelt es sich um die Aminosäuresequenz von PEX26 in originärer N-C-Richtung. An dieses Konstrukt schließt sich ein kurzer Linker an, auf den eine umgekehrte Aminosäuresequenz in C-N-Richtung folgt. Dadurch erwarteten wir, dass nach Expression die C-Termini eng beieinander liegen und die Bindedomänen verlässlich zueinander finden. Die Funktionalität der inversen Aminosäuresequenz von PEX26 wurde nachgewiesen. Hierzu wurde die peroxisomale Lokalisation mittels Immunfluoreszenz gezeigt. Als peroxisomalem Marker diente *eGFP-SKL*. Hier ist grün fluoreszierendes Protein (*enhanced green fluorescent protein*, *eGFP*) an eine peroxisomale Lokalisationssequenz gebunden, die aus der Aminosäurefolge Serin-Lysin-Leucin (SKL) besteht. Zusätzlich konnten in BRET-Experimenten die Interaktionen von $PEX26_{dimer}$ mit PEX6 und PEX19 sowie die Homooligomerisierung gezeigt werden. In der Untersuchung der relativen Bindungsaffinität durch BRET-Sättigungsexperimente zeigten PEX26, PEX26Δex5 und $PEX26_{dimer}$ eine vergleichbare Affinität für die Bindung von PEX6. Die Affinität für die Bindung von PEX14 war jedoch für PEX26Δex5 und $PEX26_{dimer}$ höher als für PEX26. Dies legt nahe, dass der Oligomerisierungsgrad einen Einfluss auf die Bindung von PEX14 hat.

Im nächsten Schritt untersuchten wir die Komplementation der PEX26-defizienten Zelllinie GM17398 durch PEX26, PEX26Δex5 und $PEX26_{dimer}$. Alle drei Konstrukte komplementierten erfolgreich. PEX26Δex5 und $PEX26_{dimer}$ zeigten zusätzlichen zur peroxisomalen auch eine zytosolische Lokalisation. $PEX26_{dimer}$ zeigte die höchste Anzahl an nachweisbaren Peroxisomen. Die Größe der entstandenen Peroxisomen und der Anteil von importiertem Marker (*eGFP-SKL*) lagen für alle 3 Konstrukte in einem vergleichbaren Bereich. Die bereits erwähnten Mutationskonstrukte (C173S, *HR1*- und *HR2*-Mutationen) komplementierten PEX26-defiziente Zellen (GM17398) und zeigten die zu erwartenden Lokalisationen: PEX26-C173S und PEX26 peroxisomale, PEX26Δex5-C173S sowie

PEX26Δex5 peroxisomale und zytosolische Lokalisation. Halbach und Kollegen zeigten für PEX26-Konstrukte, denen aa275-305 fehlen und damit *HR2*, eine mitochondriale Lokalisation (43). Auch PEX26_HR1HR2 zeigte eine mitochondriale Lokalisation. Weller und Kollegen beschrieben für PEX26Δex5 eine ER-, aber keine peroxisomale Lokalisation (40). PEX26Δex5-HR2 zeigte ebenfalls dieses Lokalisationsmuster.
Zusätzlich untersuchten wir den Einfluss von PEX26, PEX26Δex5 und $PEX26_{dimer}$, sowie des Verkürzungskonstruktes PEX26aa29-174 als Kontrolle, auf die β–Oxidation überlangkettiger Fettsäuren in PEX26-defizienten Zellen. Hierzu bestimmten wir die Carnitinester der Fettsäure C20:0 nach Beladung mit der überlangkettigen Fettsäure Lignocerinsäure (C24:0). Alle 4 Konstrukte zeigten eine C20:0 Erhöhung, was für eine erfolgreiche Wiederherstellung der β–Oxidation spricht. $PEX26_{dimer}$ induzierte den höchsten Anteil an C20:0.

2.4 Diskussion

Peroxisomale Biogenesestörungen umfassen ein breites klinisches Spektrum, wobei früh letale Multisystemerkrankungen als schwerste Manifestationsform auftreten. Bisher sind lediglich symptombezogene und keine kausalen Therapien etabliert (35). Die Physiologie und Pathophysiologie des Peroxisoms bleibt trotz eines großen Wissenszuwachses in den vergangenen Jahren weiterhin unvollständig verstanden (4, 30). Die vorliegende Arbeit soll einen Beitrag zum Verständnis der peroxisomalen Physiologie durch die umfassende Charakterisierung eines bisher wenig beschriebenen peroxisomalen Proteins leisten.
Homooligomerisierung ermöglicht die Entstehung größerer Proteinstrukturen mit hoher Stabilität. Dadurch können spezifische zelluläre Funktionen wahrgenommen werden (50, 55), beispielsweise können zusätzliche Bindestellen entstehen. Wir konnten die Homooligomerisierung von PEX26 und PEX26Δex5 nachweisen, wobei PEX26Δex5 eine deutlich geringere Homooligomerisierungsaffinität als PEX26 aufwies. Zusätzlich konnten wir zeigen, dass beide Proteinspezies miteinander interagieren, was das *in vivo* Vorkommen von Heterooligomeren nahe legt. Dadurch könnten unterschiedliche strukturelle Eigenschaften und Funktionen entstehen. Unsere Interaktionsstudien zeigten mit verschiedenen Methoden (BRET, BiFC) positive Ergebnisse für PEX26 und PEX26Δex5 mit Markierungen am N-Terminus. PEX26 ist mit dem C-Terminus in der peroxisomalen Membran verankert. Die Markierung am C-Terminus von PEX26 scheint durch räumliche oder sterische Effekte Interaktionen zu verhindern. Diese Hypothese wird dadurch unterstützt, dass PEX26Δex5, dem die TMD zur Verankerung in der peroxisomalen Membran fehlt, binäre Interaktionen für alle vier möglichen N- und C-terminalen Markierungskombinationen aufweist. Hierbei ist jedoch zu beachten, dass der fehlende Nachweis einer Interaktion, nicht zwingend bedeutet, dass keine Interaktion vorliegt.
Die Homooligomerisierung scheint durch zwei Motive im Bereich von aa175-251 (*Motif 1*) und aa270-305 (*Motif 2*) vermittelt zu werden. In diesen Regionen zeigten sich Heptadenmuster (*HR1, HR2*), die in Säugetieren hochkonserviert sind. In den Sequenzabschnitten von *HR1* und *HR2* fanden sich Leucine und Isoleucin, die als Leucin-Zipper konfiguriert eine Protein-Protein-Interaktion vermitteln können. Die Mutation bereits eines der beiden Heptadenmotive beeinträchtigte die Homooligomerisierung deutlich. *HR2* beinhaltet zusätzlich einen Abschnitt mit basischen, positiv geladenen Aminosäuren (*basic charge motif*), das für die peroxisomale Lokalisation relevant ist (56). Bei Mutation von *HR2* kommt es zu einer Fehllokalisation in Mitochondrien. Dies wurde bereits früher für Deletionen der Aminosäuren 275-305 im C-terminalen Bereich von PEX26 gezeigt (43). Damit scheint *Motif 2* für die Dimerisierung notwendig. Für die peroxisomale Lokalisation ist es jedoch nicht ausreichend. In der Splicevariante PEX26Δex5 fehlt *Motif 1*. Bei Überexpression bildet das Konstrukt Dimere, ist jedoch hauptsächlich – im Gegensatz zum peroxisomalen PEX26 - im ER lokalisiert. Der Verlust beider Motive führt darüber hinaus zum Verlust der Dimerisierung. Unter der Hypothese, dass eine Dimerisierung Voraussetzung für eine regelhafte Proteinfunktion ist, könnte der Verlust der Dimerisierungsfähigkeit zu einer Funktionseinschränkung führen. Diese Funktionseinschränkung könnte Krankheitssymptome verursachen. Außerdem könnte der Verlust von Proteininteraktionenspartnern durch Mutation von Interaktionsdomämen oder die Fehllokalisation peroxisomaler Proteine in andere Organellen zu einer Krankheitsentstehung beitragen.

Um den möglichen Einfluss einer Disulfidbrücke auf die Oligomerisierung zu analysieren, untersuchten wir das Cystein an Position 173 (C173) der Aminosäuresequenz. PEX26 verfügt über vier weitere Cysteine in der PEX6-Bindedomäne, die jedoch nicht oligomerisiert, und ein Cystein in der TMD, welche in PEX26Δex5 fehlt. Wir zeigten in Proteininteraktionsanalysen mittels BRET, dass die Mutagenese des Cysteins zu einem Serin (C173S) das Bindungsverhalten schwächt. Die subzelluläre Lokalisation der Mutationskonstrukte PEX26-C173S und PEX26Δex5-C173S blieb unbeeinträchtigt, jedoch war die funktionelle Komplementation PEX26-defizienter Zellen eingeschränkt. Nicht-reduzierende PAGE-Experimente zeigten ebenfalls Dimere, die unter reduzierenden Bedingungen nicht mehr nachweisbar waren. Diese Ergebnisse sprechen für eine funktionelle Relevanz von Disulfidbrücken bei der Oligomerisierung. Bei vorhandenem C173, jedoch fehlenden Heptadenmustern (z.B. in PEX26-R192X, einer pathogenen, in Patienten nachgewiesenen STOPP-Variante) ist die Homooligomerisierung gestört. Somit schlussfolgern wir, dass die Homooligomerisierung durch die Heptadenmuster vermittelt und durch eine Disulfidbrücke C173-C173 unterstützt wird.

Die physiologische Relevanz der Homooligomerisierung zeigt sich in der Untersuchung bekannter pathogener Varianten. Die Varianten W99X und R192X, denen *Motif 1* und *Motif 2* fehlen, zeigten in BRET-Experimenten keine Homooligomerisierung. Die Variante M1T (aa96-305), zeigte eine Homooligomerisierung. Diese Variante kann den peroxisomalen Proteinimport wieder herstellen, obwohl die Bindung zu PEX6 reduziert ist (38, 42).

Im Rahmen der erweiterten Funktion von PEX26 mit Beeinflussung des Translocons konnten wir die neu beschriebene Interaktion zu PEX14 und die PEX6-Bindedomäne (aa29-174) bestätigen. Darüber hinaus konnten wir erstmalig eine Interaktion zwischen PEX26 und PEX13 beschreiben. PEX26Δex5 interagiert nicht mit PEX13. Zusätzlich zu *Motif 2* scheint auch die TMD für eine Interaktion mit PEX13 erforderlich zu sein.

Die Proteinaufreinigung von PEX26 gelang nicht, so dass wir die Kristallstruktur nicht untersuchen konnten. Um eine Quartärstruktur zu erhalten, erstellten wir eine 3D-Struktur *in silico*. In dieser Strukturvorhersage ist die N-terminale PEX6-Bindedomäne als siebenfache Helix dargestellt, die räumlich durch die TMD und eine Linker-Region vom C-terminalen Proteinteil getrennt ist. *Motif 1* und *2* zeigten sich ebenfalls als Helices, mit einer Orientierung, die eine Protein-Protein-Interaktion möglich erscheinen lässt. Die Kristallstruktur von Pex15, dem PEX26 Ortholog in Hefe, zeigte eine vergleichbare Domänenverteilung (41). Es besteht zwar Analogie für die Funktion als Pex6-Anker und die Topologie als Typ-II-Membranprotein, jedoch lediglich eine geringe Sequenzidentität von 12 % (40).

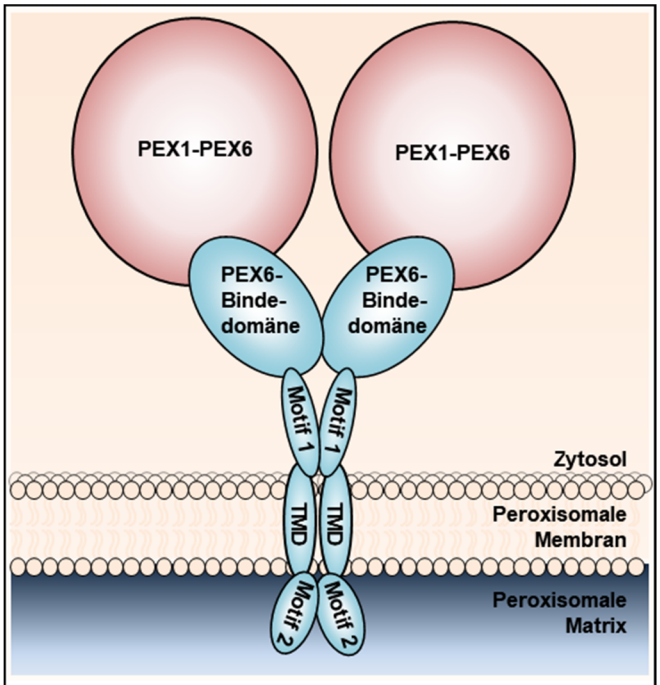

Abb. 4: Schematisches PEX26 Dimermodell. Modellvorschlag zur möglichen räumlichen Bindung von zwei PEX26-Proteinen (blau), die über *Motif 1* und *2* verbunden als Dimer interagieren und mit der TMD in der peroxisomalen Membran verankert sind. Über die PEX6-Bindedomäne bindet PEX26 Cluster des PEX1-PEX6-Komplexes (rot).

In einem weiteren Schritt untersuchten wir den Einfluss der Konformation und der Organisation verschiedener Domänen auf die Funktion. PEX26, PEX26Δex5 und $PEX26_{dimer}$ zeigten unterschiedlich hohe Wahrscheinlichkeiten, Homooligomere auszubilden, banden PEX6 jedoch mit ähnlichen Affinitäten. Wir entwarfen ein Modell (Abb. 4), in dem zwei PEX26-Proteine aneinander gelagert mit dem C-Terminus in der peroxisomalen Membran verankert sind und einen PEX1-PEX6-Komplex binden. Dieses Modell deckt sich mit einer *in silico* Dimerisierungsvorhersage.

Das obligate PEX26$_{dimer}$-Konstrukt zeigt die höchste Bindungsaffinität zu PEX14. Deshalb schlagen wir vor, dass ein PEX26-Dimerkomplex mit einem Bindungskomplex aus PEX13 und PEX14 interagiert. Bisher sind zwei verschiedene Arten von peroxisomalen Vorläuferorganellen beschrieben. Eine Art beinhaltet PEX2 und PEX10. Dabei handelt es sich um Ligasen, die für die Ubiquitinierung von PEX5 verantwortlich sind. Die andere Art beinhaltet PEX13 und PEX14 als Teile des Bindungskomplexes. PEX26 bindet nur an PEX13 und PEX14, jedoch nicht an die Ligasen. PEX26Δex5 bindet lediglich PEX14 und zeigt eine ER-Lokalisation statt einer peroxisomalen. Sowohl der Oligomerisierungsgrad als auch das Fehlen von *Motif 1* intensiviert die Bindung zu PEX14. Somit scheint es möglich, dass PEX26 und PEX26Δex5 über die unterschiedliche Lokalisation und das unterschiedliche Bindungsverhalten verschiedene Rollen in der peroxisomale Biogenese und dem Proteinimport einnehmen könnten. Hier könnte PEX26Δex5 aus folgenden Gründen in einen frühen Schritt der peroxisomalen Biogenese eingebunden sein: 1) peroxisomale Organellsynthese im ER (16), 2) unterschiedliche zelluläre Lokalisation (ER und Zytosol), 3) unterschiedliche Interaktionspartner, 4) unterschiedliche Interaktionsaffinitäten. PEX26 könnte hingegen hauptsächlich die beschriebene Rolle beim Import von peroxisomalen Membranproteinen in reifen Peroxisomen einnehmen. Für eine Evaluation dieser Hypothese sind weitere Untersuchungen notwendig. Wir haben einen zusammenfassenden Modellvorschlag (Abb. 5.) entwickelt, wie PEX19 und PEX3 PEX26 in die peroxisomale Membran

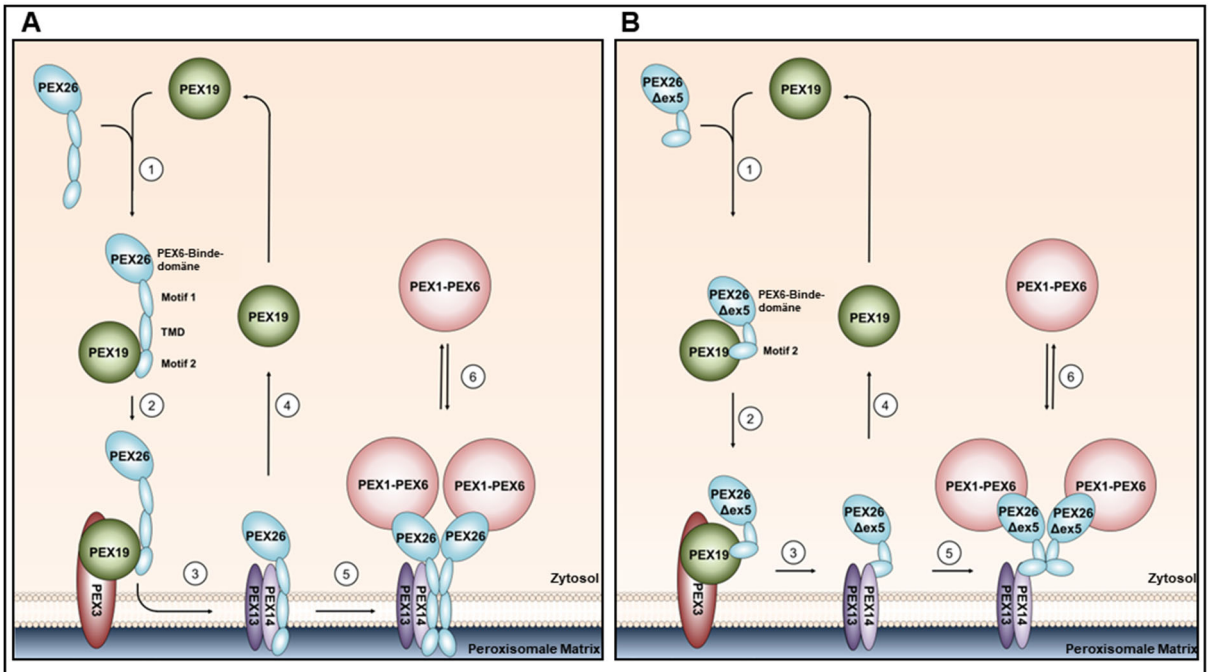

Abb. 5: Zusammenfassender Modellvorschlag zur Integration von PEX26 in (A) und PEX26Δex5 an (B) die peroxisomale Membran und Komplexbildung mit weiteren Peroxinen.
(**A**) (1) C-terminale Interaktion von PEX26 (Motif 2 und TMD) mit PEX19 im Zytosol, (2) PEX26 bildet einen Komplex mit PEX19 und PEX3 an der peroxisomalen Membran und (3) wird in die Membran integriert. (4) PEX19 verlässt den Komplex und rezyklisiert. (5) PEX26-Dimere bilden höhergradige Proteinkomplexe mit PEX13, PEX14 und dem PEX1-PEX6 AAA+ ATPasen-Komplex. (6) Anschließend löst sich der PEX1-PEX6-Komplex von der peroxisomalen Membran. (**B**) (1) C-terminale Interaktion von PEX26Δex5 (Motif 2) mit PEX19 im Zytosol und (2) anschließender Komplexbildung mit PEX3 an der peroxisomalen Membran. (3) PEX26Δex5 wird auf Grund der fehlenden Transmembrandomäme (TMD) nicht in die peroxisomale Membran integriert. Es findet eine Interaktion zwischen PEX26Δex5 und PEX14 über Motif 2 statt. Der C-Terminus von PEX26Δex5 befindet sich somit weiterhin im Zytosol. (4) PEX19 verlässt den Komplex und rezyklisiert. (5) PEX26Δex5-Dimere interagieren mit PEX14 und dem PEX1-PEX6 AAA+ ATPasen-Komplex. (6) Anschließend löst sich der PEX1-PEX6-Komplex von der peroxisomalen Membran.

integrieren und PEX26Δex5 an der Membran über die Interaktion mit PEX14 ohne transmembranöse Integration assoziiert werden könnte.

Bei Komplementation von PEX26-defizienten Zellen zeigten PEX26, PEX26Δex5 und $PEX26_{dimer}$ keinen Unterschied in der Effizienz des Matrixproteinimports. Größe und Fluoreszenzintensität der nach Komplementation entstandenen Peroxisomen zeigten sich für die untersuchten Konstrukte vergleichbar. Für $PEX26_{dimer}$ zeigte sich eine höhere Anzahl an Peroxisomen mit wiederhergestelltem Proteinimport. Dies werten wir als Einfluss auf die Homöostase. Der Oligomerisierungsstatus scheint somit einen Einfluss auf die peroxisomale Funktion zu haben, unabhängig von der Fähigkeit den PEX1-PEX6-Komplex zu binden. Dies hat die Untersuchung der β-Oxidation ebenfalls bestätigt, da $PEX26_{dimer}$ den größten Anteil von abgebauten überlangkettigen Fettsäuren zeigte. Eine verbesserte β-Oxidation kann als Folge der erhöhten Anzahl an Peroxisomen gedeutet werden. Spekulativ könnte es sich auch um einen anderen, unbekannten Einflussfaktor handeln, der nach Dimerisierung die metabolische Funktion verbessert. Dieser Aspekt benötigt ebenfalls weitere Untersuchungen.

Zusammenfassend zeigte die Analyse der Tertiär- und Quartärstruktur von PEX26 eine Homooligomerisierung, die durch die beiden Motive *Motif 1* und *Motif 2* mit Leucin-Zippern vermittelt wird. Diese Motive befinden sich N-terminal (zytosolisch) und C-terminal (luminal) an die Transmembrandomäne angrenzend. Sie unterscheiden sich in Struktur und Lokalisation von der N-terminal gelegenen PEX6-Bindedomäne. Eine Disulfidbrücke an Position 173 scheint einen stabilisierenden Einfluss auf die Dimerisierung zu haben. *Motif 1* und Transmembrandomäne fehlen in PEX26Δex5. *Motif 2* beinhaltet einen Abschnitt mit basischen, positiv geladenen Aminosäuren. Dieser Abschnitt ist verantwortlich für die peroxisomale Lokalisation. Wir erstellten ein Modell, das zeigt wie PEX26 als Dimer PEX1-PEX6-Komplexe und PEX13-PEX14-Komplexe (Bindungskomplex) bindet, und schlagen einen alternativen Bindungsmechanismus für die physiologische Isoform PEX26Δex5 vor. Auf funktioneller Ebene beeinflusst die isoformspezifische Domänenorganisation die Oligomerisierung und Interaktionen mit peroxisomalen Proteinen. Unsere Ergebnisse liefern somit Hinweise für eine erweiterte Funktion von PEX26 in Bezug auf peroxisomale Funktionen sowie Biogenese und Homöostase.

2.4.1 Weiterführende Diskussion

In dieser Arbeit wurde Biolumineszenz-Resonanz-Energie-Transfer (BRET) als Technologie zur Untersuchung von Protein-Protein-Interaktionen verwendet. Der Vorteil dieser Methode gegenüber anderen Methoden zur PPI-Bestimmung liegt in der Möglichkeit der Untersuchung von Interaktionen in der lebenden Zelle (45). Somit kann ein Organismus-spezifischer Zelltyp gewählt werden, der ein hohes Maß an physiologischer Umgebung für die entsprechende Interaktion liefert, darüber hinaus bleiben Transport und Modifikationsprozesse erhalten. Eingeschränkt wird der physiologische Aspekt durch die Notwendigkeit der Überexpression der verwendeten Proteine, sowie durch die Größenzunahme der zu untersuchenden Proteine durch Markierungen (*Rluc, YFP*). Wir verwendeten zwei verschieden Varianten der BRET-Methode. Zur Identifikation unbekannter Interaktionen wählten wir einen Screeningansatz. In diesem verwendeten wir eine bestimmtes Akzeptor(*YFP*)-Donor(*Rluc*)-Verhältnis und kombinierten die beiden Zielproteine jeweils am N- und C-Terminus sowohl mit *Rluc* als auch mit *YFP*. Aus diesen Zielproteinen ergaben sich acht verschiedene Kombinationsmöglichkeiten. Durch diese Kombinationen erhalten wir eine deutlich erhöhte Sensitivität im Vergleich zu anderen Protein-Protein-Interaktionsbestimmungen. Um verschiedene, neu identifizierte Interaktionen genauer beschreiben zu können (z.B. Bindungsaffinität, Konformationsänderung durch Mutation) haben wir Sättigungskurven erstellt. Hierbei wird das Verhältnis von Akzeptor (*YFP*) zu Donor (*Rluc*) soweit erhöht bis sich das Plateau einer Sättigungskurve einstellt (45). Eine dritte Variante haben wir im Rahmen der Untersuchung von Disulfidbrücken in PEX26 erprobt. Hier haben wir die Zellen vor der Messung lysiert und mit reduzierenden Substanzen behandelt. Dieser Prozess hat jedoch auch die Interaktion in den Kontrollzellen zerstört. Deshalb haben wir dieses Ergebnis nicht in die Publikation aufgenommen.
Zur Bestätigung der BRET-Daten verwendeten wir BiFC. Diese Methode detektiert ebenfalls PPI in lebenden Zellen, jedoch mit geringerer Sensitivität. Als weitere Bestätigungsmethode wurde zusätzlich Lumier etabliert (höhere Sensitivität im Vergleich zu BiFC (57)). Bei dieser Methode sind Lyseschritte notwendig. Es handelt sich um eine Immunpräzipitation mit Detektion einer Luciferase. PEX26-Interaktionen konnten nicht nachgewiesen werden. Deshalb findet sich die Methode nicht in der

Publikation. BiFC und Lumier wurden vom Doktoranden etabliert und an eine automatische Pipettierplattform adaptiert.

3. Zusätzliche im Rahmen der Doktorarbeit entstandene Arbeiten

Zu Beginn der Arbeit wurde eine cDNA-Datenbank mit n = 105 peroxisomalen Proteinen angelegt, mit dem Ziel, das Proteom des gesamten Organells abzudecken. Wir erreichten eine Deckungsrate von 92% verglichen mit der Referenzdatenbank www.peroxisomedb.org (58). Unsere Datenbank wurde manuell mit vollständigen Gensequenzierungen kuriert. Zur Beschreibung des peroxisomalen Interaktoms (= Darstellung aller binären PPI, die sich aus der Kombination der als peroxisomal beschriebenen Proteine ergeben) wurden alle vorhandenen Konstrukte in binären Paaren mittels BRET untersucht. Es wurde der bereits oben beschriebene Screeningansatz mit acht Kombinationsmöglichkeiten für ein einzelnes Proteinpaar gewählt. Somit wurden 5565 Proteinpaarmessungen auf einer informatikgestützten, automatisierten Pipettierplattform vorgenommen. Nach Etablierung weiterer Protein-Protein-Interaktionsmethoden (BiFC, Lumier), sowie der Adaptation an die automatisierte Pipettierplattform, wurden die positiven Screeningergebnisse mit diesen beiden unabhängigen Methoden kontrolliert. Die Datenauswertung ist aktuell noch nicht abgeschlossen.
Für die Untersuchung der Ursache der ausgeprägten phänotypischen Variabilität bei Vorliegen von Mutationen im *PEX26*-Gen wurde das Interaktionsnetzwerk von PEX26 und dessen Interaktionspartnern erstellt. Dieses Netzwerk wurde ebenfalls mit verschiedenen, in Patienten als pathogen beschriebenen, Varianten gemessen. In diesen Netzwerken zeigte sich, dass die Anzahl der verloren gegangenen Interaktionspartner mit der Schwere des klinischen Phänotyps korreliert. Das Manuskript zur Veröffentlichung wird derzeit erstellt.
Auch für das bekannte Krankheitsgen *ABCD1*, das bei Veränderung zur Adrenoleukodystrophie (ALD) führt, erstellten wir ein peroxisomales Protein-Protein-Interaktionsnetzwerk mittels BRET. Bei dieser Erkrankung ist die Pathogenese bisher noch unvollständig verstanden. In unserem Netzwerk konnten bisher nicht beschriebene PPI identifiziert werden. Die Proteinpartner gehörten dabei teilweise zu übergeordneten zellulären Prozessen, die bisher bei der Suche nach der Pathogenese nicht berücksichtigt wurden (z.B. Interaktion mit Pipecolinsäureoxidase (PIPOX), die am Lysinstoffwechsel beteiligt ist, oder Interaktion mit PEX5, PEX10 und PEX13, Proteine des peroxisomalen Matrixproteinimports (mit den weiter oben bereits detailliert beschriebenen Funktionen)). Diese Daten wurden auf der jährlichen internationalen Tagung für angeborene Stoffwechselerkrankungen vorgetragen (O-051, Abstracts of the SSIEM 2014 Annual Symposium). Das Manuskript zur Publikation befindet sich ebenfalls in Vorbereitung.
In einem weiteren Projekt wurde ein PPI-Netzwerk für *CLPB* (Caseinolytic peptidase B homolog), das in die AAA+-Proteinfamilie gehört, erstellt. Pathogene Varianten in *CLPB* führen zu einem Syndrom bestehend aus kognitiver Einschränkung, kongenitaler Neutropenie, progressiver Gehirnatrophie, Bewegungsstörung, Katarakt und 3-Methylglucagonazidurie. Zur Netzwerkerstellung wurden 100 Proteine aus unserer cDNA-Bibliothek ausgewählt, die aufgrund räumlicher oder funktioneller Beschreibungen mit CLPB interagieren könnten. Die Analyse binärer PPI erfolgte mittels BRET. Es konnte eine Interaktion zu ATP2A2 gezeigt werden. HAX1 interagiert ebenfalls mit ATP2A2. Varianten in *HAX1* führen zu schwerer, kongenitaler Neutropenie (SCN3; Morbus Kostmann). Hierbei handelt es sich um eine möglicherweise gemeinsame pathogene Ursache der verschiedenen Erkrankungen mit teilweise überlappendem Phänotyp (60).

Im Rahmen der Promotionsarbeit erhielt ich durch das Erlernen etablierter molekularbiologischer Methoden einen Einstieg in die Laborarbeit. Selbstständig durchgeführte Etablierungen von Methoden vertieften dieses Wissen und förderten den kritischen Umgang mit Messwerten und Ergebnisinterpretationen. Inhaltlich konnte ich einen fundierten Einblick in die Peroxisomologie gewinnen. Hierzu gehört auch die Erkenntnis, dass die Betrachtung eines Zellorganells nur im zellulären Kontext möglich ist, da Funktionen in dynamischen biologischen Prozessen selten isoliert untersucht werden können. Weiterhin erlernte ich im Rahmen der Promotionsarbeit wissenschaftliches Denken und Handeln, welche es mir ermöglichen Forschungsergebnisse und Fakten kritisch zu hinterfragen und zu beurteilen sowie selbst wissenschaftliche Fragstellungen zu entwickeln.

4. Abbildungsverzeichnis

5. Literaturverzeichnis

1. De Duve C, Baudhuin P. Peroxisomes (microbodies and related particles). Physiological reviews. 1966;46(2):323-57.
2. Islinger M, Cardoso MJ, Schrader M. Be different--the diversity of peroxisomes in the animal kingdom. Biochim Biophys Acta. 2010;1803(8):881-97.
3. Wanders RJ, Waterham HR. Biochemistry of mammalian peroxisomes revisited. Annu Rev Biochem. 2006;75:295-332.
4. Walter T, Erdmann R. Current Advances in Protein Import into Peroxisomes. Protein J. 2019.
5. Jones JM, Morrell JC, Gould SJ. PEX19 is a predominantly cytosolic chaperone and import receptor for class 1 peroxisomal membrane proteins. J Cell Biol. 2004;164(1):57-67.
6. Gandre-Babbe S, van der Bliek AM. The novel tail-anchored membrane protein Mff controls mitochondrial and peroxisomal fission in mammalian cells. Mol Biol Cell. 2008;19(6):2402-12.
7. Van Veldhoven PP. Biochemistry and genetics of inherited disorders of peroxisomal fatty acid metabolism. J Lipid Res. 2010;51(10):2863-95.
8. Brites P, Waterham HR, Wanders RJ. Functions and biosynthesis of plasmalogens in health and disease. Biochim Biophys Acta. 2004;1636(2-3):219-31.
9. Ferdinandusse S, Houten SM. Peroxisomes and bile acid biosynthesis. Biochim Biophys Acta. 2006;1763(12):1427-40.
10. Salido E, Pey AL, Rodriguez R, Lorenzo V. Primary hyperoxalurias: disorders of glyoxylate detoxification. Biochim Biophys Acta. 2012;1822(9):1453-64.
11. Waterham HR, Ferdinandusse S, Wanders RJ. Human disorders of peroxisome metabolism and biogenesis. Biochim Biophys Acta. 2016;1863(5):922-33.
12. Sugiura A, Mattie S, Prudent J, McBride HM. Newly born peroxisomes are a hybrid of mitochondrial and ER-derived pre-peroxisomes. Nature. 2017;542(7640):251-4.
13. Waterham HR, Ebberink MS. Genetics and molecular basis of human peroxisome biogenesis disorders. Biochim Biophys Acta. 2012;1822(9):1430-41.
14. Fujiki Y, Matsuzono Y, Matsuzaki T, Fransen M. Import of peroxisomal membrane proteins: the interplay of Pex3p- and Pex19p-mediated interactions. Biochim Biophys Acta. 2006;1763(12):1639-46.
15. Kim PK, Mullen RT, Schumann U, Lippincott-Schwartz J. The origin and maintenance of mammalian peroxisomes involves a de novo PEX16-dependent pathway from the ER. J Cell Biol. 2006;173(4):521-32.
16. van der Zand A, Gent J, Braakman I, Tabak HF. Biochemically distinct vesicles from the endoplasmic reticulum fuse to form peroxisomes. Cell. 2012;149(2):397-409.
17. Erdmann R, Schliebs W. Peroxisomal matrix protein import: the transient pore model. Nature Reviews Molecular Cell Biology. 2005;6:738.
18. Braverman N, Dodt G, Gould SJ, Valle D. An isoform of pex5p, the human PTS1 receptor, is required for the import of PTS2 proteins into peroxisomes. Hum Mol Genet. 1998;7(8):1195-205.
19. Erdmann R, Schliebs W. Peroxisomal matrix protein import: the transient pore model. Nat Rev Mol Cell Biol. 2005;6(9):738-42.
20. Meinecke M, Cizmowski C, Schliebs W, Kruger V, Beck S, Wagner R, et al. The peroxisomal importomer constitutes a large and highly dynamic pore. Nat Cell Biol. 2010;12(3):273-7.
21. Meinecke M, Bartsch P, Wagner R. Peroxisomal protein import pores. Biochim Biophys Acta. 2016;1863(5):821-7.
22. Platta HW, El Magraoui F, Baumer BE, Schlee D, Girzalsky W, Erdmann R. Pex2 and pex12 function as protein-ubiquitin ligases in peroxisomal protein import. Mol Cell Biol. 2009;29(20):5505-16.
23. Williams C, van den Berg M, Geers E, Distel B. Pex10p functions as an E3 ligase for the Ubc4p-dependent ubiquitination of Pex5p. Biochem Biophys Res Commun. 2008;374(4):620-4.

24. Law KB, Bronte-Tinkew D, Di Pietro E, Snowden A, Jones RO, Moser A, et al. The peroxisomal AAA ATPase complex prevents pexophagy and development of peroxisome biogenesis disorders. Autophagy. 2017;13(5):868-84.
25. Matsumoto N, Tamura S, Fujiki Y. The pathogenic peroxin Pex26p recruits the Pex1p-Pex6p AAA ATPase complexes to peroxisomes. Nat Cell Biol. 2003;5(5):454-60.
26. Birschmann I, Stroobants AK, van den Berg M, Schafer A, Rosenkranz K, Kunau WH, et al. Pex15p of Saccharomyces cerevisiae provides a molecular basis for recruitment of the AAA peroxin Pex6p to peroxisomal membranes. Mol Biol Cell. 2003;14(6):2226-36.
27. Purdue PE, Lazarow PB. Peroxisome biogenesis. Annu Rev Cell Dev Biol. 2001;17:701-52.
28. Hoepfner D, Schildknegt D, Braakman I, Philippsen P, Tabak HF. Contribution of the endoplasmic reticulum to peroxisome formation. Cell. 2005;122(1):85-95.
29. Schrader M, Bonekamp NA, Islinger M. Fission and proliferation of peroxisomes. Biochim Biophys Acta. 2012;1822(9):1343-57.
30. Wanders RJA. Peroxisomal disorders: Improved laboratory diagnosis, new defects and the complicated route to treatment. Mol Cell Probes. 2018;40:60-9.
31. Krause C, Rosewich H, Thanos M, Gartner J. Identification of novel mutations in PEX2, PEX6, PEX10, PEX12, and PEX13 in Zellweger spectrum patients. Hum Mutat. 2006;27(11):1157.
32. Klouwer FC, Berendse K, Ferdinandusse S, Wanders RJ, Engelen M, Poll-The BT. Zellweger spectrum disorders: clinical overview and management approach. Orphanet J Rare Dis. 2015;10:151.
33. Engelen M, Kemp S, Poll-The BT. X-linked adrenoleukodystrophy: pathogenesis and treatment. Curr Neurol Neurosci Rep. 2014;14(10):486.
34. Smith CE, Poulter JA, Levin AV, Capasso JE, Price S, Ben-Yosef T, et al. Spectrum of PEX1 and PEX6 variants in Heimler syndrome. Eur J Hum Genet. 2016;24(11):1565-71.
35. Braverman NE, Raymond GV, Rizzo WB, Moser AB, Wilkinson ME, Stone EM, et al. Peroxisome biogenesis disorders in the Zellweger spectrum: An overview of current diagnosis, clinical manifestations, and treatment guidelines. Mol Genet Metab. 2016;117(3):313-21.
36. Tanaka AJ, Okumoto K, Tamura S, Abe Y, Hirsch Y, Deng L, et al. A newly identified mutation in the PEX26 gene is associated with a milder form of Zellweger spectrum disorder. Cold Spring Harb Mol Case Stud. 2019;5(1).
37. Ebberink MS, Mooijer PA, Gootjes J, Koster J, Wanders RJ, Waterham HR. Genetic classification and mutational spectrum of more than 600 patients with a Zellweger syndrome spectrum disorder. Hum Mutat. 2011;32(1):59-69.
38. Matsumoto N, Tamura S, Furuki S, Miyata N, Moser A, Shimozawa N, et al. Mutations in novel peroxin gene PEX26 that cause peroxisome-biogenesis disorders of complementation group 8 provide a genotype-phenotype correlation. Am J Hum Genet. 2003;73(2):233-46.
39. Tamura S, Matsumoto N, Takeba R, Fujiki Y. AAA peroxins and their recruiter Pex26p modulate the interactions of peroxins involved in peroxisomal protein import. J Biol Chem. 2014;289(35):24336-46.
40. Weller S, Cajigas I, Morrell J, Obie C, Steel G, Gould SJ, et al. Alternative splicing suggests extended function of PEX26 in peroxisome biogenesis. Am J Hum Genet. 2005;76(6):987-1007.
41. Gardner BM, Castanzo DT, Chowdhury S, Stjepanovic G, Stefely MS, Hurley JH, et al. The peroxisomal AAA-ATPase Pex1/Pex6 unfolds substrates by processive threading. Nat Commun. 2018;9(1):135.
42. Furuki S, Tamura S, Matsumoto N, Miyata N, Moser A, Moser HW, et al. Mutations in the peroxin Pex26p responsible for peroxisome biogenesis disorders of complementation group 8 impair its stability, peroxisomal localization, and interaction with the Pex1p x Pex6p complex. J Biol Chem. 2006;281(3):1317-23.
43. Halbach A, Landgraf C, Lorenzen S, Rosenkranz K, Volkmer-Engert R, Erdmann R, et al. Targeting of the tail-anchored peroxisomal membrane proteins PEX26 and PEX15 occurs through C-terminal PEX19-binding sites. J Cell Sci. 2006;119(Pt 12):2508-17.
44. James JR, Oliveira MI, Carmo AM, Iaboni A, Davis SJ. A rigorous experimental framework for detecting protein oligomerization using bioluminescence resonance energy transfer. Nat Methods. 2006;3(12):1001-6.
45. Gersting SW, Lotz-Havla AS, Muntau AC. Bioluminescence resonance energy transfer: an emerging tool for the detection of protein-protein interaction in living cells. Methods Mol Biol. 2012;815:253-63.
46. Ensenauer R, Fingerhut R, Schriever SC, Fink B, Becker M, Sellerer NC, et al. In situ assay of fatty acid beta-oxidation by metabolite profiling following permeabilization of cell membranes. J Lipid Res. 2012;53(5):1012-20.

47. Ciniawsky S, Grimm I, Saffian D, Girzalsky W, Erdmann R, Wendler P. Molecular snapshots of the Pex1/6 AAA+ complex in action. Nat Commun. 2015;6:7331.
48. Tan D, Blok NB, Rapoport TA, Walz T. Structures of the double-ring AAA ATPase Pex1-Pex6 involved in peroxisome biogenesis. FEBS J. 2016;283(6):986-92.
49. Itoh R, Fujiki Y. Functional domains and dynamic assembly of the peroxin Pex14p, the entry site of matrix proteins. J Biol Chem. 2006;281(15):10196-205.
50. Ali MH, Imperiali B. Protein oligomerization: how and why. Bioorg Med Chem. 2005;13(17):5013-20.
51. Ispolatov I, Yuryev A, Mazo I, Maslov S. Binding properties and evolution of homodimers in protein-protein interaction networks. Nucleic Acids Res. 2005;33(11):3629-35.
52. Robert X, Gouet P. Deciphering key features in protein structures with the new ENDscript server. Nucleic Acids Res. 2014;42(Web Server issue):W320-4.
53. Roy A, Kucukural A, Zhang Y. I-TASSER: a unified platform for automated protein structure and function prediction. Nat Protoc. 2010;5(4):725-38.
54. Burkhard P, Stetefeld J, Strelkov SV. Coiled coils: a highly versatile protein folding motif. Trends Cell Biol. 2001;11(2):82-8.
55. Hashimoto K, Panchenko AR. Mechanisms of protein oligomerization, the critical role of insertions and deletions in maintaining different oligomeric states. Proc Natl Acad Sci U S A. 2010;107(47):20352-7.
56. Yagita Y, Hiromasa T, Fujiki Y. Tail-anchored PEX26 targets peroxisomes via a PEX19-dependent and TRC40-independent class I pathway. J Cell Biol. 2013;200(5):651-66.
57. Braun P, Tasan M, Dreze M, Barrios-Rodiles M, Lemmens I, Yu H, et al. An experimentally derived confidence score for binary protein-protein interactions. Nat Methods. 2009;6(1):91-7.
58. Schluter A, Fourcade S, Domenech-Estevez E, Gabaldon T, Huerta-Cepas J, Berthommier G, et al. PeroxisomeDB: a database for the peroxisomal proteome, functional genomics and disease. Nucleic Acids Res. 2007;35(Database issue):D815-22.
59. Abstracts of the SSIEM 2014 Annual Symposium, 2-5 September, 2014, Innsbruck, Austria. J Inherit Metab Dis. 2014;37 Suppl 1:27-185.
60. Wortmann SB, Zietkiewicz S, Kousi M, Szklarczyk R, Haack TB, Gersting SW, et al. CLPB mutations cause 3-methylglutaconic aciduria, progressive brain atrophy, intellectual disability, congenital neutropenia, cataracts, movement disorder. Am J Hum Genet. 2015;96(2):245-57.

6. Zusammenfassung

Peroxisomale Biogenesestörungen bilden ein breit gefächertes klinisches Spektrum. Die schwerste Manifestationsform stellen Multisystemerkrankungen mit Letalität im ersten Lebensjahr dar. Aktuell bestehen symptomatische, jedoch keine kausalen Therapien.
In dieser Arbeit wurden durch strukturelle und funktionelle Untersuchungen das Peroxin PEX26 und dessen Splicevariante PEX26Δex5 genauer charakterisiert. Die Analyse der Tertiär- und Quartärstruktur von PEX26 zeigte eine Homooligomerisierung. Diese wurde durch die beiden Motive *Motif 1* und *Motif 2* vermittelt. In beiden Motiven konnten wir Leucin-Zippern nachweisen. Sie grenzen zytosolisch und luminal an die Transmembrandomäne. Die Motive unterscheiden sich in Struktur und Lokalisation von der vorbeschriebenen N-terminal gelegenen PEX6-Bindedomäne. Die Dimerisierung scheint durch eine Disulfidbrücke an Position 173 stabilisiert zu werden. *Motif 2* beinhaltet einen Abschnitt mit basischen, positiv geladenen Aminosäuren, der für die peroxisomale Lokalisation verantwortlich ist. Wir beschreiben ein Modell, das zeigt, wie PEX26 als Dimer PEX1-PEX6- und PEX13-PEX14-Komplexe bindet. Für PEX26Δex5 schlagen wir einen alternativen Bindungsmechanismus vor, da dieser physiologischen Isoform *Motif 1* und die Transmembrandomäne fehlen. Die isoformspezifische Domänenorganisation beeinflusst die Oligomerisierung und Interaktionen mit peroxisomalen Proteinen auf funktioneller Ebene. In unseren Ergebnissen beschreiben wir eine erweiterte peroxisomale Funktion von PEX26 in Biogenese und Homöostase.

Summary

Peroxisomal biogenesis disorders show a broad clinical spectrum. Multi-systemic diseases represent the most severe clinical phenotype resulting in death in the first year of life. Currently there are supportive but no causative therapies available.
This work aimed to further characterize the peroxin PEX26 and its splice variant PEX26Δex5 by structural and functional investigations. The analysis of the ternary and quaternary structure revealed homooligomerization of PEX26 mediated by *Motif 1* and *Motif 2* harboring leucine zipper. These motifs are located adjacent at the luminal as well as at the cytosolic side of the transmembrane domain. The motifs differ in structure and localization in comparison to the N-terminally located PEX6-binding domain. A disulfide bond at position 173 seems to stabilize dimerization. *Motif 2* contains a basic charge motif that is responsible for peroxisomal targeting. We propose a model for the interaction of a PEX26 dimer with PEX1-PEX6 and PEX13-PEX14 complexes. We suggest an alternative binding mechanism for the physiological splice variant PEX26Δex5 due to the lack of *Motif 1* and the transmembrane domain. Isoform specific domain organization influences oligomerization and interaction with peroxisomal proteins on a functional level. For PEX26 we describe an extended peroxisomal function in biogenesis and homeostasis.

7. Erklärung des Eigenanteils an der Publikation

Der Doktorand P. Guder erstellte die peroxisomale cDNA Datenbank, führte die BRET-Experimente durch und betreute die automatisierte Pipettierplattform. BiFC wurde zuerst etabliert und an die automatisierte Pipetierplattform adaptiert. Ebenfalls wurde der Metabolitenassay durchgeführt. Für diese Experimente erfolgte die Datenauswertung. Die Abbildungen wurden erstellt. Das Manuskript wurde verfasst.
A.S. Lotz-Havla führte BRET-, CoIP- und Immunofluoreszenz-Experimente durch. Die Daten wurden von ihr analysiert und das Manuskript erstellt. M. Woidy erstelle Vorhersagemodelle, führte Sequenzanalysen durch und wertete die Daten der automatisierten Pipettierplattform aus. L. Büttner war an den Sequenzanalysen beteiligt und gestaltete Abbildungen. M.K. Danecka führte Western Blots und Immunfluoreszenz-Experimente durch. D.D. Reiß erstellte Co-IPs und Western Blots. Die PEX26-Verkürzungskonstrukte wurden von U.A. Schatz erstellt. M. Becker, R. Ensenauer und P. Pagel stellten die Logistik für den Metabolitenassay zur Verfügung und waren an der Auswertung beteiligt. A.C. Muntau und S.W. Gersting planten die Studie und überarbeiteten das Manuskript.

8. Danksagung

An dieser Stelle möchte ich mich zu allererst bei meiner Doktormutter Prof. A. C. Muntau für die Überlassung des Themas und die Unterstützung bei Durchführung und Anfertigung der vorliegenden Arbeit bedanken. Darüber hinaus gebührt Prof. S. W. Gersting mein Dank für die intensive Betreuung, sowie die Einführung in das wissenschaftliche Arbeiten. Meiner Betreuerin Dr. A. S. Lotz-Havla danke ich für die umfassende Supervision, sowie das kollegiale und freundschaftliche Verhältnis. Der Arbeitsgruppe University Children's Research@Kinder-UKE gebührt Dank für Unterstützung bei den Revisionen der Publikation. Insbesondere Dr. M. K. Danecka und M. Woidy waren hierbei maßgeblich beteiligt. Den Kolleginnen und Kollegen im Kinderforschungszentrum der Ludwig-Maximilians-Universität München danke ich für die stets kooperative und supportive Zusammenarbeit über Arbeitsgruppengrenzen hinweg. Die Arbeit wurde im Rahmen des Promotionsstudiengangs „systembiologische Medizin" im Förderprogramm für Forschung und Lehre (FöFoLe) der Ludwig-Maximilians-Universität gefördert.
Meiner Familie und insbesondere meiner Frau Stephanie danke ich für den Rückhalt und die Unterstützung sowie die Motivation in allen Phasen der Arbeit.

9. Lebenslauf

Lebenslauf wurde aus datenschutzrechtlichen Gründen entfernt

10. Eidesstattliche Versicherung

Ich versichere ausdrücklich, dass ich die Arbeit selbständig und ohne fremde Hilfe verfasst, andere als die von mir angegebenen Quellen und Hilfsmittel nicht benutzt und die aus den benutzten Werken wörtlich oder inhaltlich entnommenen Stellen einzeln nach Ausgabe (Auflage und Jahr des Erscheinens), Band und Seite des benutzten Werkes kenntlich gemacht habe.
Ferner versichere ich, dass ich die Dissertation bisher nicht einem Fachvertreter an einer anderen Hochschule zur Überprüfung vorgelegt oder mich anderweitig um Zulassung zur Promotion beworben habe.
Ich erkläre mich einverstanden, dass meine Dissertation vom Dekanat der Medizinischen Fakultät mit einer gängigen Software zur Erkennung von Plagiaten überprüft werden kann.

Unterschrift: .....